การหาขนาดและโมดการควบคุมที่เหมาะสมของการผลิตไฟฟ้าจากเซลล์แสงอาทิตย์ในระบบจำหน่ายโดยพิจารณาเสถียรภาพแรงดัน

นายตอง ดาย อัน

วิทยานิพนธ์นี้เป็นส่วนหนึ่งของการศึกษาตามหลักสูตรปริญญาวิศวกรรมศาสตรมหาบัณฑิต
สาขาวิชาวิศวกรรมไฟฟ้า ภาควิชาวิศวกรรมไฟฟ้า
คณะวิศวกรรมศาสตร์ จุฬาลงกรณ์มหาวิทยาลัย
ปีการศึกษา 2557

DETERMINING APPROPRIATE SIZE AND CONTROL MODE OF PV GENERATION IN DISTRIBUTION SYSTEMS CONSIDERING VOLTAGE STABILITY

Mr. Tong Duy Anh

A Thesis Submitted in Partial Fulfillment of the Requirements
for the Degree of Master of Engineering Program in Electrical Engineering
Department of Electrical Engineering
Faculty of Engineering
Chulalongkorn University
Academic Year 2014

Thesis Title	DETERMINING APPROPRIATE SIZE AND CONTROL MODE OF PV GENERATION IN DISTRIBUTION SYSTEMS CONSIDERING VOLTAGE STABILITY
By	Mr. Tong Duy Anh
Field of Study	Electrical Engineering
Thesis Advisor	Assistant Professor Kulyos Audomvongseree, Ph.D.

Accepted by the Faculty of Engineering, Chulalongkorn University in Partial Fulfillment of the Requirements for the Master's Degree

.....Dean of the Faculty of Engineering

(Professor Bundhit Eua-arporn, Ph.D.)

THESIS COMMITTEE

.....Chairman

(Assistant Professor Thavatchai Tayjasanant, Ph.D.)

.....Thesis Advisor

(Assistant Professor Kulyos Audomvongseree, Ph.D.)

.....Examiner

(Surachai Chaitusaney, Ph.D.)

.....External Examiner

(Pradit Fuangfoo, Ph.D.)

ตอง ดาย อัน : การหาขนาดและโมดการควบคุมที่เหมาะสมของการผลิตไฟฟ้าจากเซลล์แสงอาทิตย์ในระบบจำหน่ายโดยพิจารณาเสถียรภาพแรงดัน (DETERMINING APPROPRIATE SIZE AND CONTROL MODE OF PV GENERATION IN DISTRIBUTION SYSTEMS CONSIDERING VOLTAGE STABILITY) อ.ที่ปรึกษาวิทยานิพนธ์หลัก: ผศ. ดร. กุลยศ อุดมวงศ์เสรี, หน้า.

ตั้งแต่ระบบผลิตไฟฟ้าพลังงานแสงอาทิตย์เริ่มมีบทบาทสำคัญในระบบจำหน่าย การประเมินผลกระทบทางด้านเสถียรภาพทางแรงดันของระบบผลิตไฟฟ้าพลังงานหมุนเวียนจึงเป็นสิ่งสำคัญ ในวิทยานิพนธ์ฉบับนี้ได้พิจารณาแบบจำลองของแผงเซลล์แสงอาทิตย์ซึ่งเป็นแบบจำลองแบบไดโอดเดียวที่มี 5 พารามิเตอร์พร้อมทั้งพิจารณาเงื่อนไขของสภาพแวดล้อมโดยรอบ โดยที่พลังงานไฟฟ้าผลิตได้จากระบบผลิตไฟฟ้าพลังงานแสงอาทิตย์และโหลดในระบบมีการเปลี่ยนแปลงตามเวลา ในแต่ละขั้นตอนของการควบคุมระบบไฟฟ้าที่สภาวะอยู่ตัวได้ใช้วิธีการวิเคราะห์การคำนวณการไหลของกำลังไฟฟ้ากระแสสลับ ผลลัพธ์ที่ได้จากการคำนวณการไหลของกำลังไฟฟ้าทำให้ทราบว่าดัชนีเสถียรภาพแรงดัน PQ (PQVSI) สามารถแสดงให้เห็นถึงสถานะปัจจุบันของระบบไฟฟ้าว่ามีความใกล้เคียงกับเงื่อนไขของการสูญเสียเสถียรภาพทางแรงดันมากน้อยเพียงใด ดัชนีนี้เป็นเกณฑ์การประเมินหลักของวิทยานิพนธ์ฉบับนี้ ซึ่งจะหาตำแหน่งและขนาดที่เหมาะสม ตลอดจนการควบคุมระบบผลิตไฟฟ้าพลังงานแสงอาทิตย์ นอกจากนี้ยังมีเงื่อนไขอื่นๆ ได้แก่ การสูญเสียพลังงานของระบบและส่วนเบี่ยงเบนแรงดันไฟฟ้า ซึ่งจะรวมอยู่ในขั้นตอนของการออกแบบและการติดตั้งระบบผลิตไฟฟ้าเซลล์แสงอาทิตย์ด้วย โดยเงื่อนไขของการสูญเสียพลังงานของระบบและส่วนเบี่ยงเบนแรงดันไฟฟ้านี้ได้นำเสนอโดยดัชนีเอนกประสงค์ (MOI) วิทยานิพนธ์ฉบับนี้ได้แสดงให้เห็นถึงประโยชน์ของการทำงานของระบบการผลิตไฟฟ้าพลังงานแสงอาทิตย์ที่ตัวประกอบกำลังน้อยกว่าหนึ่ง โดยวิทยานิพนธ์ฉบับนี้ได้ทดสอบกับระบบไฟฟ้าจริงของประเทศไทยและผลลัพธ์ที่ได้จากการทดสอบสามารถยืนยันความถูกต้องของวิธีการได้ นอกจากนี้ได้มีการเพิ่มกรณีศึกษาต่างๆ ได้แก่ โหมดการควบคุมแรงดันไฟฟ้าและการกระจายตัวของระบบผลิตไฟฟ้าพลังงานแสงอาทิตย์

ภาควิชา วิศวกรรมไฟฟ้า ลายมือชื่อนิสิต .....

สาขาวิชา วิศวกรรมไฟฟ้า ลายมือชื่อ อ.ที่ปรึกษาหลัก .....

ปีการศึกษา 2557

5570580021 : MAJOR ELECTRICAL ENGINEERING
KEYWORDS: PV GENERATION, PQ VOLTAGE STABILITY INDEX, MULTIOBJECTIVE INDEX, AC POWER FLOW ANALYSIS, VOLTAGE-DEPENDENT LOAD.

TONG DUY ANH: DETERMINING APPROPRIATE SIZE AND CONTROL MODE OF PV GENERATION IN DISTRIBUTION SYSTEMS CONSIDERING VOLTAGE STABILITY. ADVISOR: ASST. PROF. KULYOS AUDOMVONGSEREE, Ph.D., pp.

Since PV generation starts to play a vital role in distribution networks, the requirement to assess the effect of this type of renewable energy source on the system voltage stability becomes important. In this research, the PV modules model based on the single-diode five-parameter model considering environmental conditions is used. Then, the output power from PV is generated every time-step throughout a pre-defined duration, along with the load data using different types of time-varying load models. At each time-step, the steady-state operation of the system is analyzed by AC Power Flow calculation. From the results of the Power Flow analysis, the general PQ Voltage Stability Index (PQVSI) can be determined to indicate how close the system's current operating condition to the voltage instability condition. Using this index as a main criterion, this research shows how to specify the appropriate location, size, as well as control mode of the PV farm. In addition, the other criteria including system power losses and voltage deviation are also taken into consideration in the process of PV design and installation to fulfil the study. These supplementary criteria are represented by a common index named Multiobjective Index (MOI). Furthermore, this research also demonstrates the benefit of operating the PV generation system at the power factor less than unity. Utilizing a real distribution network in Thailand, this research will clarify the simulation results to confirm the validity of the methodology. The research is also expanded to satisfy various case-studies such as voltage control mode and scattered PV units.

Department: Electrical Engineering Student's Signature .....
Field of Study: Electrical Engineering Advisor's Signature .....
Academic Year: 2014

ACKNOWLEDGEMENTS

This research has been conducted under the supervision and financial support of ASEAN University Network/ Southeast Asia Engineering Education Development Network (AUN/SEED – Net) Program of Japan International Cooperation Agency (JICA).

First of all, I would like to express my sincerest appreciation to my supervisor, Assistant Professor Kulyos Audomvongseree, who has supported me throughout my research with his excellent advices, patience, and caring. The conversations with him about specialized fields have inspired me to go through the long term of conducting the research. Without his conscientious guidance and encouragement, I would never have been able to complete my dissertation.

I would also like to take this opportunity to gratefully thank the committee members including Asst. Prof. Dr. Thavatchai Tayjasanant, Dr. Surachai Chaitusaney, and Dr. Pradit Fuangfoo for giving me their valuable time and recommendations to fulfil my study. My sincere thanks go to all professors, lecturers at Faculty of Engineering, who provided me the basic understanding and advanced knowledge of electrical engineering. I also would like to extend my gratitude to all members of Power System Research Laboratory (PSRL) for their kindly assistances during my study in Chulalongkorn University, Bangkok, Thailand. My appreciation also goes to Dr. Le Viet Tien, my co-advisor from Hanoi University of Science and Technology, Hanoi, Vietnam, for his technical support.

Finally, I wish to thank my beloved parents and my family, who always give me unconditional love and stand by me through the good times and bad.

CONTENTS

Page

Page

Page

Page

LIST OF FIGURES

LIST OF TABLES

CHAPTER I
Introduction

1.1 Motivation

Nowadays, a large number of photovoltaic (PV) generation units have been integrated into power systems. The penetration level of PV generators is increasing rapidly worldwide because of numerous benefits over conventional power plants. Solar PV is now one of the main solutions to capture the interests of distributed generations. Indeed, PV technology produces no greenhouse gas, so it is beneficial to the environment in comparison with fossil fuel power plants. In addition, since PV panels can be integrated among load areas, they reduce power transmission losses from remote power sources. Simultaneously, they may enhance network performances by reducing system congestion and meeting peak demands. Finally, PV technology does not require cooling water during the power production process, and then it helps preserve water resources for other uses. By installing PV panels combined with inverter systems to generate electricity, this modern technology is suitable for the areas of high solar intensity such as Southern Vietnam and Thailand. In Vietnam, a few small PV farms are under experimentation and construction, and they can be a huge potential energy source in the next decades. By the end of 2012, the global cumulative solar power capacity had passed the 100 GW milestone [1] and it is expected that this growth will continue in the near future.

Although this type of distributed generations has many significant advantages, it also has several unwanted impacts on the normal operation of power systems, especially distribution networks. According to intermittent behaviors of solar irradiance and ambient temperature, the power system stability can be influenced considerably. Among stability problems, static voltage instability is one of the major issues. This phenomenon occurs because of reactive power shortages during strained working conditions. In fact, the uncertain supply of PV reactive power can be the reason of undesirable voltage fluctuations [2]. Furthermore, in the large scale grid-

connected PV station, the step-up transformer between the PV system and the utility grid may consume a considerable amount of reactive power leading to some voltage troubles. Currently, most power grids are operating near their static stability limits, which may cause the voltage instability at any possible time. If such a system with the appearance of PV units faces the voltage instability, it can make a great possibility to have the blackout in a wide area. Fortunately, with a suitable operating condition, PV farms do not adversely affect system stability but can possibly help increase the performance of power networks [3, 4]. Indeed, when the PV station is operated in constant voltage control mode or fixed power factor (PF) scheme with non-unity PF, the grid may receive the reactive power support and then, the voltage instability can be reduced. Furthermore, the reduction of system power losses and voltage deviation due to the PV support is also a major benefit. Therefore, determination of the appropriate PV generation becomes an important issue. The proper PV farm should be integrated to bring maximum benefits to the utility grids and PV producers, concurrently guarantee the system stability. In fact, there are many criteria that need to be considered when choosing the location, size and control mode of PV arrays, such as environmental conditions, degree of power quality, and etc. However, in this study, the static voltage stability and system power losses will be taken into account.

To determine properties of PV farms based on these criteria, it is necessary to analyze the effects of large-scale PV generations on system steady-state voltage stability and power losses. Conventionally, the static voltage analysis based on Power Flow technique to draw *P-V* and *Q-V* curves at a particular bus is used. Then, voltage collapse condition can be specified. In [5], various methods such as *Q-V* modal analysis, loading margin, and bus participation are utilized for this purpose. Another group of quick performance measures is used to assess steady-state voltage stability that includes Fast Voltage Stability Index (FVSI), Line Stability Index (L_{mn}), Line Stability Factor (LQP), PQ Voltage Stability Index (PQVSI), and etc. Most of these indices are referred to a transmission line to indicate how far current system operating condition from voltage collapse condition. On the other hand, to study the

PV impact on system power losses and voltage deviation, several indices are utilized such as active power loss index (PLI), reactive power loss index (QLI) and voltage deviation index (VDI). Based on the advantages and disadvantages of each approach, a proper tool will be chosen to conduct this research.

1.2 Specific Objectives

Main objective of this research is to develop the methodology to determine the appropriate photovoltaic (PV) generation size, location and its operating mode in a distribution system considering the static voltage stability constrains. In addition, the standards for system power loss and voltage deviation can be added to fulfill the investigation. Specifically, the objectives of this research are:

1. To study the impacts of PV penetration on system's static voltage stability as well as system power losses and voltage deviation:
   - Determining the appropriate size and location of the PV system.
   - Specifying the proper control mode of the PV system.
   - Verifying the suitable PV penetration: centralized or scattered PV units.
2. To develop a suitable Matlab-based software to determine the impacts of PV penetration on system's static voltage stability, system power losses and voltage deviation.

1.3 Scope of Works

This research is limited by following scopes:

1. The work focuses on the steady-state analysis. The effects of large scale grid-connected PV generation on system static voltage stability and power losses are studied. From then on, the proper sizes, positions, as well as the control modes, are specified.
2. Both concentrated PV system and scattered PV system will be taken into account.

3. PV farm is represented as follows:
    - PV modules model is based on the well-known single-diode five-parameter model considering environmental conditions.
    - The inverter's steady-state model is simply considered as a coefficient (*eff*) representing the energy conversion efficiency.
    - The step-up transformer is simplified as a line reactance (X_T).
    - The PV station is supposed to have ability to control the required reactive power to keep the constant terminal voltage magnitude or power factor at the terminal node (connected bus).
4. Time varying load models are used to simulate the loading data at every load (PQ) bus.
5. The simplified configuration of a real distribution power network in Thailand named TahSai system is used to test the performance of the algorithm.
6. Time-series AC Power Flow analysis is applied to compute the static Voltage Stability Indices (VSI) and the general index of system power losses and voltage deviation.

1.4 Methodology

1. Conduct literature reviews on:
    - Theory of probabilities.
    - Photovoltaic generation technologies and modelling.
    - Static voltage stability assessments.
    - Power loss and voltage deviation assessments.
    - Time-series AC Power Flow analysis.
2. Identify the specific objectives and scope of study.
3. Determine the proper solution method.
4. Collect the relevant historical data.
5. Establish and test the mathematical models of system components.
6. Develop computer programs to analyze the problem.
7. Simulate, evaluate, and verify the results.

8. Draw conclusions and complete relevant documents for publication and final thesis.

1.5 Expected Contribution

This research aims to provide the background knowledge of the impacts of PV penetration on the system static voltage stability and power losses. When these effects along with their mechanisms are clearly specified, the utilities and the PV owners can determine the strategies to exploit the positive impacts as well as limit the negative influences. Based on these understandings, it is expected that the installation and utilization of this renewable energy source will become more efficient. The PV farms should be integrated to gain the maximum benefits while maintaining the normal stability condition of the power system. In the specific application, this study can help make the right decision in choosing the size and location of the PV farm to satisfy the voltage stability and power loss criteria. Furthermore, the study will show the worth of controlling the power factor of PV farm at non-unity condition. This operation not only brings more financial benefits to PV owners but also helps maintain the normal voltage stability and provide the necessary reactive power to utilities. In addition, a completed and detailed mathematical model of PV generation has been established through the research. Hence, this model can be applied to other studies related to integration of solar PV generation to the distribution system.

1.6 Literature Reviews

Impacts of PV generation on system static voltage stability has been mentioned in some previous studies. Rakibuzzaman Shah, N.Mithulananthan, R.C.Bansal, K.Y.Lee, and A.Lomi [5] conducted this research topic by using *Q-V* modal analysis and bus participation factor. Various case studies are presented to verify the effects of different PV locations and penetrations. However, the results are still theoretical when using the IEEE 14 bus test system instead of utilizing a real network configuration. Furthermore, the PV generator model was not described in detail, so that it is quite difficult for other researchers to consult and apply to their works. An

investigation of PV effects on system stability in the case of Ontario, Canada is introduced by Behnam Tamimi, Claudio Cañizares and Kankar Bhattacharya [6]. In this research, distributed PV units and centralized farms with and without voltage regulation are considered. Based on these scenarios, the PV impacts are studied by using eigenvalue and voltage stability analysis. It is illustrated that PV generators contribute significantly to system stability. In [7] and [8], impacts of large-scale PV generation on static and dynamic voltage stability in sub-transmission networks are taken into account. The study utilizes *P-V* curve, singular vectors of power-flow Jacobian matrix and modal analysis to investigate properties of the designed power system. Recently, Duong Quoc Hung, Nadarajah Mithulananthan and Kwang Y. Lee have just established an index named Multiobjective Index (MOI) to present the general PV effect on system power losses and voltage deviation [9]. However, this index is formulated by using the quite complicated equations that can be simplified in some specific applications.

1.7 Outline of Thesis

The thesis contains 7 chapters presented as follows:

Chapter II introduces an overview of photovoltaic (PV) technology in term of definition and composition. Some common PV influences on power networks are also presented. The main point at issue in this chapter is how to establish a suitable PV generation model describing its electrical behavior. Based on this model, the impacts of PV systems on distribution networks can be verified by using simulation programs.

Chapter III recapitulates the available approaches for steady-state voltage stability analysis. From this summarization, a suitable method is specified to assess static voltage stability of power systems in this research.

Chapter IV raises the problem formulation and a detailed methodology to evaluate static voltage stability of distribution systems integrated PV units based on the specified method. From this assessment, the appropriate PV system will be determined to satisfy voltage stability criterion in the next parts. In this chapter,

beside the model of PV systems discussed in chapter II, the other network component models are established in details.

Chapter V presents Multiobjective Index (MOI) as a general indicator for system power loss and voltage deviation assessment. This index is also used in the determination of the proper PV system to fulfil more requirements. A computational procedure is suggested to apply in this specific study.

Chapter VI shows the simulation results and discussion. In this chapter, many case-studies are implemented to verify the impacts of PV sizes, locations as well as control modes on system voltage stability, system power losses and voltage deviation. From then on, the appropriate PV systems are well determined.

Chapter VII concludes the research and suggests future works.

CHAPTER II
Photovoltaic Generation

2.1 Overview of Photovoltaic Technology

Photovoltaic (PV) technology is an application to generate electricity from solar energy by using semiconductors that exhibit the PV effects and DC-AC inverter systems [10]. PV panels composed of a large quantity of solar cells play the role in converting from solar radiation into direct electrical current. The main materials utilized for PV cells contain polycrystalline silicon, monocrystalline silicon, cadmium telluride, amorphous silicon, and copper indium gallium selenide. When these special materials are under the sunlight, photons of light with suitable wavelength and energy can cause some electrons in covalent bonds to break of their atoms and move freely throughout the crystal. If an electric field is supplied, those electrons can move in a certain direction generating a direct electric current. Then, inverters transform the generated DC power into standard AC electricity before delivering to utility grids.

PV arrays can be dispersedly integrated on the roofs or walls of buildings, or they can be constructed as a small power plant. By the end of 2012, the 100 GW solar power capacity was installed around the world, in more than 100 countries [1]. With the development of technologies, the competition between manufactures and the financial incentives from responsible organizations, the cost of PV panels has steadily decreased leading to the increasing penetration of PV in power systems. Due to many global problems such as climate changes, greenhouse effects and the depletion of fossil fuels, this renewable energy source is expected to become an efficient solution for power industry in the near future.

The PV generated electrical power strongly depends on solar irradiance and ambient temperature, which are intermittent variables. As a result, PV generation delivers an uncertain amount of active and reactive power in to the grids causing some troubles for system stability, system reliability, power quality, and etc. The uncertainty of generated active power will affect the system frequency stability,

while the change of reactive power is consistent with system voltage fluctuation issue [2]. However, with the appearance of PV generators, power networks may receive the additional assistances and hence, the power system stability can be increased [11]. For instance, when the PV station is operated in constant voltage control mode or fixed power factor (PF) scheme with non-unity PF, it can support utility grids in maintaining the voltage stability. Therefore, many researches have been conducted to explore the impacts of PV on power systems; then, the positive effects are absolutely exploited while the negative influences are limited.

2.2 Theory of PV Generation Modelling

In the analysis of power systems integrated PV generations, it is necessary to construct the mathematical model of solar cells to describe their electrical behavior. Over the years, the PV model has been established by using the circuit based method [10]. The simplest equivalent circuit representing the PV cell model consists of an ideal current source and a real diode connected in parallel. The current source is assumed to generate current in proportion to the solar intensity, so that the relationship between solar energy and electricity is depicted. On the other hand, the diode represents the physical essence of a PV cell that is a p-n junction.

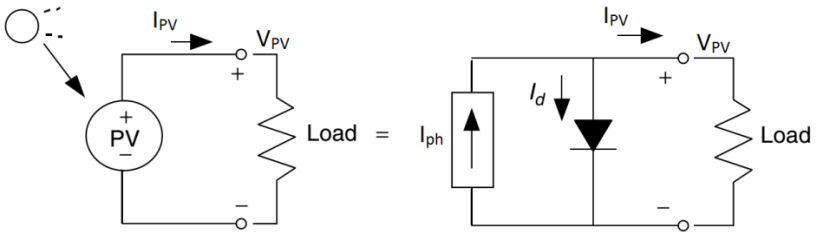

Figure 2. 1 The simplest equivalent circuit for a PV cell.

However, this model has the limits in describing the true behavior of PV cells. Indeed, suppose that two PV cells are connected in series and one of them is shaded (in the dark). By using the discussed model, we can draw the circuit as in Figure 2. 2.

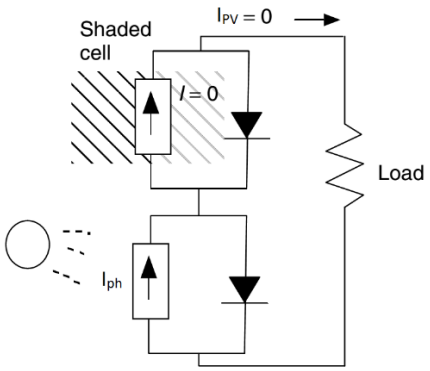

Figure 2. 2 The simplest equivalent circuit of a string of cells in series.

For the shaded cell with the corresponding solar intensity is zero, there is no current through its current source at all. Furthermore, its diode is back biased so it does not allow the current to pass over. In conclusion, the circuit shows that no current or power will be delivered to the load if one of the cells is shaded. However, this result does not reflect the real phenomenon when in facts, the load still receives the power although it is very small. An improved version is obtained by adding an additional parallel resistance (R_{sh}) into the circuit. This resistance will create the path for current to flow through, so the power can be transferred to the load. The value of R_{sh} should be large enough to ensure the small amount of delivered power as in the real situation.

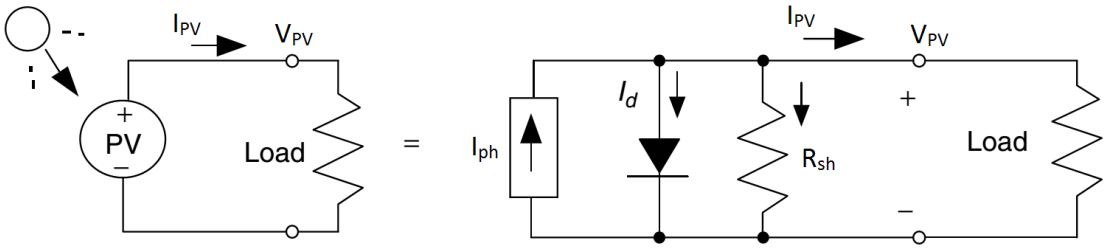

Figure 2. 3 The simplest equivalent circuit of a PV cell with an additional parallel resistance.

A further modification that contains a series resistance, R_s was offered by various researchers. This resistance includes the contact resistance related to the bond between the cell and its wire leads, and the self-resistance of the semiconductor. Finally, the well-known single-diode five-parameter model of PV cell or module is obtained that guarantees the simplicity and the accuracy [12]. In Figure 2. 4, I_{ph}

represents photovoltaic current that is proportional to solar intensity; I_d and V_d are diode current and voltage, respectively; I_{sh} is shunt resistor current; R_{sh} and R_s are shunt and series resistances, respectively; I_{PV} and V_{PV} are PV current and voltage.

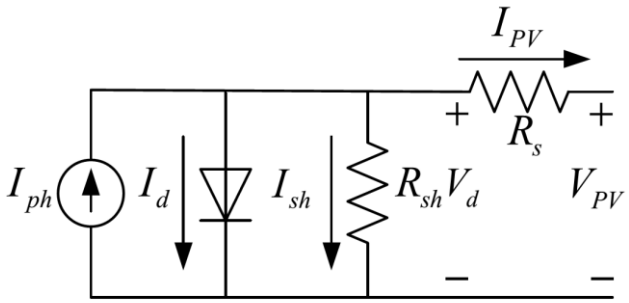

Figure 2. 4 Five-parameter model of PV module.

Many studies were conducted to evaluate the values of five unknown parameters including I_{ph}, I_0, V_T, R_{sh} and R_s that are strongly depend on solar irradiance and ambient temperature. At a particular environmental condition, if these parameters are specified, so the *V-I* curve can be plotted by using the proper tools. As a result, the *V-P* curve can be drawn as well. These curves are very important in representing the electrical characteristics of PV modules. Of course, different conditions of solar intensity and temperature will result different characteristic curves of the same PV module. The process of constructing the PV module model will be discussed in details in the next section, and it is an important part of this research.

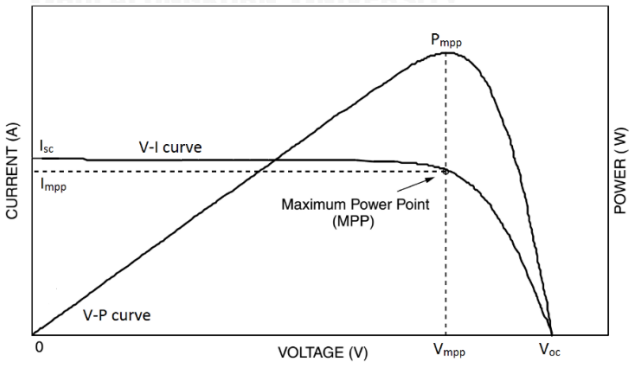

Figure 2. 5 *V-I* and *V-P* curves of a PV module.

2.3 Establishing PV Generation Model for Research

Typically, a PV system consists of a large number of PV modules connected in series or parallel, an inverter system, and a step up transformer to link to the utility

grid as in Figure 2. 6 [13]. The bus between the inverter and the transformer is named photovoltaic bus. The theoretical model of each component will be discussed in details as follows.

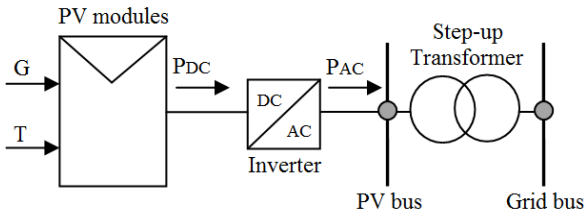

Figure 2. 6 Topology of a grid-connected PV system.

2.3.1 Photovoltaic Array Model

As above mention, only one PV module is too small to generate a considerable amount of electricity; therefore, the modules are connected in series to form a PV string, and the strings will be wired in parallel to create a PV array. By using this combination, both voltage and current can be increased causing the increase of PV power. This section starts from the well-known single-diode five-parameter model of PV module; then, given the specific values of light intensity and temperature, these parameters are modified to get the accurate numerical model in that situation; finally, the PV array model along with its voltage-current (*V-I*) equation could be specified at any environmental condition. Using these models, the thesis will show how to obtain the DC active power from PV farm.

2.3.1.1 Single-diode Five-parameter Model of PV Module

This model is illustrated in Figure 2. 7 [12]. The basic concepts to construct this equivalent circuit can be found in the previous section.

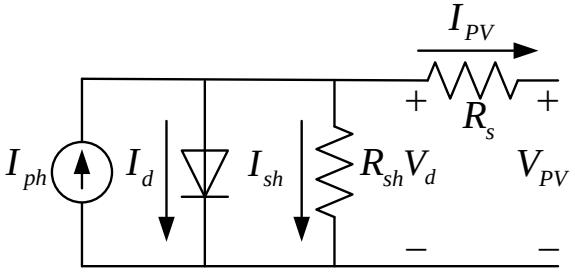

Figure 2. 7 Five-parameter model of PV module.

In above diagram, I_{ph} is photo-generated current; I_d and V_d are diode current and voltage, respectively; I_{sh} is shunt resistor current; R_{sh} and R_s are shunt and series resistances, respectively; I_{PV} and V_{PV} are PV current and voltage. To analyze this circuit, starting with the simple current equation by the Kirchhoff's law

$$I_{PV} = I_{ph} - I_d - I_{sh} \tag{2.1}$$

I_d is modelled by using Shockley equation for an ideal diode [14]

$$I_d = I_0\left(exp\left(\frac{V_d}{nV_T}\right) - 1\right) \tag{2.2}$$

where I_0 is dark saturation current, n is the number of PV cells inside one module, and V_T is the thermal voltage as given by

$$V_T = \frac{kA(T_{module} + 273)}{q} \tag{2.3}$$

where k is Boltzmann's constant (1.381×10^{-23} J/K), A is diode quality factor, T_{module} is module temperature in Celsius scale and q is Coulomb charge (1.60210^{-19} C).

From the circuit, V_d can be represented as

$$V_d = V_{PV} + I_{PV}R_s \tag{2.4}$$

According to (2.2) and (2.4), the formula for I_d is written as

$$I_d = I_0\left(exp\left(\frac{V_{PV} + I_{PV}R_s}{nV_T}\right) - 1\right) \tag{2.5}$$

In addition, based on the circuit and (2.4)

$$I_{sh} = \frac{V_d}{R_{sh}} = \frac{V_{PV} + I_{PV}R_s}{R_{sh}} \tag{2.6}$$

From (2.1), (2.5) and (2.6), the relationship between current and voltage of PV module is derived as

$$I_{PV} = I_{ph} - I_0\left(exp\left(\frac{V_{PV} + I_{PV}R_s}{nV_T}\right) - 1\right) - \frac{V_{PV} + I_{PV}R_s}{R_{sh}} \tag{2.7}$$

Equation (2.7) is the key to find the output power from PV modules. It is obvious to see that five unknown parameters in (2.7) are I_{ph}, I_0, V_T, R_{sh} and R_s. If the numerical values of them are identified, the *V-I* curve and hence, the voltage-power (*V-P*) relationship can be drawn. It is very important to be noticed that these parameters strongly depend on the natural environment. Thus, under the actual solar and thermal conditions, their values have to be adjusted to achieve the exact characteristic curves at that moment.

2.3.1.2 Modification of Five Parameters

First of all, equation (2.7) will be considered under standard test conditions (STC) (1000W/m^2 of solar intensity (G_{STC}), 25°C of cell temperature (T_{STC})). Normally, manufacturers provide the PV datasheet (Table A.1 – Appendix) that includes all electrical characteristics at STC such as maximum power ($P_{max,n}$), voltage and current at $P_{max,n}$ ($V_{mpp,n}$ and $I_{mpp,n}$), short circuit current ($I_{sc,n}$), open circuit voltage ($V_{oc,n}$), temperature coefficients of short circuit current and open circuit voltage (K_I and K_V, respectively), nominal operating cell temperature (*NOCT*), number of cells within module (*n*), and etc. Obviously, the *V-I* curve passes through three important points (short circuit point (0, $I_{sc,n}$), open circuit point ($V_{oc,n}$, 0) and max power point ($V_{mpp,n}$, $I_{mpp,n}$)) resulting three equations of five unknown variables.

$$I_{sc,n} = I_{ph} - I_0\left(exp\left(\frac{I_{sc,n}R_s}{nV_T}\right) - 1\right) - \frac{I_{sc,n}R_s}{R_{sh}} \tag{2.8}$$

$$0 = I_{ph} - I_0\left(exp\left(\frac{V_{oc,n}}{nV_T}\right) - 1\right) - \frac{V_{oc,n}}{R_{sh}} \tag{2.9}$$

$$I_{mpp,n} = I_{ph} - I_0\left(exp\left(\frac{V_{mpp,n} + I_{mpp,n}R_s}{nV_T}\right) - 1\right) - \frac{V_{mpp,n} + I_{mpp,n}R_s}{R_{sh}} \tag{2.10}$$

In addition, the derivative of power with respect to voltage at maximum power point is zero, and based on the slope of *V-I* curve at short circuit point, two remaining equations are formulated.

$$\frac{dP_{PV}}{dV_{PV}}\Big|_{\substack{V_{PV}=V_{mpp,n} \\ I_{PV}=I_{mpp,n}}} = 0 \tag{2.11}$$

$$\frac{dI_{PV}}{dV_{PV}}\Big|_{\substack{V_{PV}=0 \\ I_{PV}=I_{sc,n}}} = -\frac{1}{R_{sho}} \tag{2.12}$$

where R_{sho} is the effective resistance at short circuit, that approximates to R_{sh}. Combining all five equations, the five unknown parameters are well specified at STC by using iterative methods such as Gauss-Seidel [12].

According to [15] and [16], these parameters can be modified from the standard case to any other case of solar irradiance G (W/m^2) and temperature T (^{o}C) as follows

$$T_{module} = T + \left(NOCT - 20\right) \times G / 800 \tag{2.13}$$

$$V_T = V_{T,n} \times \left(T_{module} + 273\right) / \left(T_{STC} + 273\right) \tag{2.14}$$

$$I_{sc} = I_{sc,n} \times G / G_{STC} + K_I \times \left(T_{module} - T_{STC}\right) \tag{2.15}$$

$$V_{oc} = V_{oc,n} + V_T \times \log\left(G / G_{STC}\right) + K_V \times \left(T_{module} - T_{STC}\right) \tag{2.16}$$

$$R_{sh} = R_{sh,n} \times G_{STC} / G \tag{2.17}$$

$$R_s = R_{s,n} \tag{2.18}$$

$$I_o = \left(I_{sc} - \left(V_{oc} / R_{sh}\right)\right) / \left(\exp\left(V_{oc} / \left(n \times V_T\right)\right) - 1\right) \tag{2.19}$$

$$I_{ph} = I_o \times \left(\exp\left(V_{oc} / \left(n \times V_T\right)\right) - 1\right) + V_{oc} / R_{sh} \tag{2.20}$$

2.3.1.3 Characteristic Equation of PV Arrays

Suppose that a PV array consists of N_s strings in parallel, and each string has N_m modules in series. In accordance with [12], module parameters are adjusted as

$$I_{sc}^{ar} = N_s \times I_{sc} \tag{2.21}$$

$$V_{oc}^{ar} = N_m \times V_{oc} \tag{2.22}$$

$$I_{ph}^{ar} = N_s \times I_{ph} \tag{2.23}$$

$$I_o^{ar} = N_s \times I_o \tag{2.24}$$

$$R_s^{ar} = R_s \times N_m / N_s \tag{2.25}$$

$$R_{sh}^{ar} = R_{sh} \times N_m / N_s \tag{2.26}$$

$$V_T^{ar} = V_T \tag{2.27}$$

All above equations are substituted into (2.7) to obtain the *V-I* equation of PV arrays as

$$I_{PV}^{ar} = N_s I_{ph} - N_s I_0 \left(exp\left(\frac{V_{PV}^{ar} + I_{PV}^{ar} R_s N_m / N_s}{N_m n V_T} \right) - 1 \right) - \frac{V_{PV}^{ar} + I_{PV}^{ar} R_s N_m / N_s}{R_{sh} N_m / N_s} \quad (2.28)$$

It should be noticed that, in the above equation, I_{ph}, I_o, V_T, R_s and R_{sh} are parameters of one PV module; and currently, they are clearly specified at any environmental conditions.

2.3.1.4 DC Active Power from PV Arrays

Until now, the relationship between current and voltage of PV arrays under any given outside condition is clearly specified through (2.28). Consequently, the *V-I* and *V-P* characteristics have been plotted by using Matlab tools as in Figure 2. 8, for example. It should be aware that PV generation usually works in the control of maximum power point tracking (MPPT) system. One of the functions of MPPT is to keep the generated power at the maximum point on *V-P* curve [17]. Hence, this peak value is assumed to be the DC active power (P_{DC}) that the PV farm supplies into the grid.

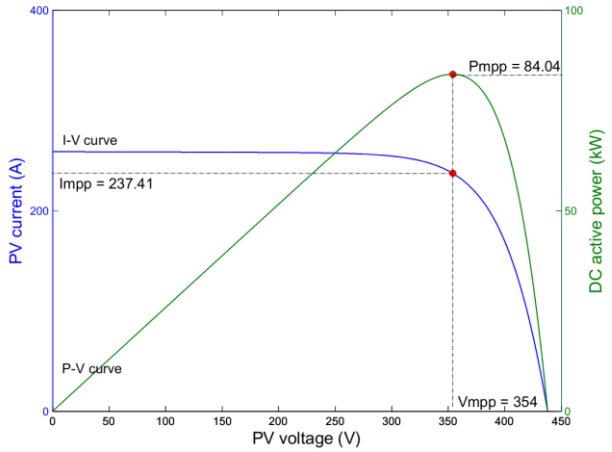

Figure 2. 8 *V-I* and *V-P* characteristics of a PV array under STC.

2.3.2 Inverter and Step-up Transformer Models

In fact, the inverter plays an important role in PV systems. The basic function of this essential device is to transform the generated DC power into standard AC electricity before delivering to utility grids. Based on the steady-state properties of this research, the inverter model can be simply considered as a coefficient *eff*

representing the energy conversion efficiency [18]. The injected three-phase active power at the photovoltaic bus (in Figure 2. 6) is calculated as

$$P_{AC} = eff \times P_{DC} \tag{2.29}$$

In addition, it could be assumed that the converter system has ability to control the required reactive power to keep the constant terminal voltage or power factor at the photovoltaic bus. In the fixed power factor control mode, the corresponding reactive power from PV generation can be easily computed and the photovoltaic bus is treated as a PQ bus. Alternatively, in the constant terminal voltage scheme, this node will be viewed as a voltage-controlled bus with its voltage magnitude is decided by the operators.

Finally, the step-up transformer will be simplified as a line reactance X_T with the transformer off nominal turn ratio is set to be unity. So far, the PV generation model is completed for power system analysis.

CHAPTER III

Static Voltage Stability Assessment

3.1 An Elementary View of Static Voltage Stability Assessment

In power systems, voltage stability can be defined as the ability of a power network to maintain all bus voltages within the limits when the network is normally operated or under a disturbance [19]. Conventionally, the steady-state analysis utilizes Power Flow technique to draw *P-V* and *Q-V* curves at a particular bus to observe the relationship between bus voltage magnitude and corresponding active (reactive) power. Normally, when the active power at that bus keeps increasing, the bus voltage magnitude will decrease until it reaches the voltage collapse point. This approach requires a considerable amount of computation time. At some nodes, this method may not capture the *Q-V* curve completely because of the power flow divergence caused by several problems in the other parts of the network. Recently, *Q-V* modal analysis and bus participation factor are used to assess voltage stability [5]. For modal analysis, the critical eigenvalues of *Q-V* modal matrix will provide the information about system static voltage stability. Following this method, a system is considered as voltage stable if all corresponding eigenvalues are positive; and it is in the unstable state if at least, one of the eigenvalues is negative. The eigenvalue of zero denotes that the system is operating at voltage collapse condition. For bus participation factor, these indices give the measures of the association between buses and modes; in which, the critical mode is related to the smallest eigenvalue of power flow reduced Jacobian matrix. Nodes with the largest participation factors to the critical mode are viewed as the weakest buses of the power system. When these critical buses are close to each other, the weakest area supersensitive to voltage instability is defined. This approach can play an important role in identifying the proper location of PV generators to support the system stability. However, in the real application, these methods have the limits when it is complicated to establish the mathematical model governing the real network. Even that the complete set of

equations describing the power system can be constructed, the computation to find the eigen characteristics often consumes lots of time.

In practical applications, to make the timely decision when operating the electrical system, a fast and accurate voltage stability evaluation is indispensable. Generally, the quick voltage assessment is expressed through voltage stability indices. Several quick measures are used to evaluate static voltage stability such as Fast Voltage Stability Index (FVSI) [20], Line Stability Index (L_{mn}) [21], Line Stability Factor (LQP) [22], PQ Voltage Stability Index (PQVSI) [23], and etc. All of these indices are referred to a transmission line to indicate how close the system's current operating condition to the voltage instability condition. When these indicators reach the value close to unity, it means that the system operates at the voltage collapse point and hence, the blackout in wide areas may occur. The main interests of these methods are: the fast and accurate voltage assessment, the small amount of calculation time required, the simple computation process based on AC Load Flow program.

3.2 Typical Voltage Stability Indices

3.2.1 Fast Voltage Stability Index (FVSI)

Fast Voltage Stability Index (FVSI) is suggested by Ismail Musirin and Titik Khawa Abdul Rahman in [20]. This voltage index is derived by first formulating the current flow equation in a common transmission line between sending bus *i* and receiving bus *j* as in Figure 3. 1.

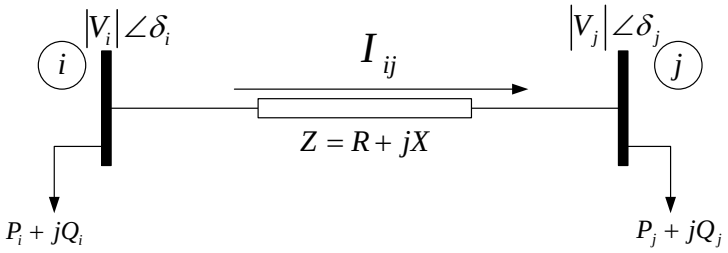

Figure 3. 1 Buses transmission line model.

The equation of current flow can be obtained as

$$I_{ij} = \frac{|V_i|\angle\delta_i - |V_j|\angle\delta_j}{R + jX} \tag{3.1}$$

where $|V_i|$ and $|V_j|$ are voltage magnitudes at sending and receiving buses, respectively; δ_i and δ_j are corresponding voltage angles; R and X are total line resistance and reactance. Then, the equation to compute $|V_j|$ is determined

$$|V_j|^2 + \left(\frac{R}{X}\sin\delta - \cos\delta\right)|V_i||V_j| + \left(X + \frac{R^2}{X}\right)Q_j = 0 \tag{3.2}$$

where δ is the difference between the voltage angles at sending bus and receiving bus $(\delta_i - \delta_j)$. The mathematical condition to get the real roots for $|V_j|$ is represented as

$$\left[\left(\frac{R}{X}\sin\delta - \cos\delta\right)|V_i|\right]^2 - 4\left(X + \frac{R^2}{X}\right)Q_j \geq 0 \tag{3.3}$$

Or

$$\frac{4|Z|^2 Q_j X}{|V_i|^2 \left(R\sin\delta - X\cos\delta\right)^2} \leq 1 \tag{3.4}$$

Normally, phase angle difference is very small $(\delta \approx 0)$. Thus, the formulation of FVSI for each transmission line can be defined from the left expression of above equation as follows

$$FVSI_{ij} = \frac{4|Z|^2 Q_j}{|V_i|^2 X} \tag{3.5}$$

The maximum value among these line indices will indicate the general system voltage stability.

$$FVSI_{system} = \max\left\{FVSI_{ij}\right\} \tag{3.6}$$

The above equation implies that the value of $FVSI_{system}$ should be less than unity, otherwise the power system voltage may be collapsed leading to the collapse of the whole system.

3.2.2 Line Stability Factor (LQP)

Line Stability Factor *(LQP)* is developed by A. Mohamed, G.B. Jasmon, and S. Yusoff in [22]. By using the same line transmission model as in Figure 3. 1, another form of current flow can be derived

$$I_{ij} = \left(\frac{P_j + jQ_j}{|V_j| \angle \delta_j} \right)^* \tag{3.7}$$

Combining (3.1) and (3.7), a resulting equation can be obtained as

$$P_j - jQ_j = \frac{|V_i||V_j| \angle \delta - |V_j|^2}{(R + jX)} \tag{3.8}$$

Separating the real part and the imagine part of above equation, with an assumption that the resistance is very small $(R \approx 0)$, the sub-equations are specified as

$$P_j = \frac{|V_i||V_j| \sin\delta}{X} \tag{3.9}$$

$$Q_j = \frac{|V_i||V_j| \cos\delta - |V_j|^2}{X} \tag{3.10}$$

Rewriting (3.9) and (3.10) in terms of $\sin\delta$ and $\cos\delta$ and applying identity

$$(\sin x)^2 + (\cos x)^2 = 1 \tag{3.11}$$

the equation to compute $|V_j|^2$ is determined as

$$\left(|V_j|^2 \right)^2 + \left(2XQ_j - |V_i|^2 \right) |V_j|^2 + \left(X^2 Q_j^2 + X^2 P_j^2 \right) = 0 \tag{3.12}$$

The mathematical condition to get the real roots for $|V_j|^2$ is represented as

$$\left(2XQ_j - |V_i|^2 \right)^2 - 4\left(X^2 Q_j^2 + X^2 P_j^2 \right) \geq 0 \tag{3.13}$$

Or

$$4\left(\frac{X}{|V_i|^2}\right)\left(\frac{X}{|V_i|^2}P_j^2+Q_j\right)\leq 1 \tag{3.14}$$

When the resistance is negligible, the magnitudes of active power at sending and receiving buses are equal ($|P_j| \approx |P_i|$). Hence, LQP can be defined as the left expression of above equation

$$LQP_{ij}=4\left(\frac{X}{|V_i|^2}\right)\left(\frac{X}{|V_i|^2}P_i^2+Q_j\right) \tag{3.15}$$

The maximum value among these line indices will indicate the general system voltage stability.

$$LQP_{system}=\max\left\{LQP_{ij}\right\} \tag{3.16}$$

The above equation indicates that the value of LQP_{system} should be less than unity, otherwise the power system will face to the voltage collapse.

3.2.3 Line Stability Index (L_{mn})

Line Stability Factor (L_{mn}) is published by M. Moghavvemi and F. M. Omar in [21]. This fast voltage index is also defined by using the line model as in Figure 3. 1. From (3.1) and (3.7), the equation to compute Q_j can be derived as

$$Q_j=\frac{|V_i||V_j|}{|R+jX|}\sin\left(\theta-\delta\right)-\frac{|V_j|^2}{|R+jX|}\sin\left(\theta\right) \tag{3.17}$$

where θ is the angle of the total line impedance ($Z = R + jX$). Then, from the above equation, $|V_j|$ is calculated as

$$|V_j|=\frac{|V_i|\sin\left(\theta-\delta\right)\pm\sqrt{\left[|V_i|\sin\left(\theta-\delta\right)\right]^2-4XQ_j}}{2\sin\left(\theta\right)} \tag{3.18}$$

The condition to get the real roots for $|V_j|$ is identified as

$$\left[|V_i|\sin\left(\theta-\delta\right)\right]^2-4XQ_j\geq 0 \tag{3.19}$$

Or

$$\frac{4XQ_j}{\left[|V_i|\sin(\theta-\delta)\right]^2} \leq 1 \tag{3.20}$$

Finally, L_{mn} can be defined as the left expression of above equation

$$Lmn_{ij} = \frac{4XQ_j}{\left[|V_i|\sin(\theta-\delta)\right]^2} \tag{3.21}$$

Similarly, the maximum value among these branch indices will represent the general voltage stability of power systems.

$$Lmn_{system} = \max\left\{Lmn_{ij}\right\} \tag{3.22}$$

The value of Lmn_{system} should be less than unity to maintain the system voltage stability.

3.2.4 PQ Voltage Stability Index (PQVSI)

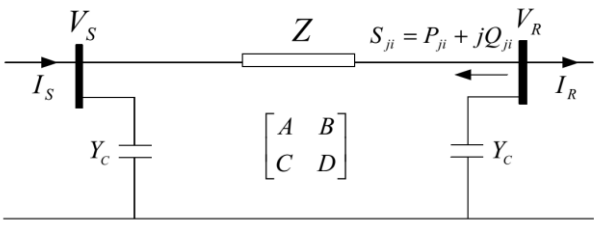

Figure 3. 2 $\prod$ model of a common transmission line.

Figure 3. 2 represents the $\prod$ model of a common transmission line. As in the figure, sending and receiving buses are defined based on the actual direction of the active power flow on the line. P_{ji} and Q_{ji} depict the active and reactive power flowing from receiving bus to sending bus, and hence, the value of P_{ji} should be negative. The complex voltages at the sending and receiving ends are V_S and V_R, respectively. The network parameters can be computed as

$$A = 1 + ZY_C \tag{3.23}$$

$$B = Z \tag{3.24}$$

where Z is the total line impedance and Y_C is the half line charging admittance of the transmission line. From this configuration, the real power flow at the collapse point P_{ji}^{NP} can be derived as follows [23]

$$P_{ji}^{NP} = \frac{\left|V_S\right|^2}{2\left[Im\left\{AB^*\right\}\tan\theta_{ji} - Re\left\{AB^*\right\} + \left|A\right|\left|B\right|\sec\theta_{ji}\right]} \tag{3.25}$$

In this method, the increase of load demands is assumed to be under a constant power factor. Then, the corresponding reactive power at the collapse condition can be derived as

$$Q_{ji}^{NP} = P_{ji}^{NP}\tan\theta_{ji} \tag{3.26}$$

where θ_{ji} is the power flow angle computed by

$$\tan\theta_{ji} = \frac{Q_{ji}^{O}}{P_{ji}^{O}} \tag{3.27}$$

where P_{ji}^{O} and Q_{ji}^{O} are active and reactive power flows at current operating condition that can be calculated by AC Power Flow technique. Figure 3. 3 illustrates the relationship between the current working condition and the voltage collapse condition of a transmission line.

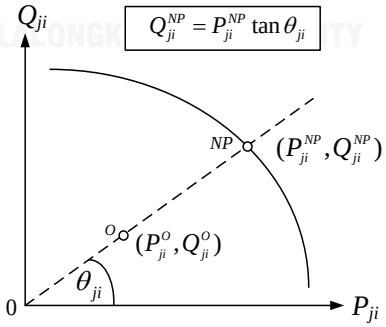

Figure 3. 3 Relationship between the current working condition and the voltage collapse condition.

Consequently, the PQ Voltage Stability Index for each line is determined by the ratio between magnitude of apparent power at normal working point and the one at voltage collapse point. The equation can be written as

$$PQVSI_{ji} = \sqrt{\frac{\left(P_{ji}^{O}\right)^2 + \left(Q_{ji}^{O}\right)^2}{\left(P_{ji}^{NP}\right)^2 + \left(Q_{ji}^{NP}\right)^2}} \tag{3.28}$$

When representing the reactive power in the term of real power as in (3.26) and (3.27), PQVSI can be computed as

$$PQVSI_{ji} = \frac{P_{ji}^{O}}{P_{ji}^{NP}} \sqrt{\frac{\left(1+\tan^2\theta_{ji}\right)}{\left(1+\tan^2\theta_{ji}\right)}} \tag{3.29}$$

Finally, the PQVSI can be obtained as

$$PQVSI_{ji} = \frac{P_{ji}^{O}}{P_{ji}^{NP}} \tag{3.30}$$

The above equation indicates that, if one of PQ Voltage Stability Indices is close to unity, the associated transmission line will be operated near the critical point leading to the voltage collapse of the whole system. The max value of line indices will be the representative of the network.

$$PQVSI_{system} = \max\left\{PQVSI_{ji}\right\} \tag{3.31}$$

Among these fast voltage stability measures, PQ Voltage Stability Index approach provides the reliable index values that reflect the true working condition of networks. This method proposes an accurate formula to compute the voltage stability index, while the other methods use the approximate equations. With the considerable advantages, this tool will be used in the research to study the impacts of PV farms on system static voltage stability.

CHAPTER IV

Problem Formulation and Solution

4.1 Problem Formulation

As the previous mention in chapter I and chapter II, PV systems may contribute both positive and negative impacts to power networks. Therefore, it is necessary to determine the appropriate PV systems to bring the maximum benefits to utilities and PV producers, while the adverse effects are minimized. In this research, the PV impact on system static voltage stability will be the first concern. Based on the theory of PQVSI index discussed in chapter III, this chapter will present a detailed methodology to calculate the general PQVSI of the distribution system connected PV units. This indicator not only shows the degree of system static voltage stability, but also helps identify the proper PV systems to reduce system voltage instability. It is noted that, the computation of this index requires power flow and bus voltage data, which are the results of Load Flow calculation. Secondly, system power losses and voltage deviation are taken into account as the additional criteria in the determination of PV systems, and they will be represented in chapter V.

4.2 Novel Algorithm for Load Flow Calculation

Load Flow study is one of the most important techniques in power system analysis and design [24]. By utilizing this method, steady-state behaviors of electrical networks can be deeply assessed through various results such as bus voltage magnitudes and angles, line flows and losses. The main objective of Load Flow analysis is to specify the node voltages when the power network is under balanced conditions. The formulation of system equations results in complicated nonlinear equations in terms of active and reactive power, known as the *power flow equations*. When the node injected power is identified, the set of these nonlinear equations can be solved by iterative techniques such as Gauss Seidel and Newton Raphson methods. Gauss Seidel technique introduces the simple formulas to estimate reactive power at PV buses and node voltages at all buses except slack bus. However, it requires a considerable amount of calculation time to converge to the roots.

Nowadays, most of Load Flow programs are based on Newton Raphson method with the high accuracy and small amount of required time. A well-known simulation tool for solving power flow and optimal power flow problems is Matpower. It is intended as a package of Matlab® M-files that is easy to use and modify. Obviously, PQVSI could be merged in Line Flow calculation and hence, static voltage appreciation is comprehensive. It should be noticed that each branch of the network configuration has its own voltage stability index and thus, the maximum value among these indices will be the representative to show the voltage stability degree of the whole system.

At normal working conditions of power systems, Matpower based on Newton Raphson method can return the accurate solution of bus voltages. However, since the load demands increase until the system faces to the voltage collapse point where the operating condition is unstable, Newton Raphson may provide inaccurate solutions due to the inaccuracy of Jacobian matrix. As a result, the computed PQVSI at this critical point may be far away from unity; hence it does not reflect the true working status of the system. To alleviate this drawback, the research suggests another algorithm to solve Load Flow problem. Although the computation time can be remarkably increased, it is expected that this algorithm with the linear equations and very few intermediate calculations will return the better solution.

This algorithm starts from the basic equation describing the relationship between node currents and node voltages through bus impedance matrix Z_{bus}. The purpose is to specify the value of V_{bus}

$$V_{bus} = Z_{bus} \times I_{bus} \tag{4.1}$$

It is the fact that, a power system contains only one slack bus, and all of the remaining buses are PQ or PV buses. Equation (4.1) is re-written as

$$\begin{bmatrix} V_s \\ V_g \\ V_l \end{bmatrix} = \begin{bmatrix} Z_{ss} & Z_{sg} & Z_{sl} \\ Z_{gs} & Z_{gg} & Z_{gl} \\ Z_{ls} & Z_{lg} & Z_{ll} \end{bmatrix} \times \begin{bmatrix} I_s \\ I_g \\ I_l \end{bmatrix} \tag{4.2}$$

where V_s and I_s are node voltage and current at slack bus; V_g and I_g are the vectors containing the node voltages and currents at all PV buses, respectively; V_l and I_l are

the voltage and current vectors for PQ buses, respectively; Z_{ss}, Z_{sg},..., Z_{ll} are sub-matrixes obtained from Z_{bus}. Equation (4.2) can be represented as a set of three equations:

$$V_s = Z_{ss} \times I_s + Z_{sg} \times I_g + Z_{sl} \times I_l \tag{4.3}$$

$$V_g = Z_{gs} \times I_s + Z_{gg} \times I_g + Z_{gl} \times I_l \tag{4.4}$$

$$V_l = Z_{ls} \times I_s + Z_{lg} \times I_g + Z_{ll} \times I_l \tag{4.5}$$

It should be noted that, the voltage at slack bus is clearly defined by operators. Hence, only V_g and V_l need to be calculated. From (4.3), I_s can be computed as

$$I_s = \frac{V_s - Z_{sg} \times I_g - Z_{sl} \times I_l}{Z_{ss}} \tag{4.6}$$

Substitute (4.6) into (4.4) and (4.5), the formulas to compute V_g and V_l are specified

$$\begin{aligned} V_g &= Z_{gs} \times \frac{V_s - Z_{sg} \times I_g - Z_{sl} \times I_l}{Z_{ss}} + Z_{gg} \times I_g + Z_{gl} \times I_l \\ &= Z_{gs} \times \frac{V_s}{Z_{ss}} + (Z_{gg} - \frac{Z_{gs} \times Z_{sg}}{Z_{ss}}) \times I_g + (Z_{gl} - \frac{Z_{gs} \times Z_{sl}}{Z_{ss}}) \times I_l \end{aligned} \tag{4.7}$$

$$\begin{aligned} V_l &= Z_{ls} \times \frac{V_s - Z_{sg} \times I_g - Z_{sl} \times I_l}{Z_{ss}} + Z_{lg} \times I_g + Z_{ll} \times I_l \\ &= Z_{ls} \times \frac{V_s}{Z_{ss}} + (Z_{lg} - \frac{Z_{ls} \times Z_{sg}}{Z_{ss}}) \times I_g + (Z_{ll} - \frac{Z_{ls} \times Z_{sl}}{Z_{ss}}) \times I_l \end{aligned} \tag{4.8}$$

All parameters in (4.7) and (4.8) are well known except I_g and I_l. To solve this problem, the iterative method will be applied

$$V_g^{(k+1)} = Z_{gs} \times \frac{V_s}{Z_{ss}} + (Z_{gg} - \frac{Z_{gs} \times Z_{sg}}{Z_{ss}}) \times I_g^{(k)} + (Z_{gl} - \frac{Z_{gs} \times Z_{sl}}{Z_{ss}}) \times I_l^{(k)} \tag{4.9}$$

$$V_l^{(k+1)} = Z_{ls} \times \frac{V_s}{Z_{ss}} + (Z_{lg} - \frac{Z_{ls} \times Z_{sg}}{Z_{ss}}) \times I_g^{(k)} + (Z_{ll} - \frac{Z_{ls} \times Z_{sl}}{Z_{ss}}) \times I_l^{(k)} \tag{4.10}$$

where k denotes the iteration index. I_l is estimated as follows

$$\begin{aligned} I_l^{(k)} &= (-\overset{*}{S_l^{(k)}}) ./ \overset{*}{V_l^{(k)}} = (-\overset{*}{P_l^{(k)}} - jQ_l^{(k)}) ./ \overset{*}{V_l^{(k)}} \\ &= (-P_l^{(k)} + jQ_l^{(k)}) ./ \overset{*}{V_l^{(k)}} \end{aligned} \tag{4.11}$$

S_l, P_l, Q_l are the vectors containing the apparent, active and reactive power at all PQ buses, respectively. In case of voltage-independent load, these vectors are kept constant all time. However, when voltage-dependent load is taken into account, load demand is the function of the corresponding voltage magnitude; so it will be updated in each iteration along with bus voltages. The sign "-" means the injected power is negative or the load demands consume the active and reactive power. $V_l^{(k)}$ contains PQ bus voltages at iteration k.

Similarly, I_g is estimated by the following equation

$$I_g^{(k)} = (P_g - jQ_g^{(k)})./V_g^{*(k)} = (P_{g,s} - P_{g,d} - jQ_g^{(k)})./V_g^{*(k)} \tag{4.12}$$

where $P_{g,s}$ and $P_{g,d}$ contain generated active power and real power demands (if any) at all PV buses. While $P_{g,s}$ is obviously constant, $P_{g,d}$ is dependent on the voltage magnitude at the connected bus. However, the voltage magnitudes at all PV buses are constant, so $P_{g,d}$ is constant as well. Q_g consists of injected reactive power at all PV buses, and each of its elements can be estimated as follows

$$Q_i^{(k)} = -\Im(V_i^{*(k)} \times \sum_{j=1}^{n} Y_{i,j} \times V_j^{(k)}) \tag{4.13}$$

where i denotes bus index, n is the number of buses in the network, and $Y_{i,j}$ is the element of admittance matrix Y_{bus}.

By using the above iterative method with the suitable initial values of PQ and PV bus voltages, the voltages at all buses are well identified at the steady state of the power system. This novel algorithm can be described by the flow chart in Figure 4. 1.

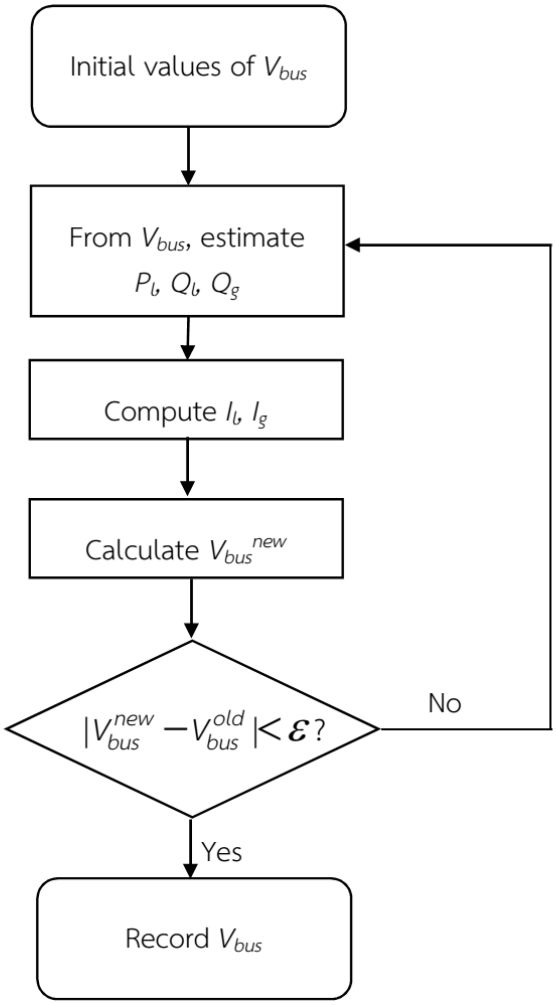

Figure 4. 1 Novel algorithm for Load Flow calculation.

Conventionally, AC Load Flow has only been applied to a single steady state of power systems. Therefore, it may be restricted in assessing the true behaviors of the system during a long period in which the load demands change frequently. Especially, when the grid is integrated the PV generation with variable characteristics of its generated power, focusing on a specific operating point becomes worthless. Although the most stressful working point could be determined without difficulty in the traditional network and Load Flow can be utilized at this time to generally evaluate the system, challenges arise with the penetration of PV. Therefore, time-series Power Flow becomes more useful in this circumstance [25]. The main concept of this approach is to collect the load and generation data every interval during a specified duration; and then, Load Flow program will be run at every time point to gather all

necessary information. Finally, the information is analyzed to return the common voltage stability index expressing general operating status of the system.

4.3 System Component Modelling

4.3.1 Review of PV Generation Model

In chapter II, the PV generation model has been well established for Load Flow analysis. Based on this model, the photovoltaic bus can be treated as a voltage-controlled (PV) bus or load (PQ) bus depending on the control mode of PV generation. Hence, this bus is connected to the power network by using the line-reactance model (X_T) of the step-up transformer. It should be noticed that, besides only one slack bus, the other buses of the considered power system can also be voltage-controlled (PV) or load (PQ) buses.

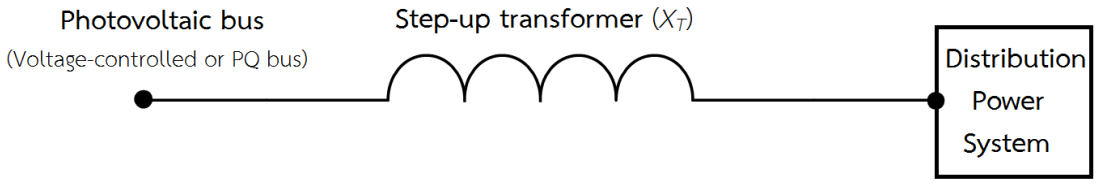

Figure 4. 2 PV generation model.

4.3.2 Distribution Line Model

Normally, transmission lines of distribution networks are short enough to apply the simple $\prod$ model (Figure 4. 3). When taking into account long line effects, the distributed-parameter line model should be considered.

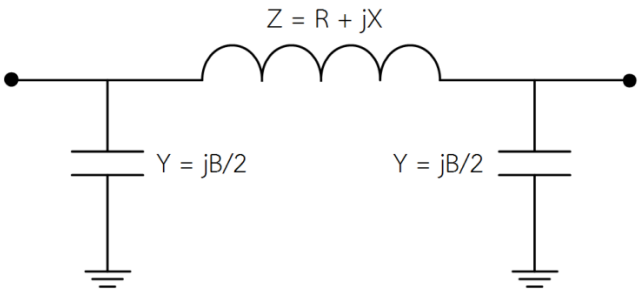

Figure 4. 3 Simple $\prod$ model of distribution lines.

4.3.3 Load Model

4.3.3.1 Voltage-independent Load Model

In accordance with time-series Power Flow, load demands have to be collected every time step Δt during the study period. Suppose that this duration consists of many hours, and the average value of the power demand in each hour has been identified based on the historical data analysis (Table A.6 – Appendix). The load at time *t* of hour *i* can be calculated from the preceding value at time $t-\Delta t$ as

$$P_{i,t} = P_{i,t-\Delta t} + \Delta P \tag{4.14}$$

where ΔP is the load difference that is described by normal distribution $N\left(0,\sigma^2\Delta t\right)$

$$\Delta P = 0 + \sigma\sqrt{\Delta t}\,Z \tag{4.15}$$

$$\sigma = \beta\sqrt{P_{avg,i}} \tag{4.16}$$

where σ is standard deviation of forecasted demands in hour *i* which can be approximated by coefficient β times of root of average value as (4.16) [26], and *Z* is a standard normal distributed random number. The mean of '0' implies that the load varies around the average value. From (4.14), (4.15) and (4.16), the stochastic model of load demands is represented as (4.17) with the starting value $P_{i,t=0}$ is assumed to be $P_{avg,i}$.

$$P_{i,\,t} = P_{i,t-\Delta t} + \beta\sqrt{P_{avg,i}}\sqrt{\Delta t}\,Z \tag{4.17}$$

It should be noticed that the reactive power demand can be directly estimated from (4.17) by an assumption of constant power factor.

4.3.3.2 Voltage-dependent Load Model

In reality, the actual load of a power system depends on the voltage magnitude at the connected bus. To study the true dynamic behavior of power systems, this issue has to be taken into account. Normally, there are three main types of loads: constant power, constant current and constant impedance loads. A good example of a constant power load is a motor-based equipment. This component has to maintain

its power into its load, so it must draw the same amount of power from its source even if the source voltage changes. For constant current load, a welding machine is a good example. Shielded metal arc welding and gas tungsten arc welding use a constant current. Finally, constant impedance load can be found in residential consumers such as light and heat elements.

It is obvious that the real power consumption of a constant power load maintains at the rated value (P_o). In case of constant current load, the real power consumption (P) is proportional to voltage magnitude at connected node ($|V|$). This proportion can be illustrated as

$$\frac{P}{|V|}=\frac{P_o}{|V_o|}=const \Rightarrow P=P_o\times\frac{|V|}{|V_o|} \tag{4.18}$$

where P_o and $|V_o|$ are rated power and voltage magnitude. Similarly, the real power consumption of a constant impedance load is proportional to square of corresponding voltage magnitude

$$\frac{|V|^2}{P}=\frac{|V_o|^2}{P_o}=const \Rightarrow P=P_o\times\frac{|V|^2}{|V_o|^2} \tag{4.19}$$

In fact, the load demand that is connected at a particular bus is the combination of all types of loads. Therefore, the voltage-dependent load model can be established as follows

$$P_{k,i,t}=P^{O}{}_{k,i,t}\times(w_1+w_2\times\frac{\left|V_{k,i,t}\right|}{\left|V^{O}_{k,i,t}\right|}+w_3\times\frac{\left|V_{k,i,t}\right|^2}{\left|V^{O}_{k,i,t}\right|^2}) \tag{4.20}$$

where $P_{k,i,t}$ and $|V_{k,i,t}|$ are the active power demand and the voltage magnitude (in per unit) at time t in hour i at bus k. The nominal value $P^{O}_{k,i,t}$ is calculated as in the case of voltage-independent load model

$$P^{O}_{k,i,t}=(P^{O}_{k,i,t-\Delta t}\times Base_{MVA}+\beta\sqrt{P_{avg,k,i}}\sqrt{\Delta t}\,Z)/Base_{MVA} \tag{4.21}$$

In addition, w_1, w_2 and w_3 are weighting factors denoting the percentage of each type of loads. The summation of these coefficients should be unity. It should be noticed that the value of $|V^{O}_{k,i,t}|$ is always assumed to be unity at any time and location.

With voltage-independent load model, at each time point, the constant values of load demands are clearly identified by using previously described stochastic process. Associated with PV generated power, the bus voltages can be easily specified by using conventional Load Flow program. However, with voltage-dependent load model, the calculation process becomes more complicated. At a particular time, Load Flow technique requires power demands (P, Q) as the input data to return bus voltages. However, in this case, power demand is the function of corresponding bus voltage magnitude that is unidentified before solving Load Flow problem. In the other words, power demands need to be given to obtain bus voltages; vice versa, bus voltages are necessary to determine power demands. Therefore, Load Flow program has to be modified to take into account this issue. Once again, iterative method plays a vital role in this situation. The calculation process can be illustrated as in Figure 4. 4. After this process, the bus voltages along with the power demands are clearly determined at every time point during study period.

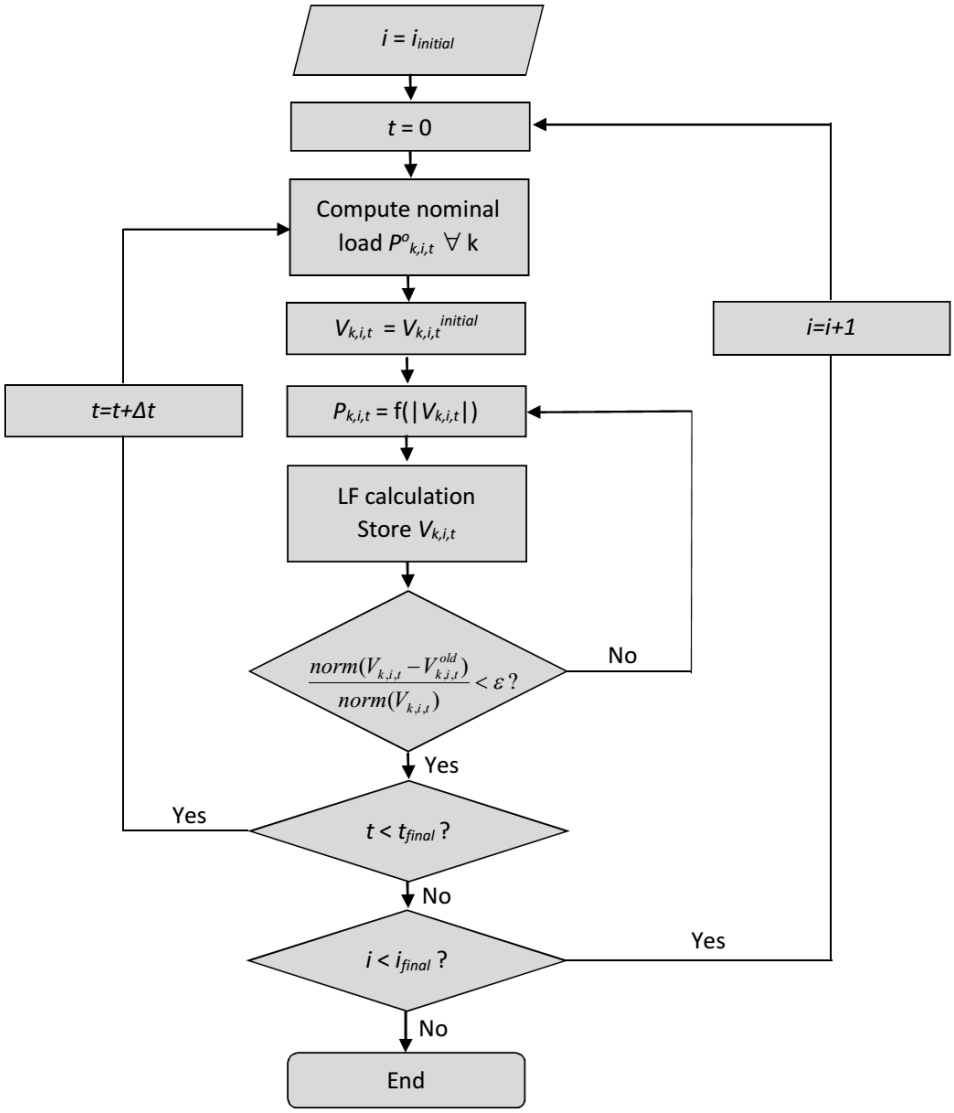

Figure 4. 4 Flow chart describing the algorithm for voltage-dependent load model.

4.4 Solution Methods

Based on time-series AC Power Flow, the main concept of this method is to collect the load and PV output data every interval during a specified duration; and then, Load Flow program will be run at every time point to gather all necessary information. After that, the information is analyzed to return the common voltage stability index to express general operating status of the system. According to this concept, some technical terms should be defined as follows:

- *Local PQVSI ($PQVSI_{local}$)*: At any time point, Load Flow is applied to return the voltage stability indices of all branches. The max value within these indices will be the general indicator of the system at that specific time and it is called *local PQ Voltage Stability Index.*
- *Global PQVSI ($PQVSI_{global}$)*: That is the maximum value of the local PQ Voltage Stability Indices considering all time. This index is the overall representative of the whole system during the study period.
- *Critical time*: Thai is the time point when the system reaches the global PQVSI.
- *Local critical line*: At a time point, it is the branch corresponding to the local PQVSI.
- *Global critical line*: That is the branch related to the global PQVSI at critical time.

Figure 4. 5 describes the research method. It should be noted that, in the case of voltage-independent load, the nominal load is also the actual load.

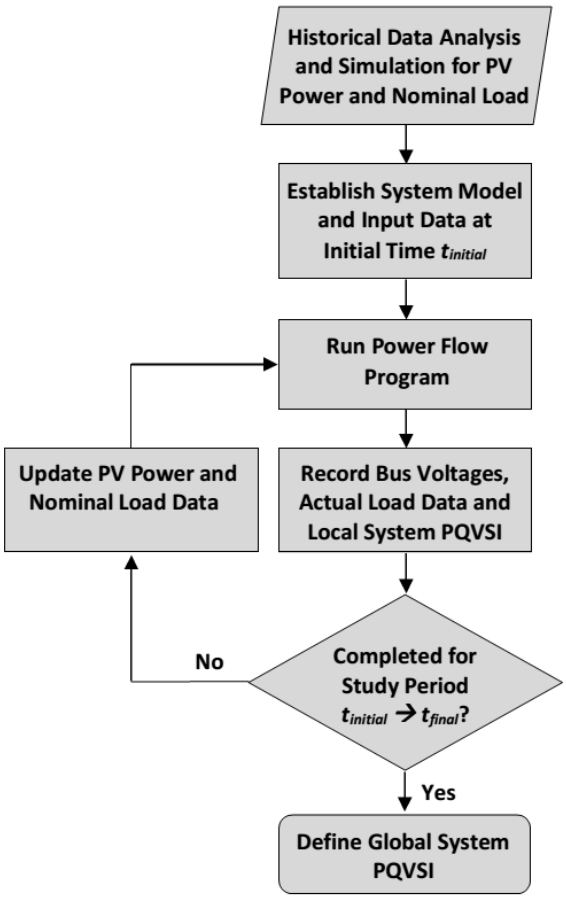

Figure 4. 5 Flow chart describing the method.

CHAPTER V

System Power Loss and Voltage Deviation Assessment

5.1 Introduction

In the previous chapters, the methods to assess static voltage stability of electric power systems integrated PV generators are presented. In fact, there are many aspects of power systems affected by PV installation, not only voltage stability but also system reliability, power quality, power losses, and etc. Although the determination of PV systems based on voltage stability criterion is particularly important, it may not satisfy the other technical requirements. To objectively and accurately determine an appropriate PV system for distribution networks, other criteria need to be taken into account. The more standards a PV system meets, the more suitable it is.

In distribution systems, power loss is always one of the big concerns. Typically, active and reactive power losses can occur in various system components such as distribution lines and transformers during the distribution process. These losses cause not only the extra fuel costs but also the additional supplying power to cover them. Since distribution losses, especially active power loss, are directly related to the profit of electrical producers, it is quite necessary to minimize these losses as much as possible. While many methods of reducing power losses can be applied to existing networks, the other approaches are utilized during the process of constructing new power systems. Strategically, beside the benefits in meeting the growth of demands and enhancing system stability, an appropriate PV system may also help reduce power losses remarkably [27]. Therefore, in this research, the standard for system power losses will be added in determining the proper PV generation. Furthermore, in the PV design and installation process, voltage deviation may be considered as a complementary criterion as well. This issue is defined as the voltage difference between the buses of a power network at steady-states [9]. For the simplicity, all

additional criteria including power losses and voltage deviation are represented by a common index that will be discussed in details in the next section.

5.2 System Power Loss and Voltage Deviation Indices

In the limitation of this research, beside voltage stability issue reflected by PQVSI, another index named Multiobjective Index (MOI) will be introduced as the combination of system active power loss index (PLI), system reactive power loss index (QLI) and system voltage deviation index (VDI) [9]. By using this combined indicator along with PQVSI, it is expected that the specified PV generator can gain more benefits for utility grids.

As the previous mention, MOI is formulated from three indices: PLI, QLI and VDI; hence, this index represents the general influence of PV penetration on system power losses and voltage deviation. First of all, it is necessary to establish the equations of three component indices.

5.2.1 Active Power Loss Index (PLI)

Suppose that a typical distribution network without PV has *n* branches as shown in Figure 5. 1 (a). P_i and Q_i are the active and reactive power flows on branch *i*, respectively; while R_i and X_i denote the corresponding line resistance and reactance. In addition, the complex voltage at bus *i* is defined as V_i.

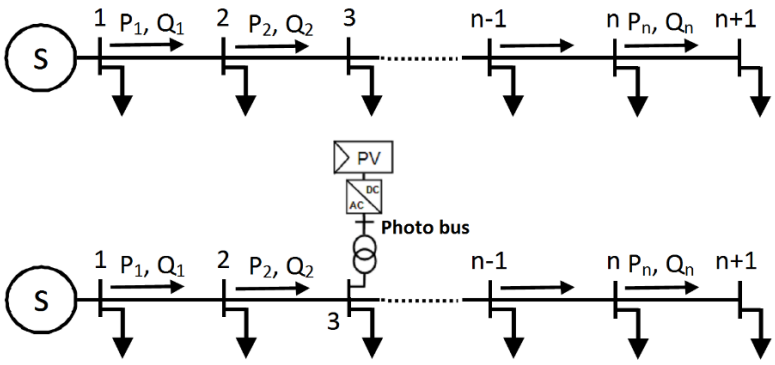

Figure 5. 1 Radial distribution system: (a) without PV and (b) with PV.

From Figure 5. 1 (a), total active power loss of the distribution system without PV is calculated as [28]

$$P_L = \sum_{i=1}^{n} \frac{P_i^2 + Q_i^2}{|V|_i^2} \times R_i \tag{5.1}$$

Without loss of generality, this equation can be applied to the power system with PV penetration as in Figure 5. 1 (b). In this case, the photovoltaic bus is simply treated as load (PQ) or voltage-controlled (PV) bus depending on the PV control modes, and the step-up transformer can be viewed as a branch with the identified resistance and reactance. So far, the system integrated PV units becomes a regular power network. Based on these calculations, the active power loss index (PLI) is defined as

$$PLI = \frac{P_L^{PV}}{P_L} \tag{5.2}$$

where P_L^{PV} is the total active power loss of the system with PV penetration. If PLI value is less than unity, it means that the appearance of PV units helps reduce the system active power loss; and vice versa.

5.2.2 Reactive Power Loss Index (QLI)

Similar to PLI, reactive power loss index (QLI) can be defined as

$$QLI = \frac{Q_L^{PV}}{Q_L} \tag{5.3}$$

where Q_L^{PV} and Q_L are the total reactive power losses of the system with PV and without PV, respectively. Both Q_L^{PV} and Q_L can be computed by using the following equation

$$Q_L = \sum_{i=1}^{n} \frac{P_i^2 + Q_i^2}{|V|_i^2} \times X_i \tag{5.4}$$

5.2.3 Voltage Deviation Index (VDI)

From Figure 5. 1, the voltage deviation or voltage difference along the branch *i* (between bus *i* and bus *i+1*) can be computed as [29]

$$|VD_i| = \frac{|P_i \times R_i + Q_i \times X_i|}{|V_{i+1}|} \tag{5.5}$$

Subsequently, the total voltage difference squared of the power system will be formulated as

$$VD^2 = \sum_{i=1}^{n} \frac{(P_i \times R_i + Q_i \times X_i)^2}{(V_{i+1})^2} \tag{5.6}$$

Finally, the ratio between the system voltage deviation squared in case of PV (VD^2_{PV}) and the system voltage deviation squared in case of no PV (VD^2) is defined as voltage deviation index (VDI)

$$VDI = \frac{VD^2_{PV}}{VD^2} \tag{5.7}$$

It should be noted that, all of these component indices are calculated based on power flows (P_i, Q_i) and bus voltages (V_i), which are the solutions of Load Flow analysis. Therefore, like PQVSI, these indices can be merged in Load Flow program.

5.2.4 Multiobjective Index (MOI)

To generally evaluate the impact of PV on system power losses and voltage profiles, the above individual indices are combined to form a common index named Multiobjective Index (MOI). The formula for MOI can be written as follows [9]

$$MOI = \alpha_1 \times PLI + \alpha_2 \times QLI + \alpha_3 \times VDI \tag{5.8}$$

where $\alpha_1, \alpha_2, \alpha_3$ are the weighting factors. These factors vary between "0" and "1"; and their summation should be one. It is obvious that, when the PV system is not connected to the utility grid, the MOI reaches the value of unity. The determination of weighting factors depends on research purposes, interests of utilities and PV producers, experiments, and etc. Based on the fact that active power loss is always one of the biggest concerns since it is directly related to the profit, the corresponding weighting factor (α_1) can be assumed to be 0.5 in this research. The other factors (α_2, α_3) are supposed to be 0.25 each because reactive power loss and voltage deviation problems often receive little attention. However, these weights can be easily adjusted to satisfy the specific requirements.

According to the methodology of this research, the study period is divided into many intervals. At each time point, Load Flow calculation will be applied to analyze

the system steady-state properties and return one individual (local) MOI. Considering all study duration, the global MOI (MOI_{global}) can be defined as the average value of all local Multiobjective Indices

$$MOI_{global} = \frac{1}{T}\sum_{t=1}^{T} MOI_t \tag{5.9}$$

where T is the number of time points, and MOI_t is the local index at time point t. By using this general index along with global PQVSI, the study of PV impacts on distribution networks will be a multi-dimensional assessment.

In some cases, to represent only the PV effect on the system active power loss, PLI_{global} can be defined as

$$PLI_{global} = \frac{1}{T}\sum_{t=1}^{T} PLI_t \tag{5.10}$$

where PLI_t is the local active power loss index at time point t. It should be noticed that, if α_1 is set to be "1"; while α_2, α_3 receive the values of "0", MOI_{global} will become PLI_{global}. Obviously, QLI_{global} or VDI_{global} can be defined in a similar way. Next section describes the calculation process.

5.3 Computational Procedure

The process to compute the global MOI of a distribution system connected PV units is summarized by following steps:

Step 1: Run Power Flow program at every time point during the specified duration for the system without PV (the base case system). The voltage-dependent load will be considered by using iterative method inside Load Flow program. At each time point, gather the system active and reactive power losses ($P_{L,t}$, $Q_{L,t}$) as well as system voltage deviation squared (VD_t^2).

Step 2: Run Power Flow program at every time point during the study period for the system with PV (the test system). Input data of PV power can also be collected every time interval as the previous discussion in chapter IV. At each time point, gather the system active and reactive power losses ($P^{PV}_{L,t}$, $Q^{PV}_{L,t}$) and system voltage deviation squared ($VD_{PV,t}^2$).

Step 3: Based on the information from steps 1&2, at each time point, compute active power loss index (PLI_t), reactive power loss index (QLI_t) and voltage deviation index (VDI_t) of the test system by using (5.2), (5.3) and (5.7).

Step 4: From the indices in step 3, at each time point, calculate Multiobjective Index (MOI_t) of the test system by using (5.8).

Step 5: Specified global MOI by using (5.9). This index will be the representative of the whole system considering the entire study period.

CHAPTER VI

Test Results and Discussion

6.1 Test System Model and Sample Data

6.1.1 Test System Model

This section describes a real distribution power network in Thailand named TahSai system. The network consists of 33 branches and 34 buses, in which bus 1 is considered as the slack bus. The remaining nodes are viewed as PQ buses in Load Flow program, but in fact there are only 18 actual load points. When the photovoltaic generator is connected to any node, that node will play the role of grid bus as in Figure 2.6 (chapter II). For convenience, the photovoltaic bus is defined as bus 35 which can be PQ or PV bus depending on the operating control mode. Utilizing this test system, time-series Power Flow studies will be carried out with different positions, sizes and control modes of PV generation. TahSai system configuration is illustrated in Figure 6. 1.

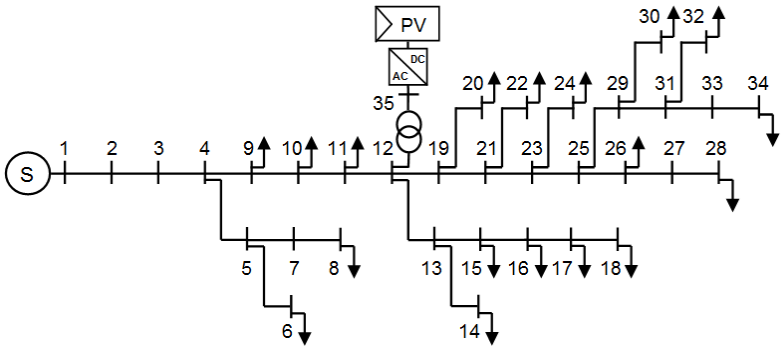

Figure 6. 1 Single diagram of TahSai distribution power network.

6.1.2 Numerical Examples of PV Generated Power and Demands

The research has been conducted in a period from 7 am to 6 pm of a typical summer working day with the time interval (Δt) of 1/60 hours. To generate the PV active power, it is required to know the input data of solar irradiance and temperature. According to [30], the irradiation and ambient temperature models have been well established. Figure 6. 2 shows the sample of environmental conditions which are simulated every minute throughout the observation period.

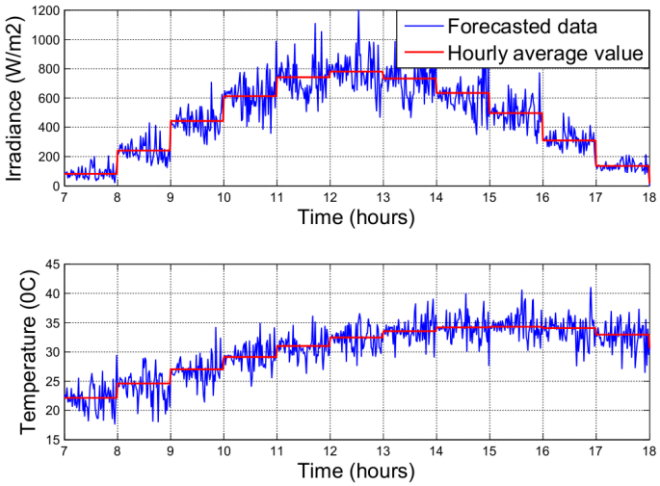

Figure 6. 2 Sampling irradiance and temperature for a typical summer day.

Consequently, the corresponding active power from the PV farm is produced as in Figure 6. 3 by using the concepts discussed in chapter II.

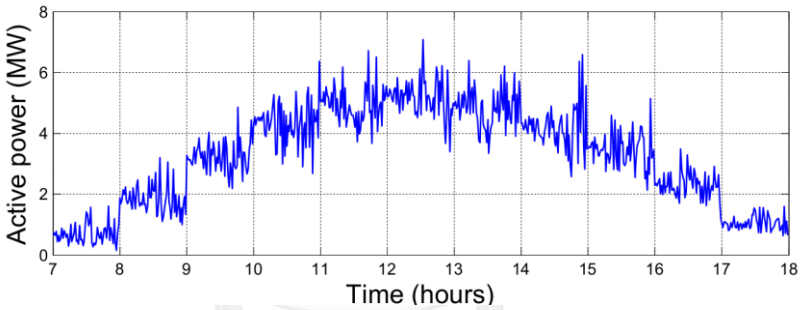

Figure 6. 3 Sampling generated active power from 8 MWp (peak) PV generation.

In addition, based on the theory mentioned in chapter IV, the load demands at all buses are determined by using voltage-independent load model as in Figure 6. 4, for example. For voltage-dependent load model, load demands along with bus voltages will be the final solutions after solving time-series Power Flow completely.

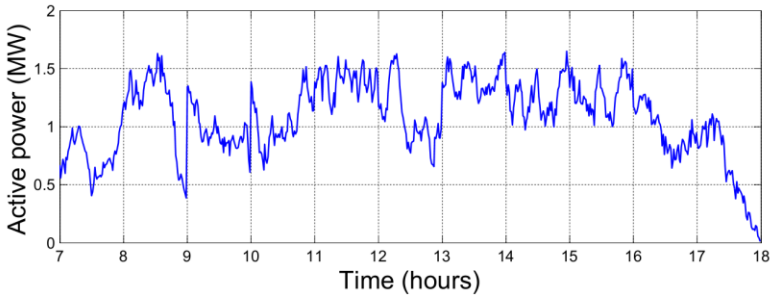

Figure 6. 4 Sampling voltage-independent active load at bus 24 for a working summer day.

6.2 Determining the Proper Centralized PV System in TahSai Distribution Network considering Static Voltage Stability

6.2.1 Effect of PV Generator on System Static Voltage Stability

Firstly, PQVSI analysis will be applied to the system without penetration of PV. In this case study, voltage-independent load model is concerned. Table 6. 1 has shown three highest voltage indices at the critical time when one of the branches reaches the highest PQVSI considering all study period.

Table 6. 1 Highest PQVSI values at critical time in base case.
(Using voltage-independent load model)

Highest PQVSI at the 5th minute of the period 1-2 pm	
Line	PQVSI
11-12 (global critical line)	0.2487 (global value)
3-4	0.1364
2-3	0.1180

At this specific time, the industrial load demands are quite high causing the large amounts of power flowing on the lines. All lines 2-3, 3-4 and 11-12 belong to the main feeder, thus their power flows are considerable. As a result, these lines become more stress leading to high values of their PQVSI. Nevertheless, voltage stability indices are also influenced by line parameters (e.g., the resistance and reactance). It can be shown that, although the power flow on branch 11-12 is smaller than the one on branch 2-3 or 3-4, the parameters of this line, however, are considerably greater than the other ones (Table A. 7 – Appendix) leading to the smaller value of power limits (P_{ji}^{NP}). As the PQVSI is the ratio between the actual power and the limit, the index of branch 11-12 can be the highest one, and in fact, it is the global value. The PQVSI of the whole system shows that, the operation is at normal conditions and does not cause the voltage instability.

Then, a PV generator of 8 MWp (Megawatt peak) is installed at bus 12 to see the impact of this renewable energy source on the system voltage stability. Both control modes are taken into account to return the results as in Table 6. 2.

Table 6. 2 PQVSI values in case of PV.

(Using voltage-independent load model)

Fixed power factor control PF=1	
Critical time (34th minute of the period 8-9 am)	
Global PQVSI	0.2150
Global critical line	11-12
Reference time (5th minute of the period 1-2 pm)	
Local PQVSI	0.1854
Local critical line	11-12
Terminal voltage control V=1.04	
Critical time (58th minute of the period 7-8 am)	
Global PQVSI	0.1669
Global critical line	11-12
Reference time (5th minute of the period 1-2 pm)	
Local PQVSI	0.1449
Local critical line	35-12

At the reference time (the critical time in case without PV), with the good conditions of sunlight and temperature, the PV farm contributes a significant amount of active power into the network causing the changes of the line flows. Specifically, in any PV control mode, the active power flow on line 11-12 is decreased comparing to the one in case of no PV, and hence, it causes the reduction of line 11-12's PQVSI. In the case of constant PF mode, even that line 11-12's PQVSI still be the local maximum index at this time, it is reduced considerably to 0.1854 and then, it is not the global PQVSI anymore. On the other hand, in constant voltage mode, PV system supports not only active but also reactive power into the network. Comparing this mode to the fixed PF regulation and considering line 11-12 at the reference time, the flow of active power is almost similar but the corresponding reactive power is decreased significantly leading to a quite small value of line 11-12's PQVSI (0.1281). As a result, branch 35-12 with the higher voltage index becomes the local critical line

at this time. In general, the new critical time can be defined when the load demand is extremely high but the network does not receive the proper contribution from PV, or it can be the time with the over support from PV generation. As in the Table 6. 2, the global PQVSI reduces from 0.2487 (the case without PV) to 0.2150 (PF control mode) or 0.1669 (voltage control mode) showing that: with the appropriate integrated PV system, the network voltage stability can be increased remarkably.

The results are also verified by using voltage-dependent load model as in Table 6. 3 and Table 6. 4. It can be seen that, both types of load models return the similar results. However, voltage-dependent load model is recommended since it reflects actual behaviors of load demands causing more reliable voltage indices. From now on, this model of load demands will be used to conduct the research.

Table 6. 3 Highest PQVSI values at critical time in base case.
(Using voltage-dependent load model)

Highest PQVSI at the 5th minute of the period 1-2 pm	
Line	PQVSI
11-12 (global critical line)	0.2464 (global value)
3-4	0.1354
2-3	0.1172

Table 6. 4 PQVSI values in case of PV.
(Using voltage-dependent load model)

Fixed power factor control PF=1	
Critical time (34th minute of the period 8-9 am)	
Global PQVSI	0.2130
Global critical line	11-12
Reference time (5th minute of the period 1-2 pm)	
Local PQVSI	0.1807
Local critical line	11-12

Terminal voltage control V=1.04	
Critical time (58th minute of the period 7-8 am)	
Global PQVSI	0.1692
Global critical line	11-12
Reference time (5th minute of the period 1-2 pm)	
Local PQVSI	0.1441
Local critical line	35-12

6.2.2 Impacts of Different PV Locations on System Static Voltage Stability

Now, a PV farm of 8 MWp under unity PF control mode will be installed at various locations to observe its effect on system voltage performance. Several positions are interested such as bus 2, bus 5, bus 12, bus 13, bus 27 and bus 33. It is noted that voltage-dependent load model is applied for the rest of this research. The results have shown in Table 6. 5.

Table 6. 5 Output data considering different PV locations.

Bus	Critical time	Global PQVSI	Global critical line
No PV	1-2 pm (5th minute)	0.2464	11-12
2	1-2pm (5th minute)	0.2464	11-12
5	1-2pm (5th minute)	0.2462	11-12
12	8-9am (34th minute)	0.2130	11-12
13	8-9am (34th minute)	0.2130	11-12
27	12-1pm (33th minute)	0.2140	26-27
33	8-9am (34th minute)	0.2130	11-12

At the locations near the slack bus (e.g., bus 2), the appearance of PV does not have noticeable impacts on the system voltage stability. In this case, PV farm combines with the slack bus to become a group of generators directing forward to the loads. With the assistance from the PV station, the conventional supply can reduce its generated power to satisfy the demands. The interaction between the PV system and the main substation can be seen as the internal support. If all generators

are considered as a united system, the total amount of supplying power from this source should be similar to the one from only slack bus in the case of no PV. In other words, at this position, with or without PV, the flows of power on the lines are almost equal leading to the same values of global PQVSI.

At bus 12, the PV system helps reduce the voltage instability as the discussion in the previous section. It should be noticed that, when the PV generation is integrated at bus 27, the amount of active power flowing from bus 27 to bus 26 reaches the highest value at the time of the best environmental conditions. In addition, based on the configuration of the system, line 26-27 has the quite high reactance and resistance causing its power limit (P_{ji}^{NP}) is restricted. By combining these two conditions, this line becomes the global critical line with the highest PQVSI at the time of the most suitable sunlight and temperature. Although the similar problem occurs to line 31-33 when the PV farm is connected at bus 33, the physical parameters of this line are very small conducting to the opposite results. In facts, line 31-33's PQVSI is only 0.0959 when the PV generated power reaches the maximum value, while the local critical line at this time is branch 35-33 with the local PQVSI is 0.1387. The actual critical time is the 34th minute of the period from 8 am to 9 am, when the active power from PV generation is only enough to supply to the demands at buses 30, 32 and 34; and the rest of power comes from the slack bus.

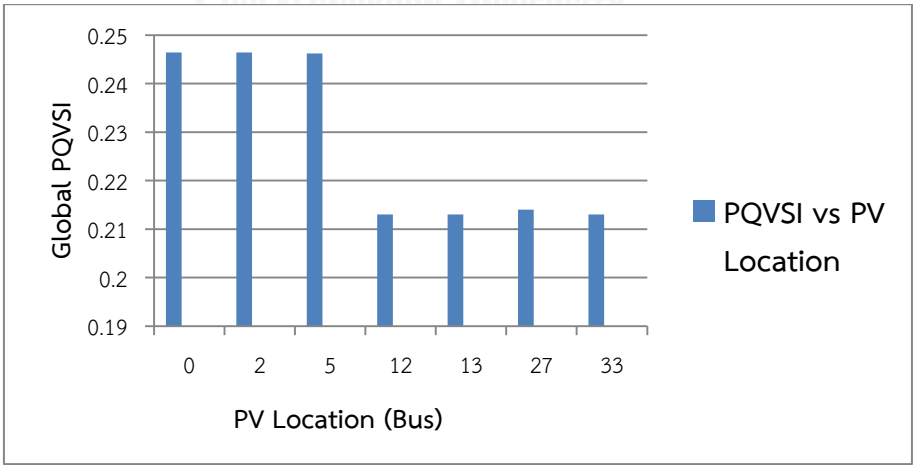

Figure 6. 5 Impacts of various locations of PV farm on static voltage stability.

6.2.3 Impacts of Different PV Sizes on System Static Voltage Stability

Repeating section 6.2.2 with different values of PV size to see the impacts of PV system on the network voltage stability. According to Grid Code, the size of PV is limited depending on the actual distribution system. In this research, the PV size is increased constantly up to 36 MWp with the 1 MWp step size; and some remarkable results are shown to observe the effects of changing PV size on the system voltage stability. In this case, PV farm is installed at bus 12.

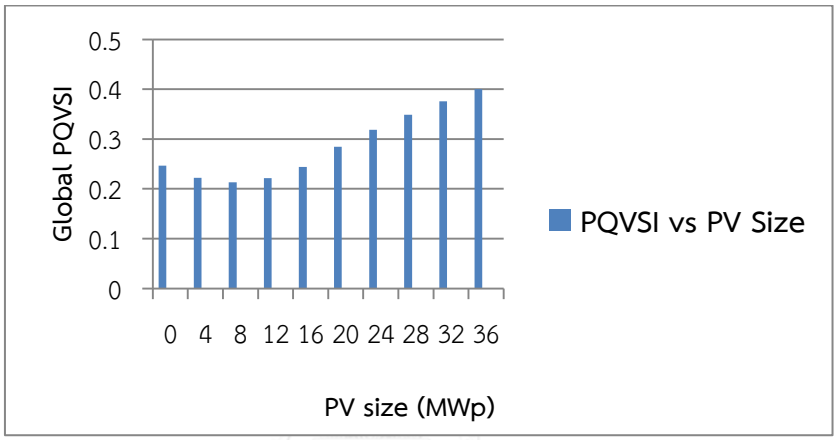

Figure 6. 6 Impacts of various sizes of PV farm on static voltage stability.

Table 6. 6 Output data considering different PV sizes.

PV Size (MWp)	Critical time	Global PQVSI	Global critical line
No PV	1-2 pm (5th minute)	0.2464	11-12
2	1-2 pm (6th minute)	0.2308	11-12
4	8-9am (34th minute)	0.2220	11-12
8	8-9am (34th minute)	0.2130	11-12
12	12-1pm (33th minute)	0.2218	11-12
16	12-1pm (33th minute)	0.2437	11-12
20	12-1pm (33th minute)	0.2844	11-12
24	12-1pm (33th minute)	0.3189	11-12
28	12-1pm (33th minute)	0.3490	11-12
32	12-1pm (33th minute)	0.3759	11-12
36	12-1pm (33th minute)	0.4001	11-12

With 2 MWp PV system, this capacity seems to be too small to cause the noticeable impact on the voltage profile. As the results, the global PQVSI as well as the critical time does not change too much in comparison to the case without PV.

When the PV size keeps rising up to 8 MWp, the voltage index decreases showing that: with the appropriate capacity, the PV system can support the network in sustaining the voltage stability. In these cases, the critical time also changes as mention in section 6.2.1. However, when the PV size is too large combine with the compatible conditions of sunlight and temperature, the generated active power can be dramatically exceeded causing the significant problems for the voltage profile. One of the disastrous consequences is the voltage collapse when the PV capacity is high enough and the global PQVSI index is very close to unity leading to the collapse of the whole system. For the exceedingly high values of PV size, 36 MWp for example, the critical time changes as in the table because at this point, with the best environmental conditions, the PV generated power reaches the maximum value during one day. In this case-study, PV generator is operated under unity power factor control mode. In the case of non-unity power factor, the research is also conducted giving the quite similar trend of the global PQVSI when the PV active power keeps increasing.

Based on the above results and discussion, it can be concluded that: when the generated power from PV is high enough, the global PQVSI will reach the value of "1" representing the collapse of the whole system. However, it is reasonable to suspect this conclusion. Indeed, if PV unit is controlled under fixed non-unity power factor, it will supply both active and reactive power with the strong relation into the grid. When the PV active power increases causing the corresponding increase of PV reactive power, the bus voltage magnitudes of the system will be raised. As a result, the system voltage profile can be far away from the collapse condition and hence, the system voltage stability will be enhanced. In the other word, the global PQVSI should be reduced in this phenomenon instead of reaching unity as the above results. To clearly explain this query, an additional case-study will be implemented as follows. Power Flow analysis is applied to TahSai distribution network at a specific

steady-state at which, the load demands are fixed as in the base case (Table A. 5 – Appendix). Based on this state, the generated power from PV is varied to observe the voltage profile of the network. Ideally, the photovoltaic bus (bus 35) is treated as a PQ bus with the constant power factor of 0.8. In order to comprehend the effect of PV size on system voltage stability, the PV injected power is supposed to be either positive (bus 35 is a generation bus – default case) or negative (bus 35 plays the role of load bus – hypothetical case). The results are shown as in Figure 6. 7. In this figure, the active power at bus 35 is represented in the form of consumption (demands) for convenience.

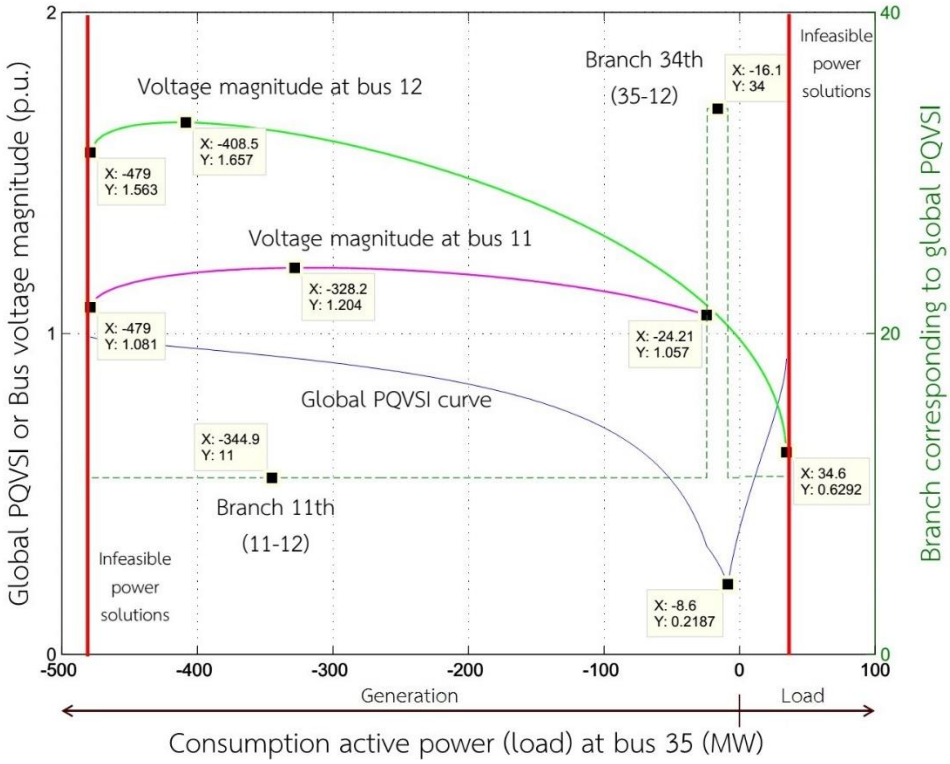

Figure 6. 7 Effect of exceeded power from PV on system voltage stability.

Firstly, the global PQVSI is calculated along with the variation of the active power at bus 35 resulting the global PQVSI curve as in the figure. It can be seen that, when the load demand increases from 0 to 34.6 MW, the voltage magnitudes at some buses (bus 12, for example) will drop until the system faces to the voltage collapse. This phenomenon has been clarified in many studies, and it is correctly reflected by the increase of the global PQVSI till this index reaches unity. Logically, when the load

at bus 35 decreases and especially, bus 35 changes the role to become the generation bus (the consumption power changes from the positive value to the negative one), the operating condition will move away from the collapse condition. This enhancement of voltage stability is still accurately presented by the reduction of the global PQVSI. However, when the PV injected power exceeds the value of 8.6 MW, the global PQVSI starts to increase again and this indicator will proceed to "1" as the previous results. This phenomenon will be the main point at issue in this case-study. With the exceeded amount of PV power, branch 11-12 is identified as the global critical line, and bus 11 is defined as the cause of the system collapse since it receives too much power. Hence, the voltage magnitude at this bus will be observed to explain this phenomenon. Indeed, when the PV supplying power keeps rising, bus 11's voltage magnitude increases as expected; but then, it drops rapidly until reaching the collapse point as in the figure. The movement to the collapse condition of the voltage magnitude at bus 11 when PV power is exceeded confirms the validity of the system PQVSI in this situation. In conclusion, this research verifies the accuracy of PQ Voltage Stability Index in presenting the system voltage stability in any circumstances.

6.2.4 Proper Location and Size of PV Generator

In this research, three properties of PV stations including size, location and control mode are taken into account. It is the fact that, PV control modes can be easily adjusted at any time by operators when running the power system; while the location and installed size must be specified before plant construction. According to this fact and to reduce the complexity, the PV control mode is assumed to be fixed at standard scheme; then, PV size and location will be varied simultaneously to identify the most suitable solution based on static voltage stability criterion. In reality, the suitable position of PV depends on various factors like light intensity, terrain, available lands, and etc. Several locations are interested such as bus 2, bus 5, bus 12, bus 13 and bus 27. To comply with Grid Code, the size of PV is also limited depending on the actual distribution system; then, the PV size is constantly increased

up to 36 MWp with the 1 MWp step size. Figure 6. 8 shows only remarkable points to depict the effect of PV penetration on the voltage stability.

At the locations near the slack bus, the increase in penetration of PV does not have noticeable influences on the system stability as previous discussion. The only reason that can make the system more unstable is the exceeded power flows on branches 1-2 and 35-2. In fact, when the PV is sized up to 36 MWp with corresponding outside conditions, line 35-2 becomes more stress causing high value of its PQVSI and then, this value plays the role of global one. At bus 12, research was completely conducted. The similar trend can be observed for bus 27. It should be aware that, the cases of bus 5 and bus 13 are not represented in the figure because they return the same results as in the cases of bus 2 and bus 12, respectively.

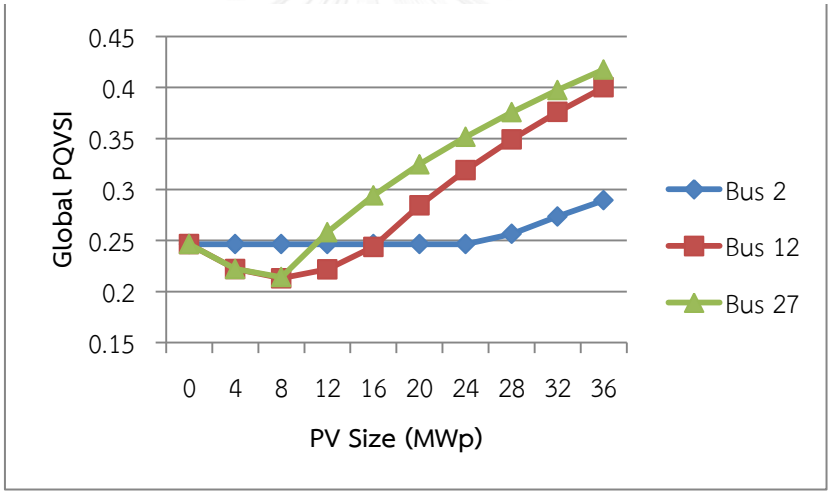

Figure 6. 8 Effect of PV penetration on voltage stability.

From Figure 6. 8, bus 12 should be chosen as the most proper location of the PV system with its corresponding suitable size of 8 MWp based on the static voltage stability criterion. This position seems the same answer with the center of loads. In this instance, the PV generator is operated at unity power factor.

6.2.5 Enhance Size of PV by Adjusting Power Factor of Inverter

Now, a PV farm of 8 MWp has been installed at bus 12 and various power factor operations of PV will be studied. It is expected that by using another power factor instead of unity value, the voltage stability index can be reduced more. Since, the PV

capacity is sized up until the global PQVSI reaches again the initial value as planned in the previous section. The article will prove that, although the degree of voltage stability does not change, this adjustment can bring more financial benefits to PV owners. Firstly, the impact of different power factors is illustrated through Figure 6. 9.

When the PF starts to decrease, the PV system supports not only active but also reactive power into the network. Hence, the flow of reactive power on branch 11-12, for example, can be reduced when compared with the case of unity PF. this reduction on some key lines can affect to the parameter θ_{ji} in equation (3.25), may increase limit values (P_{ji}^{NP}), and then, decrease the PQVSI of these lines as well as the whole system. However, when the PF is under 0.8, the supported reactive power from PV seems to be over. The trouble occurs at the time of the highest sunlight, the generated active power from PV is extremely considerable, and with the small value of PF, the amount of reactive power is quite high as well causing voltage instability. In summary, the PF of 0.8 is suggested to be used when operating the PV system.

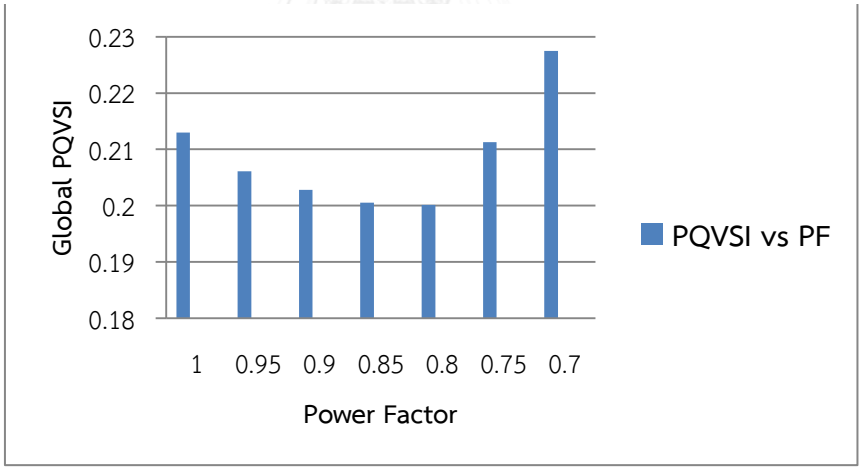

Figure 6. 9 Effect of various power factor operations of PV on voltage stability.

Nevertheless, PV producers do not want to operate their own generators at a power factor less than unity because of financial problems. For instance, with the PV arrays of 8 MWp under the unity power factor operation, the minimum size of the inverter required is 8 MVA only; while in the case of 0.8 PF, the peak values of active and reactive power from PV are 8 MW and 6 MVAr, respectively, so the inverter must be designed for the apparent power of 10 MVA. Due to high investment costs of inverters whereas the PV owners do not gain any benefit, they have the reason to

refuse to support utilities. Alternatively, private investors may want to obtain more profit by increasing the capacity of PV that is restricted by voltage stability requirements. This contradiction can be solved if the PV producers enhance electricity generation while reducing power factor of inverter to maintain the initial global PQVSI. This process, simultaneously, satisfy the requests of utilities regarding reactive power assistance. The agreement is reached as in Table 6. 7.

Table 6. 7 Adjustment of PV installation.

	Original plan	Adjusted plan
Location of PV	Bus 12	Bus 12
Size of PV (MWp)	8	9
Operated power factor	1.0	0.8
Global PQVSI	0.2130	0.2136
Size of inverter (MVA)	8	11.25

The interests of private investors will be discussed in details. According to [31], the output energy from PV in one year can be calculated as

$$A_{PV} = CF \times P_{PV}^{p} \times 8760 \tag{6.1}$$

where CF is capacity factor, P_{PV}^{p} is installed capacity of PV arrays. Based on the policy mechanism designed to accelerate investment in renewable energy technologies named Feed-in Tariff (FiT), the price of PV electricity in Thailand is specified. Then, the revenue of small power producers will be determined for a year. In addition, suppose that investment costs for solar farm are given as in Table 6. 8. From this information, the benefits of investors are illustrated as in Table 6. 9.

Table 6. 8 Example of given data.

Costs of PV modules (Million THB/ MWp)	24.75
Costs of inverters (Million THB/ MVA)	22
Costs of others (Million THB/ MWp)	8.25
Capacity factor (%)	16
PV electricity price (THB/ kWh)	5.7

Table 6. 9 Investment costs and benefits for PV owners.

	Original plan	Adjusted plan
Investment costs (Million THB)	440	544.5
Revenue (Million THB/ year)	63.9	71.9
Recovery of investment (years)	6.9	7.6

In conclusion, utilizing an appropriate power factor control mode combined with the enhanced size, PV producers not only gain more profit but also help maintain the normal voltage stability and provide the necessary reactive power to utilities.

6.2.6 Enhance Bus Voltage Performance in Network by Adjusting PV Terminal Voltage

First of all, voltage profile of all buses will be studied in the case of original plan (a PV farm of 8 MWp at bus 12 under unity PF). By running Power Flow program every minute throughout the study period, the voltage magnitudes of all buses can be clearly identified. From that, the maximum and minimum values of bus voltage magnitudes are defined for each time point. Figure 6. 10 illustrates the voltage performance of buses in the TahSai system. It can be seen that, the maximum value of bus voltage magnitudes keeps constant at 1.0455 every time, and it is the voltage magnitude at slack bus (bus 1).

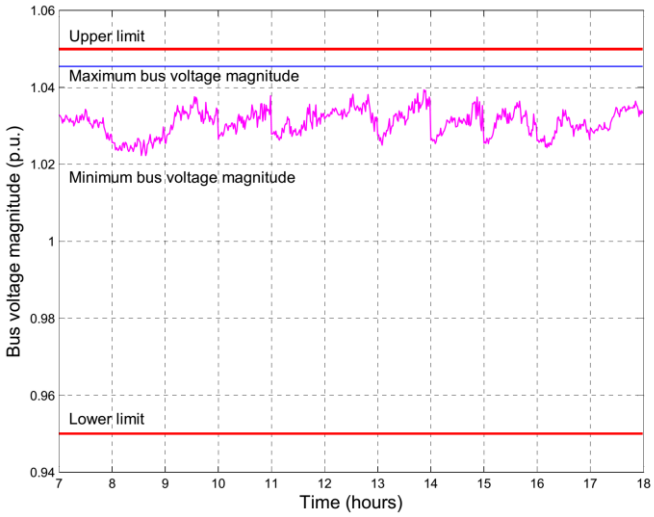

Figure 6. 10 Bus voltage performance in original plan.

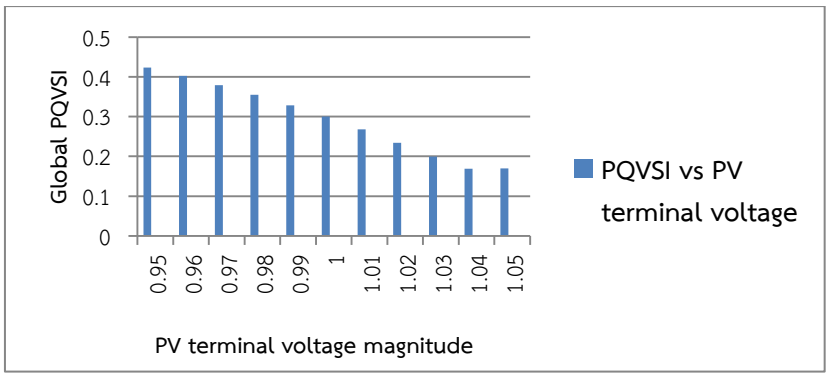

Figure 6. 11 Impacts of various PV terminal voltage magnitude on voltage stability.

Then, from this original plan, a proper voltage control mode is determined to increase the voltage stability of the network. In this research, the constant voltage magnitude at bus 35 is varied from 0.95 p.u. to 1.05 p.u. with the step size of 0.1 p.u. to specify the suitable operation state based on PQVSI. The results are represented in Figure 6. 11.

From Figure 6. 11, the constant voltage magnitude of 1.04 should be set up at PV terminal bus. Figure 6. 12 depicts the voltage performance of buses in this case. It is very clear that, using this PV control mode, not only the current condition is far away from collapse condition, but also the bus voltage profile becomes a lot better. At each time point, the voltages of all buses are kept within a small range around 1.04. Furthermore, the voltage fluctuation considering all time is reduced considerably, that can be observed through the minimum values of bus voltage magnitudes during the specified duration.

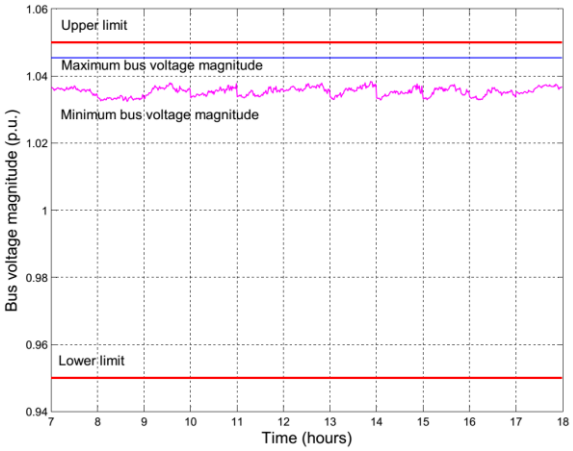

Figure 6. 12 Bus voltage performance in the case of 1.04 PV terminal voltage.

6.3 Determining the Proper PV System in TahSai Distribution Network considering Other Supplementary Criteria

6.3.1 PV Impacts on System Power Losses and Voltage Deviation

In section 6.2.1, a specific case of PV installation (A PV farm of 8 MWp is installed at bus 12 under unity PF control mode**)** is studied to verify the PV impact on system voltage stability. Now, this case study will be implemented by considering Multiobjective Index (MOI) to reflect the impact of PV penetration on system active and reactive power losses and voltage deviation. Following the computational procedure discussed in chapter V, the results are shown in Table 6. 10.

Table 6. 10 System power loss and voltage deviation indices in case of PV.

PV farm of 8 MWp at bus 12 under unity PF control mode	
MOI_{global}	0.4984
PLI_{global}	0.4558
QLI_{global}	0.6214
VDI_{global}	0.4606

It can be seen that, in this case, PV penetration helps reduce not only system active and reactive power losses (reflected by PLI_{global} and QLI_{global}) but also voltage deviation (indicated by VDI_{global}). Since these component indices are combined to form MOI_{global}, this general index of 0.4984 shows that, the power system gains the considerable benefits from the PV generator based on the power loss and voltage deviation criteria.

To carefully analyze the results, the time of the most suitable sunlight and temperature resulting the highest PV generated power will be studied. Firstly, system active power loss is taken into account as in Table 6. 11.

Table 6. 11 Active power flows and losses in two cases: without and with PV.

33rd minute of the period 12-1 pm (the time of the best conditions for PV)							
The case of no PV				The case of PV (8 MWp, bus 12, PF=1)			
$Line_{ij}$	P_{ij} (MW)	P_{ji} (MW)	P_{loss} (MW)	$Line_{ij}$	P_{ij} (MW)	P_{ji} (MW)	P_{loss} (MW)
1-2	5.5238	-5.5218	0.002	1-2	-1.5100	1.5106	0.0006
2-3	5.5218	-5.5137	0.008	2-3	-1.5106	1.5131	0.0025
3-4	5.5137	-5.503	0.0107	3-4	-1.5131	1.5164	0.0033
4-5	1.0178	-1.0174	0.0004	4-5	1.0227	-1.022	0.0004
5-6	0.4703	-0.4703	1E-05	5-6	0.4725	-0.473	1E-05
5-7	0.5471	-0.547	0.0001	5-7	0.5497	-0.55	0.0001
7-8	0.547	-0.547	4E-05	7-8	0.5496	-0.55	4E-05
4-9	4.4852	-4.4848	0.0004	4-9	-2.5390	2.5392	0.0002
9-10	4.4614	-4.4607	0.0007	9-10	-2.5628	2.5631	0.0004
10-11	4.338	-4.3366	0.0013	10-11	-2.6865	2.6872	0.0007
11-12	3.978	-3.9548	0.0232	11-12	-3.0478	3.0641	0.0162
12-13	1.9714	-1.9706	0.0008	12-13	2.0026	-2.002	0.0008
13-14	0.5036	-0.5036	5E-06	13-14	0.5116	-0.512	5E-06
13-15	1.467	-1.4665	0.0006	13-15	1.4903	-1.49	0.0006
15-16	1.4199	-1.4193	0.0006	15-16	1.4424	-1.442	0.0006
16-17	0.8945	-0.8943	0.0002	16-17	0.9087	-0.908	0.0002
17-18	0.1732	-0.1732	9E-06	17-18	0.1759	-0.176	1E-05
12-19	1.9834	-1.9833	7E-05	12-19	2.0148	-2.015	7E-05
19-20	0.0631	-0.0631	1E-07	19-20	0.0641	-0.064	1E-07
19-21	1.9202	-1.9196	0.0006	19-21	1.9506	-1.95	0.0006
21-22	0.1741	-0.1741	2E-06	21-22	0.1768	-0.177	2E-06
21-23	1.7456	-1.7451	0.0005	21-23	1.7732	-1.773	0.0005
23-24	0.9025	-0.9025	6E-05	23-24	0.9168	-0.917	6E-05

23-25	0.8426	-0.8424	0.0002	23-25	0.8559	-0.856	0.0002
25-26	0.0153	-0.0153	3E-08	25-26	0.0156	-0.016	3E-08
26-27	0.0059	-0.0059	5E-08	26-27	0.0060	-0.006	5E-08
27-28	0.0059	-0.0059	2E-08	27-28	0.0060	-0.006	2E-08
25-29	0.8271	-0.8269	0.0002	25-29	0.8402	-0.84	0.0002
29-30	0.5084	-0.5084	5E-06	29-30	0.5164	-0.516	5E-06
29-31	0.3185	-0.3185	3E-05	29-31	0.3236	-0.324	3E-05
31-32	0.2746	-0.2746	1E-05	31-32	0.2790	-0.279	1E-05
31-33	0.0439	-0.0439	5E-07	31-33	0.0445	-0.045	5E-07
33-34	0.0439	-0.0439	1E-07	33-34	0.0445	-0.045	1E-07
				35-12	7.0815	-7.082	0
System active power loss			0.0506	System active power loss			0.0282

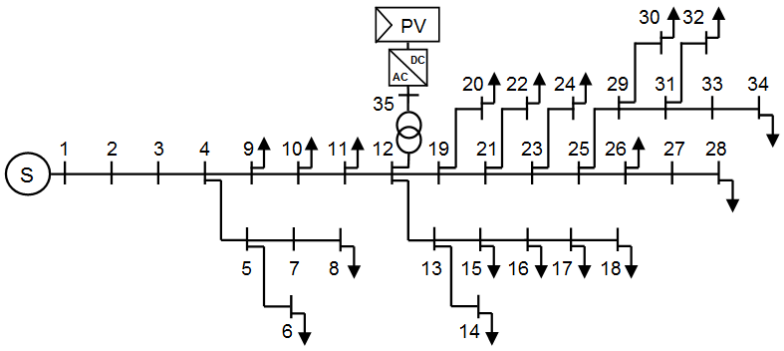

Figure 6. 13 Single diagram of TahSai distribution power network.

According to the single diagram of TahSai distribution system, the power flows on the lines to the right of the PV generator (such as lines 19-20, 19-21, 21-23, and etc.) do not change in comparison with the case of no PV. Based on the equation (5.1), the active power losses on these lines are nearly the same between two cases: with and without PV, when the bus voltage magnitudes only oscillate around 1 p.u. The results are illustrated in Table 6. 11. On the other hand, for the lines to the left of the PV farm, the power flows may change significantly with the appearance of PV. Specifically, with the support from PV generation, the power flows on these lines can be reduced or even changed the direction when the PV power is large enough to

supply back to the station (slack bus). As a result, the power losses on these lines are decreased in the case of PV. For example, without PV penetration, the active power flow on the line 1-2 reaches the value of 5.5238 MW to satisfy the load demands causing the high power loss of 0.002 MW. However, it is changed the direction and reduced to 1.5106 MW because of the exceeded power from PV resulting the decrease of power loss (0.0006 MW). In conclusion, the total active power loss is reduced from 0.0506 MW (the case of no PV) to 0.0282 MW (the case of PV).

The reduction of reactive power loss and voltage deviation at this specific time can be explained in the same way. As a result, PLI, QLI, VDI as well as MOI of the power system integrated PV at the time of the highest PV power are less than unity. When considering all time points of the study period, the maximum MOI is 0.9557 at the 58^{th} minute of the period 7-8 am, when the PV power reaches the minimum value of 0.1534 MW. In contrast, the minimum MOI is 0.3730 at the 12^{th} minute of the period 12-1 pm. In this case, the PV generated power is just enough to satisfy almost the load demands; the remaining supplied power that is quite small comes from the slack bus. For example, the power flowing from bus 1 to bus 2 is only 1.1954 MW causing a small amount of power losses and voltage deviation on this line. By using the equation (5.9), the MOI_{global} can be computed as in Table 6. 11.

6.3.2 Impacts of Different PV Locations on System Power Losses and Voltage Deviation

Now, a PV generator of 8 MWp under unity PF control mode will be installed at different locations to study its impacts on system power losses and voltage deviation. Several positions are interested such as bus 2, bus 5, bus 12, bus 13, bus 27 and bus 33. The results are shown in Table 6. 12.

Table 6. 12 System power loss and voltage deviation indices considering different PV locations.

	MOI_{global}	PLI_{global}	QLI_{global}	VDI_{global}
No PV	1.0000	1.0000	1.0000	1.0000
Bus 2	1.0249	0.9792	1.1427	0.9984
Bus 5	0.8938	0.8248	0.9888	0.9367
Bus 12	0.4984	0.4558	0.6214	0.4606
Bus 13	0.4988	0.4571	0.6227	0.4584
Bus 27	0.7414	0.7425	0.9069	0.5739
Bus 33	0.5950	0.5823	0.7473	0.4679

As previous discussion, the power flows (P, Q) on the lines to the right of PV farm do not change in comparison with the case of no PV. In the case of bus 2 as PV location, most of transmission lines satisfy this condition except only line 1-2; while the step-up transformer line (35-2) is added into the system. As a result, at this position, with or without PV, the flows of power on the lines are almost equal leading to the same values of system power losses and voltage deviation. The small difference between two cases may come from the power flows on lines 1-2 and 35-2. Indeed, all component indices and MOI_{global} are very close to unity as shown in Table 6. 12. According to QLI_{global} (1.1427), there is a slight increase of system reactive power loss when PV is connected to bus 2. To explain this result, the research focuses on the time of the highest PV power (33rd minute of the period 12-1 pm). The reactive power flows and losses at this time are calculated to compare with the case of no PV.

Table 6. 13 Reactive power flows and losses in two cases: without and with PV.

33rd minute of the period 12-1 pm (the time of the best conditions for PV)							
The case of no PV				The case of PV at bus 2 (8 MWp, PF=1)			
$Line_{ij}$	Q_{ij} (MVAr)	Q_{ji} (MVAr)	Q_{loss} (MVAr)	$Line_{ij}$	Q_{ij} (MVAr)	Q_{ji} (MVAr)	Q_{loss} (MVAr)
1-2	3.1336	-3.1297	0.0038	1-2	3.2012	-3.2	0.0012
2-3	3.1297	-3.1139	0.0159	2-3	3.1312	-3.1153	0.0159

3-4	3.1139	-3.0927	0.0212	3-4	3.1153	-3.0941	0.0212
4-5	0.5653	-0.5645	0.0008	4-5	0.5656	-0.5647	0.0008
5-6	0.2608	-0.2608	8E-06	5-6	0.2609	-0.2609	8E-06
5-7	0.3037	-0.3035	0.0002	5-7	0.3039	-0.3036	0.0002
7-8	0.3035	-0.3034	2E-05	7-8	0.3036	-0.3036	2E-05
4-9	2.5274	-2.5267	0.0007	4-9	2.5285	-2.5278	0.0007
9-10	2.5139	-2.5125	0.0014	9-10	2.515	-2.5137	0.0014
10-11	2.4446	-2.442	0.0026	10-11	2.4457	-2.4431	0.0026
11-12	2.2431	-2.1973	0.0458	11-12	2.2441	-2.1983	0.0458
12-13	1.0964	-1.0949	0.0015	12-13	1.0969	-1.0954	0.0015
13-14	0.2794	-0.2794	9E-06	13-14	0.2795	-0.2795	9E-06
13-15	0.8155	-0.8143	0.0011	13-15	0.8159	-0.8147	0.0011
15-16	0.7886	-0.7875	0.0011	15-16	0.7889	-0.7878	0.0011
16-17	0.4963	-0.4959	0.0005	16-17	0.4966	-0.4961	0.0005
17-18	0.0961	-0.0961	2E-05	17-18	0.0961	-0.0961	2E-05
12-19	1.1009	-1.1007	0.0001	12-19	1.1014	-1.1012	0.0001
19-20	0.0344	-0.0344	8E-08	19-20	0.0344	-0.0344	8E-08
19-21	1.0663	-1.0652	0.0011	19-21	1.0668	-1.0657	0.0011
21-22	0.0964	-0.0964	1E-06	21-22	0.0964	-0.0964	1E-06
21-23	0.9688	-0.9679	0.0009	21-23	0.9693	-0.9684	0.0009
23-24	0.5006	-0.5005	0.0001	23-24	0.5008	-0.5007	0.0001
23-25	0.4674	-0.467	0.0003	23-25	0.4676	-0.4672	0.0003
25-26	0.0084	-0.0084	7E-08	25-26	0.0085	-0.0085	7E-08
26-27	0.0032	-0.0032	1E-07	26-27	0.0032	-0.0032	1E-07
27-28	0.0032	-0.0032	1E-08	27-28	0.0032	-0.0032	1E-08
25-29	0.4586	-0.4583	0.0003	25-29	0.4588	-0.4585	0.0003
29-30	0.2819	-0.2818	9E-06	29-30	0.282	-0.282	9E-06
29-31	0.1764	-0.1763	5E-05	29-31	0.1765	-0.1764	5E-05

31-32	0.1521	-0.1521	6E-06	31-32	0.1521	-0.1521	6E-06
31-33	0.0243	-0.0243	1E-06	31-33	0.0243	-0.0243	1E-06
33-34	0.0243	-0.0243	8E-08	33-34	0.0243	-0.0243	8E-08
				35-2	7E-09	0.0689	0.0689
System reactive power loss			0.0998	System reactive power loss			0.1660

It can be seen from Table 6. 13 that, comparing two cases: with and without PV, most of the lines have the same reactive power losses. However, in the case of PV, the reactive power loss in the step-up transformer is considerable (0.0689 MVAr) leading to the higher system reactive power loss (0.1660 MVAr). Therefore, QLI at this specific time is greater than unity (1.6640). Considering the other time points, QLI_{global} can be higher than "1" and in fact, it receives the value of 1.1427.

At the other locations, PV generator also has the positive impact on the power network when considering power losses and voltage deviation. Figure 6. 14 represents the effect of various PV locations on the global Multiobjective Index.

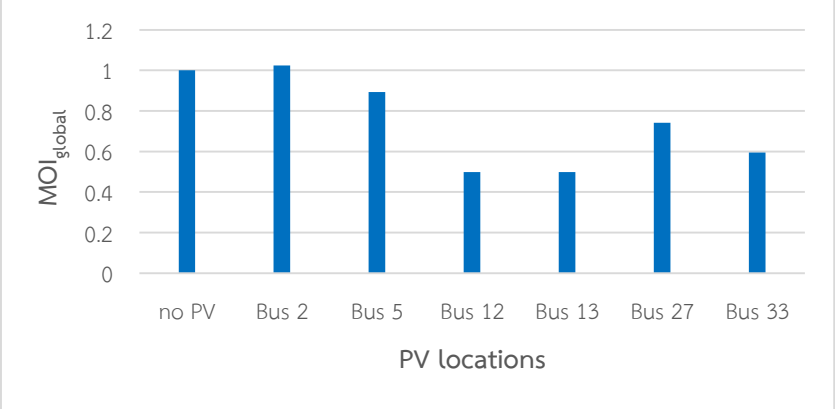

Figure 6. 14 Impacts of PV locations on system power losses and voltage deviation.

6.3.3 Impacts of Different PV Sizes on System Power Losses and Voltage Deviation

Repeating section 6.3.2 with various values of PV size to see the PV impact on the system power losses and voltage deviation. Similar to section 6.2.3, the PV size is constantly increased up to 24 MWp with the 1 MWp step size; and some remarkable

results are shown as in Figure 6. 15. In this study, PV generator is connected to bus 12 under unity PF control mode.

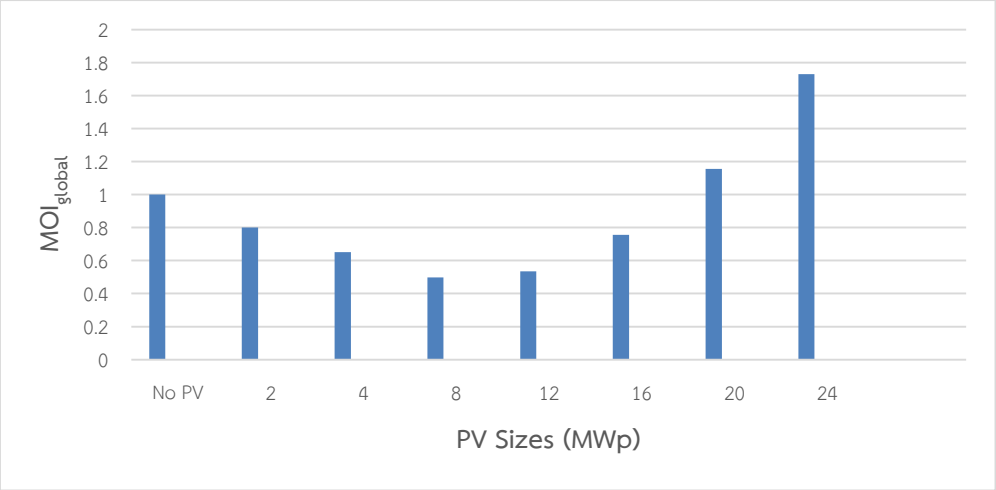

Figure 6. 15 Impacts of PV sizes on system power losses and voltage deviation.

Table 6. 14 System power loss and voltage deviation indices considering different PV sizes.

	MOI_{global}	PLI_{global}	QLI_{global}	VDI_{global}
No PV	1.0000	1.0000	1.0000	1.0000
2 MWp	0.8007	0.7866	0.7969	0.8326
4 MWp	0.6512	0.6251	0.6666	0.6878
8 MWp	0.4984	0.4558	0.6214	0.4606
12 MWp	0.5353	0.4876	0.8581	0.3079
16 MWp	0.7562	0.7167	1.3714	0.2201
20 MWp	1.1561	1.1395	2.1563	0.1889
24 MWp	1.7301	1.7528	3.2084	0.2064

It can be seen that, with the small PV size of 2 MWp, the PV penetration does not significantly affect the system power losses and voltage deviation. This conclusion is reflected by the MOI_{global} of 0.8007 that is close to unity.

When PV capacity is sized up to 8 MWp, PV system helps reduce power and voltage losses as the discussion in section 6.3.1. However, when PV size is exceeded (for example, 24 MWp), the voltage deviation can be reduced alone (VDI_{global} of

0.2064), but the system losses could be high (PLI_{global} of 1.7528 and QLI_{global} of 3.2084). As a result, the Multiobjective Index can also be high when the power losses play a main role in creating this general indicator. To verify these results, as usual, the time of the highest PV power will be the first concern. Firstly, PLI at this time is analyzed as in Table 6. 15.

Table 6. 15 Active power flows and losses in two cases: without and with PV of 24 MWp.

33rd minute of the period 12-1 pm (the time of the best conditions for PV)							
The case of no PV				The case of PV (24 MWp, bus 12, PF=1)			
$Line_{ij}$	P_{ij} (MW)	P_{ji} (MW)	P_{loss} (MW)	$Line_{ij}$	P_{ij} (MW)	P_{ji} (MW)	P_{loss} (MW)
1-2	3.1336	-3.1297	0.0038	1-2	-15.1027	15.1151	0.0124
2-3	3.1297	-3.1139	0.0159	2-3	-15.1151	15.1649	0.0499
3-4	3.1139	-3.0927	0.0212	3-4	-15.1649	15.2313	0.0663
4-5	0.5653	-0.5645	0.0008	4-5	1.0303	-1.0299	0.0004
5-6	0.2608	-0.2608	8E-06	5-6	0.4761	-0.4760	1E-05
5-7	0.3037	-0.3035	0.0002	5-7	0.5538	-0.5537	0.0001
7-8	0.3035	-0.3034	2E-05	7-8	0.5537	-0.5537	4E-05
4-9	2.5274	-2.5267	0.0007	4-9	-16.2616	16.2654	0.0038
9-10	2.5139	-2.5125	0.0014	9-10	-16.2892	16.2965	0.0074
10-11	2.4446	-2.442	0.0026	10-11	-16.4209	16.4358	0.015
11-12	2.2431	-2.1973	0.0458	11-12	-16.7997	17.1201	0.3204
12-13	1.0964	-1.0949	0.0015	12-13	2.0560	-2.0552	0.0008
13-14	0.2794	-0.2794	9E-06	13-14	0.5252	-0.5252	5E-06
13-15	0.8155	-0.8143	0.0011	13-15	1.5300	-1.5294	0.0006
15-16	0.7886	-0.7875	0.0011	15-16	1.4808	-1.4803	0.0006
16-17	0.4963	-0.4959	0.0005	16-17	0.9329	-0.9327	0.0002
17-18	0.0961	-0.0961	2E-05	17-18	0.1806	-0.1806	1E-05
12-19	1.1009	-1.1007	0.0001	12-19	2.0685	-2.0684	7E-05

19-20	0.0344	-0.0344	8E-08	19-20	0.0658	-0.0658	1E-07
19-21	1.0663	-1.0652	0.0011	19-21	2.0026	-2.0020	0.0006
21-22	0.0964	-0.0964	1E-06	21-22	0.1815	-0.1815	2E-06
21-23	0.9688	-0.9679	0.0009	21-23	1.8205	-1.8200	0.0005
23-24	0.5006	-0.5005	0.0001	23-24	0.9413	-0.9412	6E-05
23-25	0.4674	-0.467	0.0003	23-25	0.8787	-0.8786	0.0002
25-26	0.0084	-0.0084	7E-08	25-26	0.0160	-0.0160	3E-08
26-27	0.0032	-0.0032	1E-07	26-27	0.0062	-0.0062	5E-08
27-28	0.0032	-0.0032	1E-08	27-28	0.0062	-0.0062	2E-08
25-29	0.4586	-0.4583	0.0003	25-29	0.8626	-0.8624	0.0002
29-30	0.2819	-0.2818	9E-06	29-30	0.5302	-0.5302	5E-06
29-31	0.1764	-0.1763	5E-05	29-31	0.3322	-0.3322	3E-05
31-32	0.1521	-0.1521	6E-06	31-32	0.2864	-0.2864	1E-05
31-33	0.0243	-0.0243	1E-06	31-33	0.0457	-0.0457	5E-07
33-34	0.0243	-0.0243	8E-08	33-34	0.0457	-0.0457	1E-07
				35-12	21.2446	-21.2446	0
System active power loss (MW)			0.0506	System active power loss (MW)			0.4795

It is obvious that, with the highest PV generated power at this specific time, most of active power flows on the lines are increased leading to the increase of active power losses. Especially, according to the size and location of PV along with the suitable environment conditions, line 11-12 is subjected to a large amount of active power (17.1201 MW). In addition, the resistance of this line is quite high (0.1198 p.u.) in comparison with the other line resistances. Combining these conditions, the active power loss on this branch is the highest one (0.3204 MW) that is the main contribution to the system active power loss (0.4795 MW). It should be noted that, although the power flow on line 35-12 (the step-up transformer) reaches the highest value (21.2446 MW) when it is directly connected to the photovoltaic bus, its resistance is assumed to be “0” resulting the lossless active power transmission. In

conclusion, PLI at this time is extremely high (9.4756). However, there are many other time points when the PV unit is really useful in reducing the active power loss. Therefore, when the entire study period is concerned, PLI_{global} is reduced to 1.7528, but it is still higher than unity.

Secondly, QLI at the time of the best environment conditions in the case of 24 MWp PV size will be analyzed. The reactive power flows and losses are shown in Table 6. 16.

Table 6. 16 Reactive power flows and losses in two case: without and with PV of 24 MWp.

33rd minute of the period 12-1 pm (the time of the best conditions for PV)							
The case of no PV				The case of PV (24 MWp, bus 12, PF=1)			
$Line_{ij}$	Q_{ij} (MVAr)	Q_{ji} (MVAr)	Q_{loss} (MVAr)	$Line_{ij}$	Q_{ij} (MVAr)	Q_{ji} (MVAr)	Q_{loss} (MVAr)
1-2	3.1336	-3.1297	0.0038	1-2	4.6863	-4.6625	0.0238
2-3	3.1297	-3.1139	0.0159	2-3	4.6625	-4.5641	0.0984
3-4	3.1139	-3.0927	0.0212	3-4	4.5641	-4.4328	0.1313
4-5	0.5653	-0.5645	0.0008	4-5	0.5722	-0.5714	0.0008
5-6	0.2608	-0.2608	8E-06	5-6	0.2640	-0.2640	8E-06
5-7	0.3037	-0.3035	0.0002	5-7	0.3074	-0.3072	0.0002
7-8	0.3035	-0.3034	2E-05	7-8	0.3072	-0.3072	2E-05
4-9	2.5274	-2.5267	0.0007	4-9	3.8606	-3.8532	0.0074
9-10	2.5139	-2.5125	0.0014	9-10	3.8403	-3.8258	0.0145
10-11	2.4446	-2.442	0.0026	10-11	3.7569	-3.7273	0.0296
11-12	2.2431	-2.1973	0.0458	11-12	3.5255	-2.8925	0.6330
12-13	1.0964	-1.0949	0.0015	12-13	1.1434	-1.1419	0.0016
13-14	0.2794	-0.2794	9E-06	13-14	0.2914	-0.2914	9E-06
13-15	0.8155	-0.8143	0.0011	13-15	0.8505	-0.8493	0.0012
15-16	0.7886	-0.7875	0.0011	15-16	0.8224	-0.8213	0.0011
16-17	0.4963	-0.4959	0.0005	16-17	0.5176	-0.5172	0.0005

17-18	0.0961	-0.0961	2E-05	17-18	0.1002	-0.1002	2E-05
12-19	1.1009	-1.1007	0.0001	12-19	1.1481	-1.1479	0.0001
19-20	0.0344	-0.0344	8E-08	19-20	0.0359	-0.0359	8E-08
19-21	1.0663	-1.0652	0.0011	19-21	1.1121	-1.1109	0.0011
21-22	0.0964	-0.0964	1E-06	21-22	0.1005	-0.1005	1E-06
21-23	0.9688	-0.9679	0.0009	21-23	1.0104	-1.0095	0.0009
23-24	0.5006	-0.5005	0.0001	23-24	0.5221	-0.5220	0.0001
23-25	0.4674	-0.467	0.0003	23-25	0.4874	-0.4871	0.0003
25-26	0.0084	-0.0084	7E-08	25-26	0.0088	-0.0088	7E-08
26-27	0.0032	-0.0032	1E-07	26-27	0.0034	-0.0034	1E-07
27-28	0.0032	-0.0032	1E-08	27-28	0.0034	-0.0034	1E-08
25-29	0.4586	-0.4583	0.0003	25-29	0.4783	-0.4779	0.0003
29-30	0.2819	-0.2818	9E-06	29-30	0.2940	-0.2940	9E-06
29-31	0.1764	-0.1763	5E-05	29-31	0.1840	-0.1839	5E-05
31-32	0.1521	-0.1521	6E-06	31-32	0.1586	-0.1586	6E-06
31-33	0.0243	-0.0243	1E-06	31-33	0.0253	-0.0253	1E-06
33-34	0.0243	-0.0243	8E-08	33-34	0.0253	-0.0253	8E-08
				35-12	4.9E-14	0.6010	0.6010
System reactive power loss (MVAr)			0.0998	System reactive power loss (MVAr)			1.5475

Similarly, line 11-12 contributes a large amount of reactive power loss (0.6330 MVAr) into the system reactive power loss. This result can be explained by the very high active power flow on this line combining with the high value of line 11-12's reactance (X = 0.2367 p.u.). In this case, the reactive power loss in the step-up transformer is also significant (0.6010 MVAr) due to its considerable reactance (X = 0.15 p.u.) and the extremely large amount of PV power flowing through the transformer. It is noticed that, PV unit does not generate reactive power when PF = 1, so the reactive power loads are supplied by the slack bus. From the table, the reactive power flow on line 1-2 keeps the direction from bus 1 to bus 2. In

comparison with the case of no PV, this amount increases (4.6863 MVAr) to compensate the increased reactive power losses. As a result, the system reactive power loss in the case of PV (1.5475 MVAr) is much greater than the one in the base case (0.0998 MVAr) leading to extremely high value of QLI (15.5109). Combining with the other QLIs through the specified duration, the QLI_{global} becomes 3.2084. In conclusion, the high penetration of PV may cause the considerable increase of the system losses.

Finally, VDI_{global} of 0.2064 will be verified by firstly considering the time of the smallest VDI (the 47^{th} minute of the period 11-12 am). By using Load Flow calculation, the bus voltage magnitudes are represented as in Table 6. 17.

Table 6. 17 Bus voltage magnitudes between 2 cases: without PV and with PV of 24 MWp.

47^{th} minute of the period 11-12 am (the time of the smallest VDI)			
The case of no PV		The case of PV (24 MWp, bus 12, PF=1)	
Bus	Voltage magnitude (p.u.)	Bus	Voltage magnitude (p.u.)
1	1.0455	1	1.0455
2	1.0449	2	1.0454
3	1.0423	3	1.0450
4	1.0388	4	1.0444
5	1.0385	5	1.0441
6	1.0385	6	1.0441
7	1.0382	7	1.0438
8	1.0381	8	1.0437
9	1.0387	9	1.0444
10	1.0384	10	1.0444
11	1.0378	11	1.0444
12	1.0258	12	1.0445
13	1.0251	13	1.0438
14	1.0251	14	1.0438

15	1.0244	15	1.0431
16	1.0237	16	1.0424
17	1.0232	17	1.0419
18	1.0231	18	1.0418
19	1.0257	19	1.0444
20	1.0257	20	1.0444
21	1.0250	21	1.0437
22	1.0250	22	1.0437
23	1.0243	23	1.0430
24	1.0241	24	1.0428
25	1.0239	25	1.0426
26	1.0239	26	1.0425
27	1.0238	27	1.0425
28	1.0238	28	1.0425
29	1.0235	29	1.0422
30	1.0235	30	1.0421
31	1.0233	31	1.0420
32	1.0233	32	1.0420
33	1.0233	33	1.0420
34	1.0233	34	1.0420
		35	1.0444

It can be seen from the table that, although the PV size is quite high (24 MWp), the bus voltage magnitudes at this specific time are not exceeded too much (around 1.04 p.u.). This issue can be explained as follows. In fact, the capacity of 24 MW is the maximum power that PV system can generate under the most suitable conditions of solar and temperature. It does not mean that PV unit will supply 24 MW to the grid any time. In this case-study, the time of the smallest voltage deviation is considered; and at this time point, the PV power is only approximately

11 MW. Therefore, it is reasonable to get the results of voltage magnitudes as in the above table. These results are also verified by using DigSilent software as in Figure 6. 16. At the time of the highest PV power (21.2 MW), the voltage at bus 12, for example, reaches the exceeded value of 1.08 p.u. as expected.

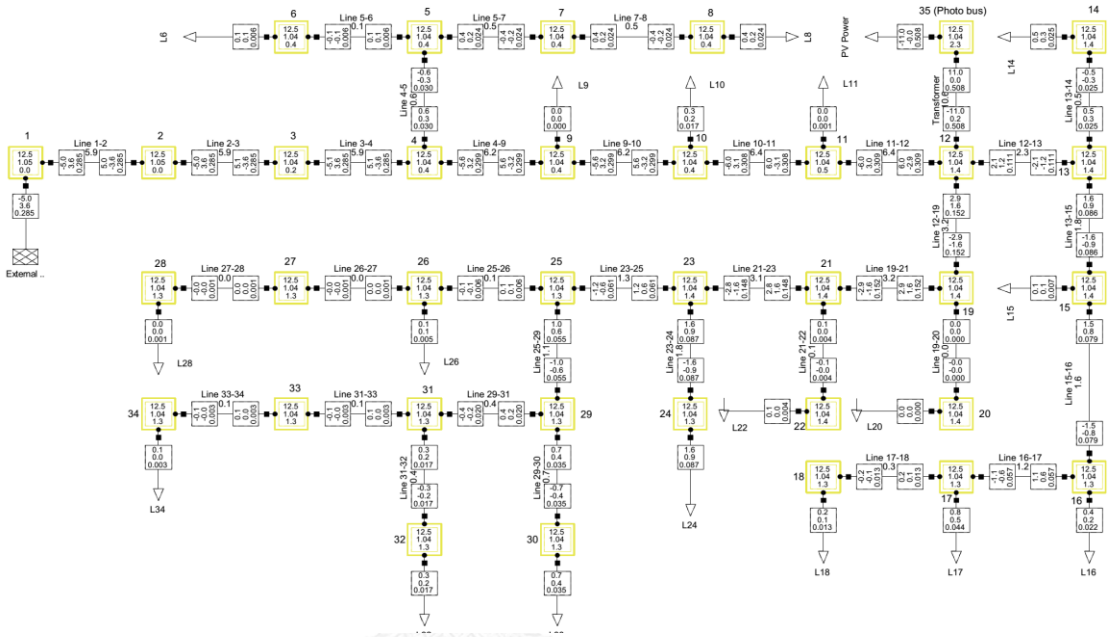

Figure 6. 16 Simulation results by using DigSilent software.

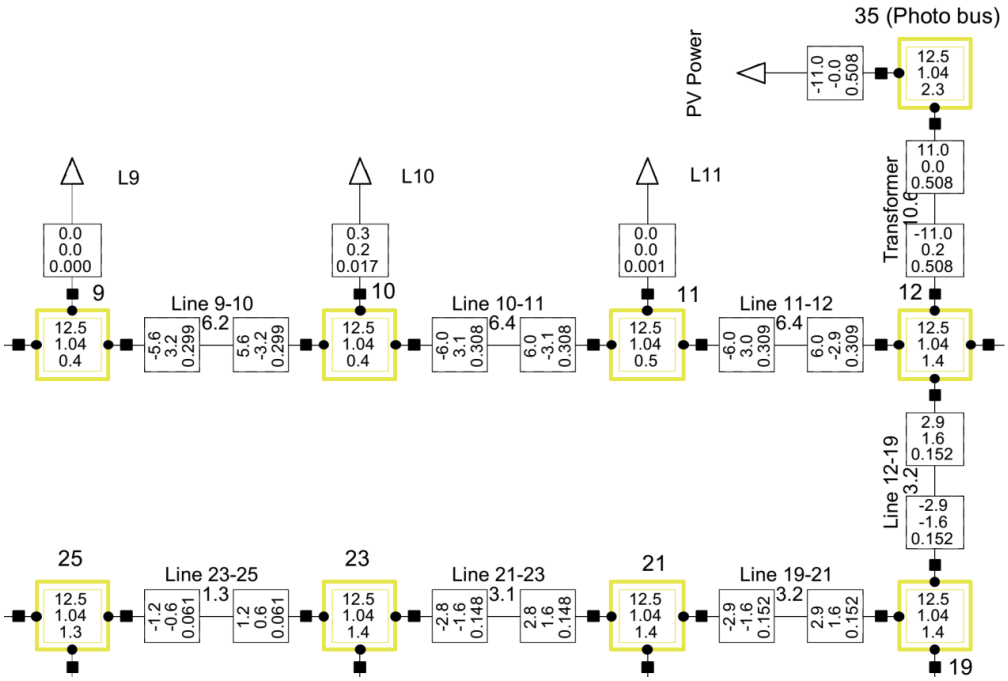

Figure 6. 17 Zoom imagine in a few specific buses.

At this particular time, by the impact of PV, the voltage magnitudes at all buses are almost equal: the maximum voltage magnitude is 1.0455 (at slack bus) while the minimum value is 1.0418 (at bus 18). As a result, the voltage deviation is very small. On the other hand, referring to the case of no PV at the same time, the voltage fluctuation is quite considerable: the maximum voltage magnitude is still 1.0455 (at slack bus) but the minimum value is 1.0231 (at bus 18). When the VDI of the power system integrated PV is defined as the ratio between the system voltage deviation in the case of PV and the one in the base case (no PV), this index becomes very small (0.0250) at this particular time. According to the research, there are 409/660 time points having the VDI smaller than 0.2. Therefore, even the VDI at the time of the best environment conditions can be high (1.0553) because of exceeded power flows, the VDI_{global} may reach the small value of 0.2064.

When all of component indices are clarified, it is convenient to get MOI_{global} of 1.7301 by using the weighting factors as previous discussion. This general index shows that, with the PV size of 24 MWp, the utility grid does not gain the benefit in reducing the system power losses and voltage deviation.

6.3.4 Proper Location, Size and PF Control Mode of PV Generator based on PQVSI and MOI

As the previous sections, it is proved that, Multiobjective Index is reliable in representing the PV impact on system power losses and voltage deviation. Now, this indicator will be combined with PQ Voltage Stability Index to determine the most suitable PV size and location. Similar to section 6.2.4, several locations are interested such as bus 2, bus 5, bus 12, bus 13 and bus 27. In addition, the PV size is constantly increased up to 24 MWp with the 1 MWp step size. The PV unit is operated in the unity power factor control mode. Figure 6. 18 shows the remarkable points to depict the impact of PV penetration on the system voltage stability as well as system power losses and voltage deviation.

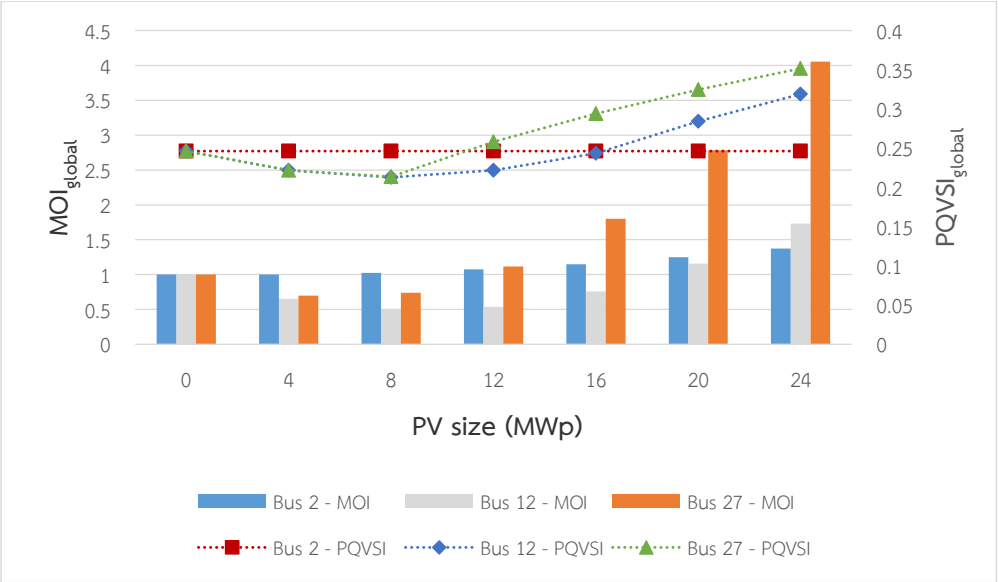

Figure 6. 18 Effects of PV penetration on system voltage stability, system power losses and voltage deviation.

At the locations near the slack bus (bus 2, for example), the increase of PV sizes does not have noticeable impact on the system power losses and voltage deviation. The only reason that can cause more system losses is the exceeded power flows on branches 1-2 and 35-2. At bus 12, the results were completely analyzed. The same trend can be observed for bus 27. According to the global Multiobjective Index, the most suitable PV location is bus 12 with the corresponding PV size of 8 MWp. In this case, the MOI_{global} of the power network integrated PV will be minimized and the utility grid will gain the maximum benefit in reducing power losses and voltage fluctuation. Fortunately, this choice is the same answer when considering only PQ Voltage Stability Index. In conclusion, a PV unit of 8 MWp connected at bus 12 will be the most appropriate PV system not only for enhancing network voltage stability bus also for minimizing system power losses and voltage deviation.

From this basic case, the PV power factor can be adjusted to specify the most proper PF control mode based on both PQVSI and MOI. The results are illustrated as in the Figure 6. 19.

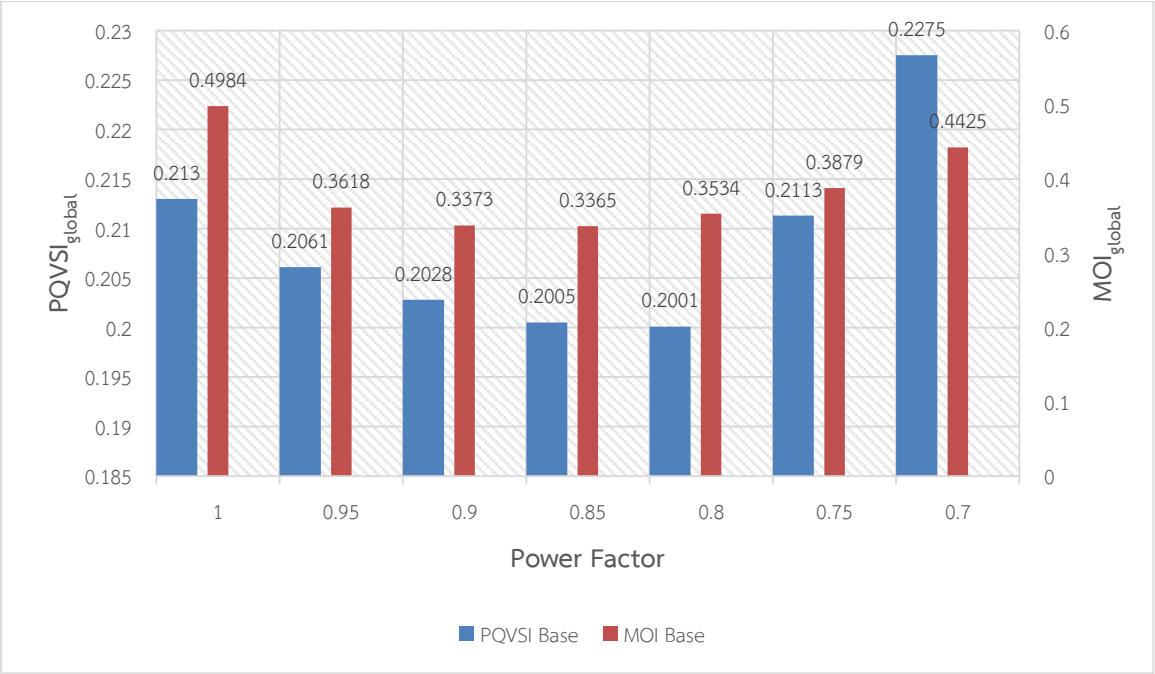

Figure 6. 19 Effect of various power factor operations of PV on voltage stability and system power losses and voltage deviation.

It can be seen that, with the PF of 0.95, the PV farm supplies not only active power but also reactive power to the utility grid. Consequently, the reactive power flows on the lines to the left of the PV unit may be decreased due to the PV reactive power assistance. As a result, the power losses and voltage deviation of these branches are reduced leading to the reduction of MOI_{global}. However, when the PF is small enough (0.7, for example), at some particular times, the PV reactive power can be over causing a large amount of exceeded reactive power back to slack bus. Then, the reactive power flows on the left-side branches not only be changed the direction but also be increased resulting the increase of the power losses and voltage fluctuation of these lines. By this reason, the MOIs at these specific times can be quite high. Combining with the other time points, the MOI_{global} can reaches the high value of 0.4425.

From the Figure 6. 19, the most suitable PV power factor control mode will be considered between two choices: PF of 0.85 and PF of 0.8. If the system voltage stability is more concerned, the PV unit should be operated under the PF of 0.8; and vice versa, PF of 0.85 is the better choice when the system operators give the priority to the reduction of power losses and voltage deviation. However, the differences

between the indices in these two cases are quite small, so both of them are satisfied the requirements.

According to section 6.2.5, the PV producers are allowed to increase the PV size from 8 MWp to 9 MWp to gain more benefit in selling PV power. Concurrently, they have to reduce the PF from unity to 0.8 to maintain the initial system voltage stability. Table 6. 18 illustrates that, this modification also brings the interest to the utility grid in reducing system power losses and voltage deviation representing by the reduction of MOI_{global}.

Table 6. 18 Adjustment of PV installation based on PQVSI and MOI.

	Original plan	Adjusted plan
Location of PV	Bus 12	Bus 12
Size of PV (MWp)	8	9
Operated power factor	1.0	0.8
Size of inverter (MVA)	8	11.25
Global PQVSI	0.2130	0.2136
MOI_{global}	0.4984	0.3789

6.4 Study of Scattered PV Installation

So far, the impacts of PV penetration on static voltage stability, power losses and voltage deviation in distribution systems have been studied with various PV sizes, locations as well as control modes. However, the research only mentions the centralized PV system. In other words, the PV system is installed at a single location as a small power producer (SPP) to support substation, feeder or peak power demands. Central PV generators are normally ground-mounted installations; therefore they may require the additional costs related to land preparation, land costs, foundations, permitting, and mounting structure. In distribution network areas, finding a wide land without shading to install a large-scale PV farm becomes a challenging issue. If PV farm is constructed in remote sites with land availability and lower land costs, access to distribution systems can be very costly. In addition, investment cost of this concentrated PV power plant can be considerable leading to

lack of investors, if utilities want to share the power market with other producers. To maintain the technical requirements such as satisfying load demands, enhancing voltage stability and minimizing power losses, while concerning the economic problems, centralized PV farm may be divided into several smaller PV generators and distributed along the main feeder of distribution networks. Of course, although central PV generation has some disadvantages, scattered PV installation is still not the optimal choice due to the limitations in shading issue, interconnection problem and other charge types. It is necessary to make the economic and technical analysis to specify the better solution.

In reality, scattered PV installation can be implemented by integrating PV arrays on rooftops of residential and commercial buildings. Sizes of residential PV systems are normally between 1 to 4 kW. System components include: PV modules, DC-AC converter system, storage system, mounting structure and wiring. Meanwhile, commercial PV systems typically range from 2 to over 1000kW in size; and PV arrays can replace curtain wall systems or be integrated in awnings, skylights or flat roofs of buildings. However, according to the scope of this research, distributed PV penetration will be considered as two or three very small power producers (VSPP) along the main feeder of the test distribution power system. The simulation will be conducted to verify the technical results as follows.

6.4.1 Scattered PV Installation as Two PV Systems

6.4.1.1 Proper Locations and Sizes

First of all, two PV generators will be installed at different buses of TahSai distribution system as in Figure 6. 20, for example. It is assumed that, the PV units are connected at the buses belonging to the main feeder to support the whole system. In this research, three locations are interested including: bus 2 (the location near slack bus), bus 12 (the middle position of the main feeder) and bus 27 (the end position of the main feeder). The other buses can be referred to one of three buses above. For instance, if PV unit is installed at bus 3 or bus 4, it may cause the same effects as the case of PV installation at bus 2. This conclusion has been verified by simulation results. In addition, it is supposed that the total PV capacity should not be

over 8 MWp for 1-feeder distribution system. For simplicity, the size of each PV unit will be limited up to 4 MWp. Then, each PV capacity is independently increased from 1 MWp to 4 MWp with the step size of 1 MWp. The sunlight and temperature conditions are assumed to be constant at any location of the distribution system area, since this site is not quite large. In this case-study, both PV units are operated under unity PF control mode. The simulation results are illustrated as in Table 6. 19 and Figure 6. 21.

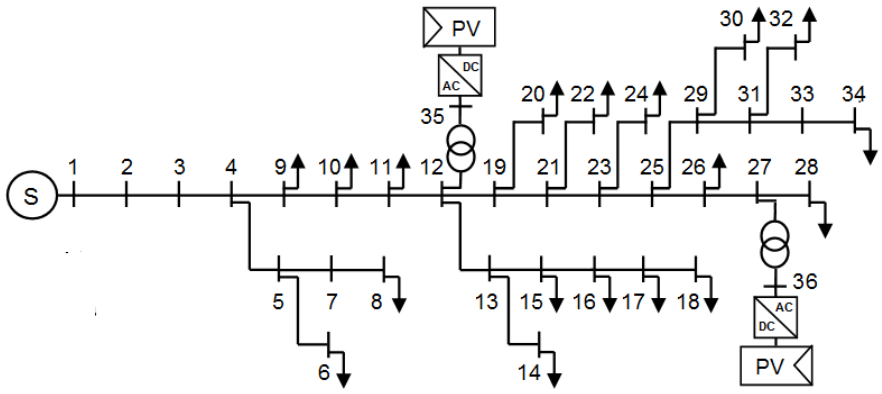

Figure 6. 20 Single diagram of TahSai distribution power network with 2 PV units.

Table 6. 19 System indices considering various (scattered) PV sizes and locations.

Location / PV Size (MWp)		Buses 2 & 12		Buses 12 & 27		Buses 2 & 27	
PV1	PV2	$PQVSI_{global}$	MOI_{global}	$PQVSI_{global}$	MOI_{global}	$PQVSI_{global}$	MOI_{global}
1	1	0.2382	0.8920	0.2307	0.7956	0.2382	0.8884
	2	0.2308	0.7989	0.2242	0.7198	0.2308	0.8019
	3	0.2243	0.7183	0.2220	0.6663	0.2243	0.7378
	4	0.2220	0.6500	0.2198	0.6346	0.2220	0.6957
2	1	0.2382	0.8915	0.2243	0.7133	0.2382	0.8880
	2	0.2308	0.7987	0.2220	0.6484	0.2308	0.8017
	3	0.2243	0.7183	0.2198	0.6055	0.2243	0.7379
	4	0.2220	0.6503	0.2175	0.5845	0.2220	0.6960

3	1	0.2382	0.8926	0.2220	0.6433	0.2382	0.8890
	2	0.2308	0.8000	0.2198	0.5892	0.2308	0.8031
	3	0.2243	0.7199	0.2175	0.5570	0.2242	0.7395
	4	0.2220	0.6522	0.2152	0.5464	0.2220	0.6979
4	1	0.2382	0.8952	0.2198	0.5856	0.2382	0.8916
	2	0.2307	0.8029	0.2175	0.5421	0.2308	0.8059
	3	0.2243	0.7231	0.2152	0.5205	0.2242	0.7426
	4	0.2220	0.6556	0.2130	0.5204	0.2220	0.7013

Summarization

Location / Total Size	Buses 2 & 12		Buses 12 & 27		Buses 2 & 27	
	$PQVSI_{global}$	MOI_{global}	$PQVSI_{global}$	MOI_{global}	$PQVSI_{global}$	MOI_{global}
2 MWp	0.2382 (1-1)*	0.8920 (1-1)	0.2307 (1-1)	0.7956 (1-1)	0.2382 (1-1)	0.8884 (1-1)
3 MWp	0.2308 (1-2)	0.7989 (1-2)	0.2243 (2-1)	0.7133 (2-1)	0.2308 (1-2)	0.8019 (1-2)
4 MWp	0.2243 (1-3)	0.7183 (1-3)	0.2220 (3-1)	0.6433 (3-1)	0.2243 (1-3)	0.7378 (1-3)
5 MWp	0.2220 (1-4)	0.6500 (1-4)	0.2198 (4-1)	0.5856 (4-1)	0.2220 (1-4)	0.6957 (1-4)
6 MWp	0.2220 (2-4)	0.6503 (2-4)	0.2175 (4-2)	0.5421 (4-2)	0.2220 (2-4)	0.6960 (2-4)
7 MWp	0.2220 (3-4)	0.6522 (3-4)	0.2152 (4-3)	0.5205 (4-3)	0.2220 (3-4)	0.6979 (3-4)
8 MWp	0.2220 (4-4)	0.6556 (4-4)	**0.2130 (4-4)**	**0.5204 (4-4)**	0.2220 (4-4)	0.7013 (4-4)

* (n-m) means the sizes of the first PV unit and the second PV unit are n and m (MWp), respectively.

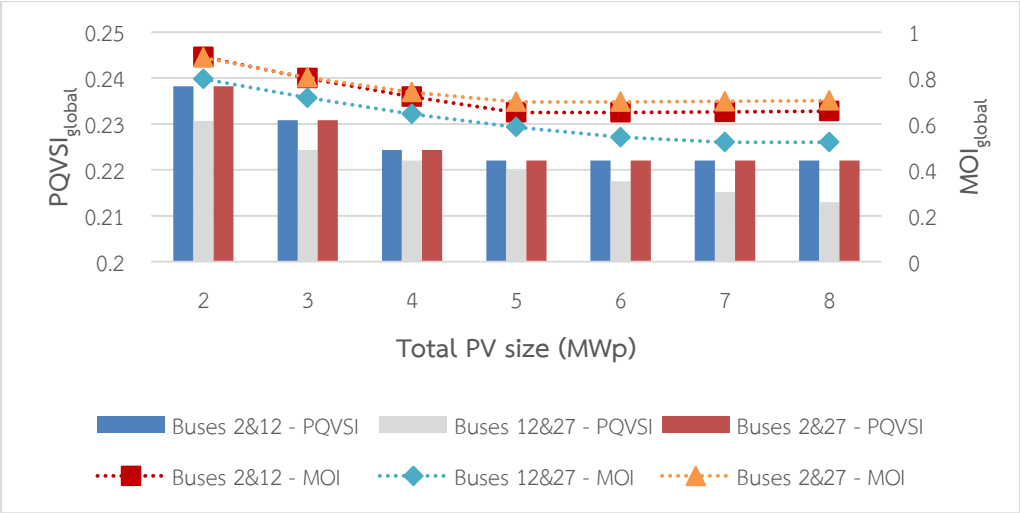

Figure 6. 21 Impacts of 2 PV units on system indices.

Based on the minimum values of $PQVSI_{global}$ and MOI_{global}, the most appropriate size of each PV unit should be 4 MWp resulting the total PV size of 8 MWp; and the corresponding locations are bus 12 and bus 27. With this choice, the $PQVSI_{global}$ reduces from 0.2464 to 0.2130, while MOI_{global} decreases from 1.0000 to 0.5204, in comparison with the case of no PV. Comparing to the base case of centralized PV installation as in section 6.3.4 (PV size of 8 MWp at bus 12 under unity PF control mode), the system voltage stability is maintained while there is a slight increase in system losses and voltage deviation. However, the system indices do not change significantly between these cases. It means that, both of these cases satisfy the same technical requirements. Hence, an economic analysis should be conducted to verify the better project. If the availability of construction sites is the first concern, the scattered PV installation seems to have more advantages, when it is quite difficult to find a large area to construct an 8 MWp central PV farm in distribution sites. The results are summarized in Table 6. 20.

Table 6. 20 Comparison between 3 scenarios (1).

Case 1: no PV		Case 2: central PV farm of 8 MWp at bus 12 under unity PF control mode		Case 3: 2 PV farms of 4 MWp each at buses 12 and 27 under unity PF control mode	
$PQVSI_{global}$	MOI_{global}	$PQVSI_{global}$	MOI_{global}	$PQVSI_{global}$	MOI_{global}
0.2464	1.0000	0.2130	0.4984	0.2130	0.5204

6.4.1.2 Adjusting PF of PV Units

Now, the power factor of each PV unit will be adjusted independently to specify the most suitable PV operating condition. The results are clearly shown in Table 6. 21.

Table 6. 21 PV power factor modification.

2 PV units of 4 MWp each at buses 12 & 27 (same environmental conditions)			
PF of PV unit at bus 12	PF of PV unit at bus 27	$PQVSI_{global}$	MOI_{global}
1.00	1.00	0.2130	0.5204
	0.95	0.2095	0.4511
	0.90	0.2079	0.4359
	0.85	0.2064	0.4317
	0.80	0.2051	0.4354
	0.75	0.2037	0.4469
	0.70	0.2065	0.4671
0.95	1.00	0.2095	0.4376
	0.95	0.2060	0.3923
	0.90	0.2044	0.3882
	0.85	0.2030	0.3936
	0.80	0.2016	0.4064
	0.75	0.2005	0.4270
	0.70	0.2058	0.4566
0.90	1.00	0.2079	0.4086
	0.95	0.2044	0.3745
	0.90	0.2028	0.3756
	0.85	0.2014	0.3855
	0.80	0.2005	0.4025
	0.75	0.2003	0.4274
	0.70	0.2054	0.4614

0.85	1.00	0.2064	0.3886
	0.95	0.2030	0.3642
	0.90	0.2014	0.3699
	0.85	0.2005	0.3835
	0.80	0.2003	0.4043
	0.75	0.2001	0.4328
	0.70	0.2051	0.4706
0.80	1.00	0.2051	0.3740
	0.95	0.2016	0.3589
	0.90	0.2005	0.3688
	0.85	0.2003	0.3861
	0.80	0.2001	0.4104
	0.75	0.2028	0.4424
	0.70	0.2111	0.4839
0.75	1.00	0.2037	0.3638
	0.95	0.2005	0.3579
	0.90	0.2003	0.3721
	0.85	0.2001	0.3932
	0.80	0.2030	0.4209
	0.75	0.2109	0.4565
	0.70	0.2191	0.5016
0.70	1.00	0.2022	0.3579
	0.95	0.2003	0.3617
	0.90	0.2001	0.3804
	0.85	0.2036	0.4053
	0.80	0.2115	0.4367
	0.75	0.2193	0.4759
	0.70	0.2272	0.5249

3 optimal choices			
0.75	0.95	0.2005	0.3579
0.70	0.95	0.2003	0.3617
0.70	0.90	0.2001	0.3804

From the simulation results, three optimal choices are selected based on the minimum values of $PQVSI_{global}$ and MOI_{global}. Among these operating modes, the $PQVSIs_{global}$ are similar representing the same system voltage stability degree. Meanwhile, in the case that the PV units at bus 12 and bus 27 are operated under 0.75 PF and 0.95 PF, respectively, system losses and voltage deviation are minimized. Therefore, this case should be chosen as the most appropriate operating condition of distributed PV generators. Table 6. 22 makes the comparison between: the case of no PV, the case of central PV system and the case of distributed PV system. It can be seen that, the appearance of PV in distribution networks brings the significant benefits in enhancing voltage stability and, especially, in reducing system losses and voltage deviation. However, distributed PV installation seems to have the same technical impacts as central PV system in this case-study. The advantages of scattered PV system may come from economic issues.

Table 6. 22 Comparison between 3 scenarios (2).

Case 1: no PV		Case 2: central PV farm of 8 MWp at bus 12 under optimal PF control mode (PF of 0.8)		Case 3: 2 PV farms of 4 MWp each at buses 12 and 27 under optimal PF control modes	
$PQVSI_{global}$	MOI_{global}	$PQVSI_{global}$	MOI_{global}	$PQVSI_{global}$	MOI_{global}
0.2464	1.0000	0.2001	0.3534	0.2005	0.3579

6.4.1.3 Adjusting Terminal Voltages of PV Units in Case of Constant Voltage Mode

From the base case (2 PV units of 4 MWp each at buses 12 & 27 under unity PF control mode), the PV operating mode is changed to the constant terminal voltage scheme. Hence, the terminal voltage magnitude of each PV generator will be

independently adjusted within the range from 0.95 p.u to 1.05 p.u. with the step of 0.01 p.u.. The results are shown in Table 6. 23.

Table 6. 23 Terminal voltage magnitude modification.

2 PV units of 4 MWp each at buses 12 & 27 (same environmental conditions)			
Voltage magnitude at bus 35 (p.u.) (PV at bus 12)	Voltage magnitude at bus 36 (p.u.) (PV at bus 27)	$PQVSI_{global}$	MOI_{global}
1.05	1.05	0.1482	0.3725
	1.04	0.1668	0.4523
	1.03	0.1858	0.8489
	1.02	0.2031	1.5618
	1.01	0.2189	2.5905
	1.00	0.2337	3.9344
	0.99	0.2835	5.5930
	0.98	0.3093	7.5658
	0.97	0.3330	9.8522
	0.96	0.3578	12.4517
	0.95	0.3792	15.3637
1.04	1.05	0.1669	0.4591
	1.04	0.1662	0.3545
	1.03	0.1728	0.5669
	1.02	0.1803	1.0955
	1.01	0.1883	1.9401
	1.00	0.1985	3.0999
	0.99	0.2149	4.5746
	0.98	0.2923	6.3634
	0.97	0.3175	8.4660
	0.96	0.3408	10.8817
	0.95	0.3652	13.6099

1.03	1.05	0.1911	1.0350
	1.04	0.1900	0.7461
	1.03	0.1982	0.7742
	1.02	0.2067	1.1187
	1.01	0.2154	1.7791
	1.00	0.2241	2.7549
	0.99	0.2334	4.0456
	0.98	0.2430	5.6505
	0.97	0.3009	7.5693
	0.96	0.3256	9.8012
	0.95	0.3485	12.3457
1.02	1.05	0.2150	2.1000
	1.04	0.2175	1.6267
	1.03	0.2260	1.4705
	1.02	0.2359	1.6308
	1.01	0.2455	2.1071
	1.00	0.2547	2.8989
	0.99	0.2636	4.0056
	0.98	0.2721	5.4267
	0.97	0.2804	7.1617
	0.96	0.3094	9.2098
	0.95	0.3336	11.5707
1.01	1.05	0.2386	3.6537
	1.04	0.2475	2.9960
	1.03	0.2568	2.6555
	1.02	0.2657	2.6316
	1.01	0.2743	2.9238
	1.00	0.2825	3.5316

	0.99	0.2905	4.4544
	0.98	0.2983	5.6917
	0.97	0.3058	7.2428
	0.96	0.3131	9.1073
	0.95	0.3202	11.2845
1.00	1.05	0.2674	5.6956
	1.04	0.2760	4.8536
	1.03	0.2843	4.3288
	1.02	0.2924	4.1208
	1.01	0.3002	4.2289
	1.00	0.3077	4.6526
	0.99	0.3151	5.3915
	0.98	0.3222	6.4449
	0.97	0.3292	7.8123
	0.96	0.3360	9.4931
	0.95	0.3426	11.4867
0.99	1.05	0.2939	8.2255
	1.04	0.3017	7.1991
	1.03	0.3093	6.4900
	1.02	0.3167	6.0978
	1.01	0.3239	6.0218
	1.00	0.3309	6.2616
	0.99	0.3377	6.8165
	0.98	0.3444	7.6861
	0.97	0.3509	8.8698
	0.96	0.3572	10.3669
	0.95	0.3635	12.1769
	1.05	0.3180	11.2428

0.98	1.04	0.3252	10.0320
	1.03	0.3323	9.1386
	1.02	0.3392	8.5622
	1.01	0.3459	8.3022
	1.00	0.3524	8.3579
	0.99	0.3588	8.7290
	0.98	0.3651	9.4148
	0.97	0.3712	10.4147
	0.96	0.3772	11.7282
	0.95	0.3831	13.3547
0.97	1.05	0.3403	14.7471
	1.04	0.3471	13.3520
	1.03	0.3537	12.2743
	1.02	0.3601	11.5137
	1.01	0.3665	11.0696
	1.00	0.3726	10.9414
	0.99	0.3787	11.1286
	0.98	0.3846	11.6306
	0.97	0.3904	12.4468
	0.96	0.3961	13.5767
	0.95	0.4017	15.0196
0.96	1.05	0.3612	18.7381
	1.04	0.3675	17.1585
	1.03	0.3738	15.8966
	1.02	0.3798	14.9518
	1.01	0.3858	14.3235
	1	0.3917	14.0114
	0.99	0.3974	14.0147

	0.98	0.4030	14.3329
	0.97	0.4086	14.9655
	0.96	0.4140	15.9118
	0.95	0.4193	17.1712
0.95	1.05	0.3810	23.2152
	1.04	0.3868	21.4512
	1.03	0.3927	20.0049
	1.02	0.3985	18.8759
	1.01	0.4042	18.0636
	1	0.4097	17.5675
	0.99	0.4152	17.3869
	0.98	0.4206	17.5214
	0.97	0.4259	17.9703
	0.96	0.4311	18.7330
	0.95	0.4362	19.8090
Two optimal choices			
1.05	1.05	0.1482	0.3725
1.04	1.04	0.1662	0.3545

As usual, two optimal choices are determined based on the minimum values of system indices. If the system voltage stability is the first consideration, both PV units should be operated under the terminal voltage magnitude of 1.05 p.u.. Vice versa, the terminal voltage magnitude of 1.04 p.u. can be a proper choice for all PV farms when the priority is given to reducing system losses and voltage deviation. Figure 6. 22 depicts the system voltage profile in the case of 1.04 p.u. terminal voltage magnitude. It can be seen that, at each time point, the voltage fluctuation is decreased significantly represented by the small gap between the maximum and minimum values of bus voltage magnitude. Table 6. 24 also represents the comparison between three cases: no PV, central PV farm of 8 MWp at bus 12 under

proper voltage control mode, and two PV units of 4 MWp each at buses 12 & 27 under proper voltage control mode.

Table 6. 24 Comparison between 3 scenarios (3).

Case 1: no PV		Case 2: central PV farm of 8 MWp at bus 12 under optimal voltage control mode (1.04 p.u.)		Case 3: 2 PV farms of 4 MWp each at buses 12 and 27 under proper voltage control modes (1.04 p.u.)	
$PQVSI_{global}$	MOI_{global}	$PQVSI_{global}$	MOI_{global}	$PQVSI_{global}$	MOI_{global}
0.2464	1.0000	0.1696	0.3336	0.1662	0.3545

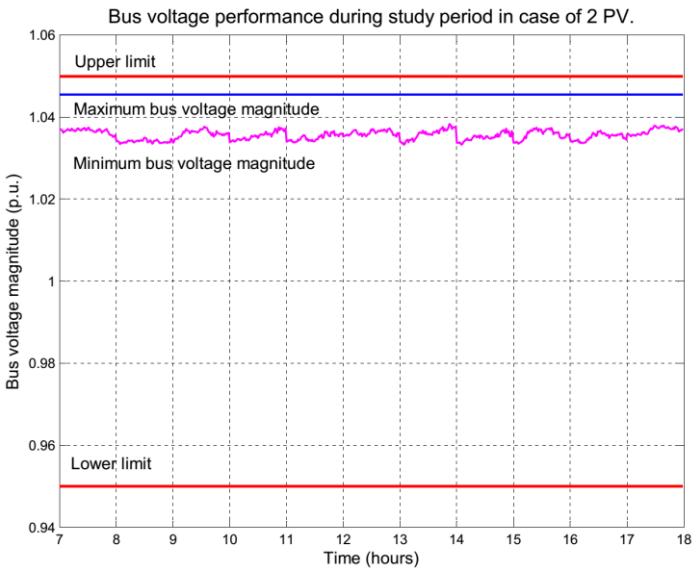

Figure 6. 22 System voltage profile in the case of 1.04 p.u. terminal voltage magnitude for each PV unit.

6.4.2 Scattered PV Installation as Three PV Systems

In this case study, three PV units will be installed at bus 2, bus 12 and bus 27, respectively. The size of each PV generator is independently adjusted from 1 MWp to 3 MWp with the size step of 1 MWp, causing the total PV capacity is limited to 9 MWp. In the base case, all PV units are operated under unity PF control mode. The results are illustrated in Table 6. 25.

Table 6. 25 System indices considering various PV sizes (scattered – 3 units).

3 PV units at buses 2, 12 & 27 under the same environmental conditions, PF = 1				
Size of PV unit at bus 2 (MWp)	Size of PV unit at bus 12 (MWp)	Size of PV unit at bus 27 (MWp)	$PQVSI_{global}$	MOI_{global}
1	1	1	0.2307	0.7939
		2	0.2242	0.7183
		3	0.2220	0.6650
	2	1	0.2243	0.7118
		2	0.2220	0.6472
		3	0.2198	0.6046
	3	1	0.2220	0.6421
		2	0.2198	0.5882
		3	0.2175	0.5563
2	1	1	0.2307	0.7937
		2	0.2242	0.7184
		3	0.2220	0.6654
	2	1	0.2243	0.7119
		2	0.2220	0.6475
		3	0.2198	0.6052
	3	1	0.2220	0.6424
		2	0.2198	0.5888
		3	0.2175	0.5572
3	1	1	0.2307	0.7950
		2	0.2242	0.7200
		3	0.2220	0.6673
	2	1	0.2243	0.7135
		2	0.2220	0.6494

		3	0.2198	0.6073
	3	1	0.2220	0.6443
		2	0.2198	0.5910
		3	0.2175	0.5596
Optimal choice				
1	3	3	0.2175	0.5563

Similarly, from this base case, the power factors of PV units are independently modified to identify the proper PF control mode for each PV farm. By using the same method, the results are shown in Table 6. 26, in comparison with the other related cases.

Table 6. 26 Comparison between 4 scenarios (1).

Case 1: no PV		Case 2: central PV farm of 8 MWp at bus 12 under optimal PF control mode (PF of 0.8)		Case 3: 2 PV farms of 4 MWp each at buses 12 and 27 under optimal PF control modes		Case 4: 3 PV farms at buses: 2 (1 MWp), 12 (3MWp) and 27 (3 MWp) under optimal PF control modes PF1 = 0.95; PF2 = 0.7; PF3 = 0.95	
$PQVSI_{global}$	MOI_{global}	$PQVSI_{global}$	MOI_{global}	$PQVSI_{global}$	MOI_{global}	$PQVSI_{global}$	MOI_{global}
0.2464	1.0000	0.2001	0.3534	0.2005	0.3579	0.2073	0.3771

If the constant voltage control mode is applied, the terminal voltage magnitude of each PV unit will be adjusted within the range from 1.05 p.u. to 0.95 p.u. as previous studies. Table 6. 27 represents the corresponding results.

In conclusion, in this case-study of 3 distributed PV units, both scattered and central PV systems bring significant technical benefits to utility grids in enhancing system stability and reducing power losses and voltage deviation. However, in comparison with the case of central PV systems, scattered PV systems have no dominance. Hence, choosing central or distributed PV generation depends on the economic advantages. One of the considerable interests when installing scattered PV

system is small areas required for PV farms. In distribution power system site, this is particularly important since the land availability is quite restricted.

Table 6. 27 Comparison between 4 scenarios (2).

Case 1: no PV		Case 2: central PV farm of 8 MWp at bus 12 under optimal voltage control mode (1.04 p.u.)		Case 3: 2 PV farms of 4 MWp each at buses 12 and 27 under proper PF control modes (1.04 p.u.)		Case 4: 3 PV farms at buses: 2 (1 MWp), 12 (3MWp) and 27 (3 MWp) under optimal voltage control modes V1 = 1.05; V2 = 1.04; V3 = 1.04	
$PQVSI_{global}$	MOI_{global}	$PQVSI_{global}$	MOI_{global}	$PQVSI_{global}$	MOI_{global}	$PQVSI_{global}$	MOI_{global}
0.2464	1.0000	0.1696	0.3336	0.1662	0.3545	0.1719	0.4353

CHAPTER VII

Conclusions and Future Works

7.1 Conclusions

Static voltage stability assessment has been conducted in a real distribution power network integrated photovoltaic generations in order to verify the PV impacts on system voltage stability. In addition, the effects of PV units on system power losses and voltage deviation are also studied to fulfill the research. Some conclusions are drawn as follows:

1. A completed PV module model has been established, which describes the true electrical behaviors of PV generators. By using this model, the researches related to PV generations can be implemented favorably.
2. A suitable method to assess system static voltage stability is specified, which is named PQ Voltage Stability Index (PQVSI). This approach brings many advantages: the fast and accurate voltage assessment, the small amount of calculation time required, the simple computation process based on AC Load Flow program. In accordance with time-series Power Flow analysis, the global PQVSI can be defined to present the degree of system voltage stability considering a study period.
3. To satisfy other technical and economic requirements, the supplementary criteria including system power losses and voltage deviation are added into the research. These issues are reflected by Multiobjective Index (MOI) as a combination of active power loss index (PLI), reactive power loss index (QLI) and voltage deviation index (VDI). Along with the global PQVSI, the global MOI is also defined through the study duration.
4. From the test results, it can be seen that: PV generations contribute the considerable impacts to system voltage stability, system power losses and voltage deviation. Specifically, with the proper PV location, size and control

mode, the utilities gain the benefits not only in enhancing system stability but also in minimizing power losses and voltage deviation.

5. By varying PV locations and sizes as well as modifying PV control modes, along with the observation of the global PQVSI and MOI in each phenomenon, the appropriate PV system can be identified.
6. The study also demonstrates the benefits of operating the PV generation system at the power factor less than unity. By setting the PV power factor at non-unity values along with increasing the PV size, the system stability is maintained as before. However, with this modification, the utilities may receive the additional supports from PV producers, while PV owners can earn more profit in selling the PV power.
7. Scattered PV penetration is taken into account by installing 2 or 3 small PV units along the main feeder of TahSai distribution network. The most suitable PV installation is determined based on the global PQVSI and MOI as the above methodology. It is verified that, both centralized and scattered PV generation bring considerable interests to utilities and PV producers in enhancing system stability and minimizing power losses as well as voltage deviation. However, in comparison with concentrated PV systems, scattered PV systems seem to have no dominance in the limitations of this research. Hence, choosing centralized or distributed PV generation depends on the other advantages. For example, one of the benefits when installing scattered PV system is the small area required for each PV unit.

7.2 Future Works

The impacts of PV penetration on distribution power systems have been investigated at some points. In the future, it is necessary to continue this research in the following issues:

1. The other criteria such as thermal limits and system frequency stability should be considered in the process of PV design and installation.

2. This research is based on steady-state analysis. Although time-series simulation is conducted to observe the system behaviors during a study period, many calculations are separately implemented in each specific time. For example, the voltage deviation between all buses of the system is considered at a particular working state, but the voltage fluctuation of a bus considering different time points (different states) is not taken into account. Specifically, it is supposed that all bus voltages nearly reach the value of 1.03 p.u. in the first time interval, while all of them change around 0.97 p.u. in the second interval. Since each bus voltage is close to the others in each time, the corresponding voltage deviation is quite small leading to a good value of the general voltage deviation index (VDI). However, comparing between two intervals, the voltage fluctuation is quite considerable. Hence, this issue should be included in the further studies.
3. In the case of PV constant power factor control mode, the generated active and reactive power from PV arrays is fully supplied into utility grids without any regulations. Since these amounts of power are uncertain according to intermittent behaviors of environmental conditions, it is necessary to put them under the control to get the better system voltage profile. For instance, the voltage regulation can be implemented by using energy storage systems (ESS) installed at PV farms. ESS may consume the exceeded power or supply the additional one following the requirements from utilities.

REFERENCES

1. G. Masson, M. L. , and D. Biancardi, *Global market outlook for photovoltaics until 2016.* European Photovoltaic Industry Association, 2012 [Online]. Available: http://www.epia.org/news.
2. Yun Tiam Tan and Daniel S. Kirschen, *Impact on the power system of a large penetration of photovoltaic generation* Power Engineering Society General Meeting, 2007. IEEE, 2007: p. 1 - 8.
3. Chowdhury, B. H. and Sawab, A. W., *Evaluating the value of distributed photovoltaic generations in radial distribution systems.* Energy Conversion, IEEE Transactions, 1996. vol. 11 (no. 3): p. 595 - 600.
4. T. Hoff, H. J. Wenger, and B. K. Farmer, *The value of grid-support photovoltaics in providing distribution system voltage support.* Proc. American Solar Energy Society Annual Conf., 1994.
5. R. Shah, N. Mithulananthan, R. C. Bansal, K. Y. Lee, and A. Lomi, *Power system voltage stability as affected by large-scale PV penetration.* ICEEI 2011, 2011: p. 1–6.
6. B. Tamimi, C. Cañizares, and K. Bhattacharya, *System stability impact of large-scale and distributed solar photovoltaic generation : the case of Ontario, Canada.* Sustainable Energy, 2013. vol. 4 (no. 3): p. 680–688.
7. S. Kabir, M. N. , and R. Bansal, *Impact of large scale photovoltaic system on static voltage stability in sub-transmission network.* ECCE Asia Downunder, 2013: p. 468–473.
8. S. Kabir, O. K. , and S. Bartlett, *Impact of large-scale photovoltaic system on short and long term voltage stability in sub transmission network.* AUPEC 2013, 2013: p. 1–6.
9. Hung, D.Q. ; Mithulananthan, N. ; and Lee, K. Y., *Determining PV penetration for distribution systems with time-varying load models.* IEEE Trans. Power Systems, 2014. volume: PP (issue: 99): p. 1-10.

10. Masters, G.M., *Renewable and Efficient Electric Power Systems.* John Wiley & Sons, Inc., Hoboken, New Jersey, 2004.
11. Eftekharnejad, S. ; Vittal, V. ; Heydt, G. T. ; Keel, B. ; and Loehr, J., *Impact of increased penetration of photovoltaic generation on power systems.* Power Systems, IEEE Transactions, 2013. vol. 28 (issue: 2): p. 893 - 901.
12. A. Chatterjee, A. Keyhani, and D. Kapoor, *Identification of photovoltaic source models.* Energy Conversion, IEEE Transactions, 2011. vol. 26 (issue: 3): p. 883 - 889.
13. Kjaer, S. B. ; Pedersen, J. K. ; and Blaabjerg, F., *A review of single-phase grid-connected inverters for photovoltaic modules.* Industry Applications, IEEE Transactions, 2005. vol. 41 (issue: 5): p. 1292 - 1306.
14. Kasap, S., *Principles of Electronic Materials and Devices.* New York: McGrawHill, 2006.
15. A. Chouder, S. Silvestre, N. Sadaoui, and L. Rahmani, *Modeling and simulation of a grid connected PV system based on the evaluation of main PV module parameters.* Simulation Modelling Practice and Theory, 2012. vol. 20 (no. 1): p. 46–58.
16. W. Desoto, S.K., and W. Beckman, *Improvement and validation of a model for photovoltaic array performance.* Solar Energy, 2006. **vol. 80**(no. 1): p. 78–88.
17. H. Koizumi and K. Kurokawa, *A novel maximum power point tracking method for PV module integrated converter.* IEEE 36th Conference on Power Electronics Specialists, 2005: p. 2081–2086.
18. C. Naksrisuk and K. Audomvongseree, *Dependable capacity evaluation of wind power and solar power generation systems.* ECTI-CON 2013, 2013: p. 1–6.
19. P. Kundur, *Power System Stability and Control.* New York: McGrawHill, 1994.
20. Ismail Musirin and Titik Khawa Abdul Rahman, *Novel Fast Voltage Stability Index (FVSI) for voltage stability analysis in power transmission system.* Research and Development, 2002. SCOReD 2002. Student Conference, 2002: p. 265–268.

21. M. Moghavvemi and F. M. Omar, *Technique for contingency monitoring and voltage collapse prediction.* IEE Proceedings - Generation, Transmission and Distribution, 1998. vol. 145 (no. 6): p. 634 - 640.

22. A. Mobamed, G. B. Jasmon, and S. Yusoff, *A static voltage collapse indicator using Line Stability Factors.* Journal of lndustrial Technology, 1989. vol. 1 (no. 1): p. 73-85.

23. K. Yimchuen and K. Udomwongseree, *Transmission expansion planning with consideration of voltage stability using genetic algorithm.* ECTI-CON 2011, 2011: p. 909–912.

24. Hadi Saadat, *Power System Analysis.* New York: McGrawHill, 1999.

25. E. Vittal, M. O. Malley, and A. Keane, *A steady-state voltage stability analysis of power systems with high penetrations of wind.* Power Systems, IEEE Transactions, 2010. vol. 25 (issue: 1): p. 433–442.

26. K. Audomvongseree and A. Yokoyama, *Risk based TRM evaluation by probabilistic approach.* Probabilistic Methods Applied to Power Systems, 2004 International Conference, 2004: p. 254–259.

27. Hoff, T. and Shugar, D. S., *The value of grid-support photovoltaics in reducing distribution system losses.* Energy Conversion, IEEE Transactions, 1995. vol. 10 (no. 3): p. 569 - 576.

28. C. Chung-Fu, *Reconfiguration and capacitor placement for loss reduction of distribution systems by ant colony search algorithm.* IEEE Trans. Power Syst., 2008. vol. 23 (no. 4): p. 1747–1755.

29. F. A. Viawan and D. Karlsson, *Combined local and remote voltage and reactive power control in the presence of induction machine distributed generation.* IEEE Trans. Power Syst., 2007. vol. 22 (no. 4): p. 2003–2012.

30. Thongsawaeng, C. and Audomvongseree, K., *Determination of the optimal battery capacity of a grid-connected photovoltaic system with power and frequency fluctuations consideration.* ECTI-CON 2013, 2013: p. 1-6.

31. J. M. Gordon and T. A. Reddy, *Generalized capacity factors for gridintertie solar photovoltaic systems.* Solar Cells, 1988. vol. 23: p. 127–137.

จุฬาลงกรณ์มหาวิทยาลัย
Chulalongkorn University

APPENDIX

Photovoltaic Generation Data

Table A. 1 Electrical characteristics of PV module (KC175GHT-2) at STC*.

Parameters	Numerical Values	Units
Maximum power ($P_{max,n}$)	175	W
Voltage at $P_{max,n}$ ($V_{mpp,n}$)	23.6	V
Current at $P_{max,n}$ ($I_{mpp,n}$)	7.42	A
Short circuit current ($I_{sc,n}$)	8.09	A
Open circuit voltage ($V_{oc,n}$)	29.2	V
Temperature coefficient of short circuit current (K_I)	0.00318	A/^{o}C
Temperature coefficient of open circuit voltage (K_V)	-0.0109	V/^{o}C
Nominal operating cell temperature (*NOCT*)	47	^{o}C
Number of cells within module (*n*)	48	cells

** STC: Standard Test Conditions (1000W/m^{2} of solar intensity, 25^{o}C of cell temperature).*

(2012, Apr.) KC175GHT-2 datasheet, Kyocera Solar, Inc. [Online]. Available: http://www.kyocerasolar.eu

Table A. 2 Five unknown parameters of PV module model at STC.

(Calculated from the data in Table A. 1)

Parameters	Numerical Values	Units
Photo-generated current ($I_{ph,n}$)	8.0909	A
Dark saturation current ($I_{0,n}$)	3.1886e-006	A
Thermal voltage ($V_{T,n}$)	0.0413	V
Shunt resistance ($R_{sh,n}$)	678.5105	Ω
Series resistance ($R_{s,n}$)	0.0769	Ω

Table A. 3 Other parameters of PV system.

Parameters	Numerical Values	Units
Number of modules in 1 string (N_m)	10	modules
Number of strings in 1 array (N_s)	6	strings
Efficiency of 3-fase inverter (*eff*)	99	%
Reactance of step-up transformer (X_T)*	0.15	p.u.

** Based on per-unit system of the test distribution network.*

Network Data

Table A. 4 Generation data of TahSai distribution system.

Parameters	Numerical Values	Units
System MVA base	100	MVA
System base voltage	12	kV
Slack bus (ordinal number)	1	
Voltage magnitude at slack bus	1.0455	p.u.
Voltage angle at slack bus	0	degrees

Table A. 5 Peak load data of TahSai distribution system.*

Load bus	Active power demand (MW)	Reactive power demand (MVAr)	Vmax (p.u.)	Vmin (p.u.)
6	0.5280	0.3270	1.05	0.95
8	0.6600	0.4090	1.05	0.95
9	0.0660	0.0400	1.05	0.95
10	0.3300	0.2040	1.05	0.95
11	0.5280	0.3270	1.05	0.95
14	0.6600	0.4090	1.05	0.95
15	0.1650	0.1020	1.05	0.95
16	0.6230	0.3860	1.05	0.95
17	0.9900	0.6130	1.05	0.95
18	0.6600	0.4090	1.05	0.95
20	0.0660	0.0400	1.05	0.95
22	0.3300	0.2040	1.05	0.95
24	1.6500	1.0220	1.05	0.95
26	0.1050	0.0650	1.05	0.95
28	0.0330	0.0200	1.05	0.95
30	0.9900	0.6130	1.05	0.95
32	0.3300	0.2040	1.05	0.95
34	0.1650	0.1020	1.05	0.95

** Peak demands of 1-year period (= summer peak demands = summer working day peak demands).*

Considering only summer working days in this research, and it is given that load data are measured every hour.

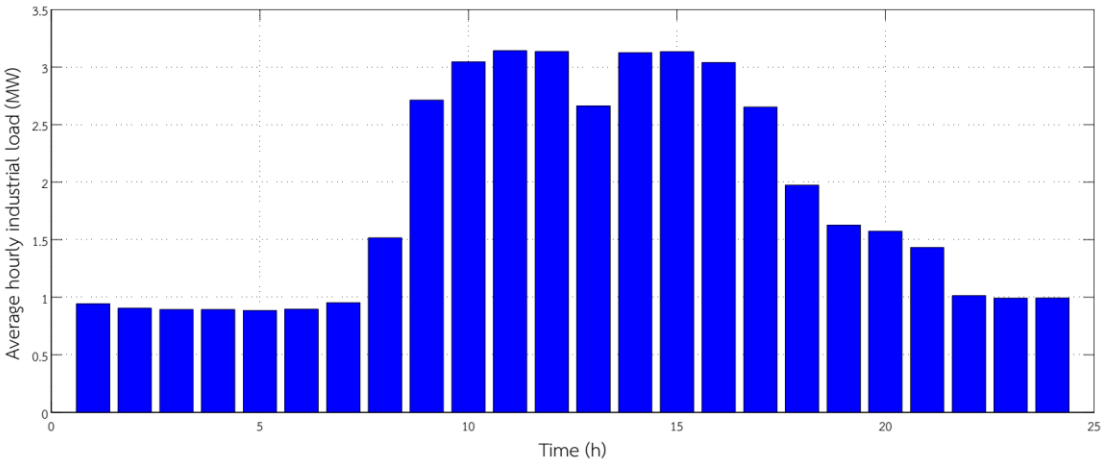

Figure A. 1 Average hourly load of a typical industrial demand considering only summer working days.

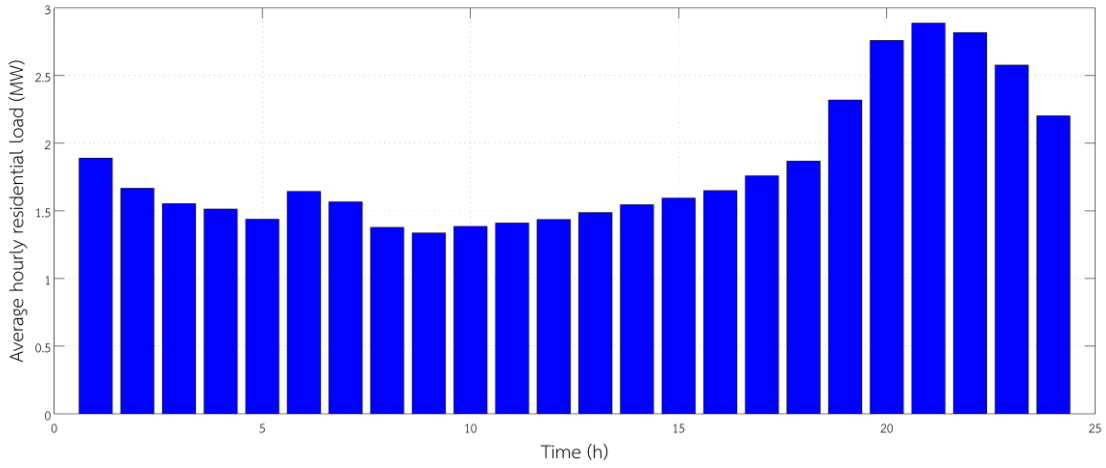

Figure A. 2 Average hourly load of a typical residential demand considering only summer working days.

In TahSai network, the bus having the peak demand greater than 0.5 MW is supposed to be industrial bus, and its average hourly load data follow the trend as in Figure A. 1. On the other hand, the other load buses will be concerned as the residential buses, and their average hourly loads follow the behavior as in Figure A. 2. For example, considering bus 34 as a residential bus. The peak demand of this bus among summer working days reaches the value of 0.165 MW (as in Table A. 5), at 8

pm (refer to Figure A. 2) of someday. The average load at this hour is assumed to be: ***k*** *x* 0.165 (MW), where ***k*** is a coefficient (0<k<1). By setting ***k*** = 0.84 and scaling the data based on Figure A. 2, the average hourly load data of bus 34 as well as the other buses considering only summer working days are specified. Table A. 6 shows only the study period from 7 am to 6 pm.

Table A. 6 Average hourly load data (MW) of TahSai network considering only summer working days.

	8 (7-8 am)	9 (8-9 am)	10 (9-10 am)	11 (10-11 am)	12 (11-12 pm)	13 (12-1 pm)	14 (1-2 pm)	15 (2-3 pm)	16 (3-4 pm)	17 (4-5 pm)	18 (5-6 pm)
Bus 6	0.2141	0.3829	0.4297	0.4435	0.4425	0.3758	0.4412	0.4423	0.4291	0.3745	0.2787
Bus 8	0.2676	0.4787	0.5372	0.5544	0.5531	0.4697	0.5515	0.5529	0.5364	0.4681	0.3483
Bus 9	0.0265	0.0257	0.0266	0.0271	0.0276	0.0285	0.0297	0.0306	0.0317	0.0338	0.0359
Bus 10	0.1323	0.1284	0.1329	0.1354	0.1379	0.1427	0.1483	0.153	0.1584	0.1689	0.1793
Bus 11	0.2141	0.3829	0.4297	0.4435	0.4425	0.3758	0.4412	0.4423	0.4291	0.3745	0.2787
Bus 14	0.2676	0.4787	0.5372	0.5544	0.5531	0.4697	0.5515	0.5529	0.5364	0.4681	0.3483
Bus 15	0.0661	0.0642	0.0665	0.0677	0.0689	0.0714	0.0742	0.0765	0.0792	0.0844	0.0896
Bus 16	0.2526	0.4518	0.5071	0.5233	0.5221	0.4434	0.5205	0.5219	0.5063	0.4418	0.3288
Bus 17	0.4014	0.718	0.8058	0.8316	0.8297	0.7046	0.8272	0.8293	0.8046	0.7021	0.5225
Bus 18	0.2676	0.4787	0.5372	0.5544	0.5531	0.4697	0.5515	0.5529	0.5364	0.4681	0.3483
Bus 20	0.0265	0.0257	0.0266	0.0271	0.0276	0.0285	0.0297	0.0306	0.0317	0.0338	0.0359
Bus 22	0.1323	0.1284	0.1329	0.1354	0.1379	0.1427	0.1483	0.153	0.1584	0.1689	0.1793
Bus 24	0.669	1.1967	1.3429	1.386	1.3828	1.1743	1.3787	1.3822	1.3409	1.1702	0.8709
Bus 26	0.0421	0.0408	0.0423	0.0431	0.0439	0.0454	0.0472	0.0487	0.0504	0.0537	0.057
Bus 28	0.0132	0.0128	0.0133	0.0135	0.0138	0.0143	0.0148	0.0153	0.0158	0.0169	0.0179
Bus 30	0.4014	0.718	0.8058	0.8316	0.8297	0.7046	0.8272	0.8293	0.8046	0.7021	0.5225
Bus 32	0.1323	0.1284	0.1329	0.1354	0.1379	0.1427	0.1483	0.153	0.1584	0.1689	0.1793
Bus 34	0.0661	0.0642	0.0665	0.0677	0.0689	0.0714	0.0742	0.0765	0.0792	0.0844	0.0896

Table A. 7 Branch data of TahSai distribution system.

Branch	R (p.u.)	X (p.u.)	B (p.u.)
1 - 2	0.0054	0.0104	0
2 - 3	0.0218	0.0430	0
3 - 4	0.0290	0.0574	0
4 - 5	0.0327	0.0646	0
5 - 6	0.0055	0.0031	0
5 - 7	0.0341	0.0674	0
7 - 8	0.0110	0.0063	0
4 - 9	0.0015	0.0029	0
9 - 10	0.0029	0.0057	0
10 - 11	0.0058	0.0115	0
11 - 12	0.1198	0.2367	0
12 - 13	0.0160	0.0316	0
13 - 14	0.0015	0.0028	0
13 - 15	0.0218	0.0430	0
15 - 16	0.0225	0.0445	0
16 - 17	0.0240	0.0473	0
17 - 18	0.0254	0.0502	0
12 - 19	0.0015	0.0029	0
19 - 20	0.0028	0.0016	0
19 - 21	0.0123	0.0244	0
21 - 22	0.0055	0.0032	0
21 - 23	0.0123	0.0244	0
23 - 24	0.0058	0.0111	0
23 - 25	0.0182	0.0359	0
25 - 26	0.0116	0.0230	0
26 - 27	0.1133	0.2238	0
27 - 28	0.0441	0.0257	0
25 - 29	0.0196	0.0387	0
29 - 30	0.0015	0.0028	0
29 - 31	0.0211	0.0416	0
31 - 32	0.0110	0.0064	0
31 - 33	0.0225	0.0445	0
33 - 34	0.0055	0.0032	0

VITA

Mr. Tong Duy Anh was born in Thanh Hoa, Vietnam in 1989. He received the Bachelor's Degree of Engineer in Electrical Engineering from Hanoi University of Science and Technology, Hanoi, Vietnam, in 2012. He has been granted a scholarship by AUN/SEED-Net (JICA) to prosecute the Master's Degree in Electrical Engineering at Chulalongkorn University, Bangkok, Thailand, since 2012. He conducted his research at Power System Research Laboratory (PSRL), Department of Electrical Engineering, Faculty of Engineering, Chulalongkorn University. His research interests are power system stability, photovoltaic generation modelling and renewable energy.